TÉCNICO LISBOA

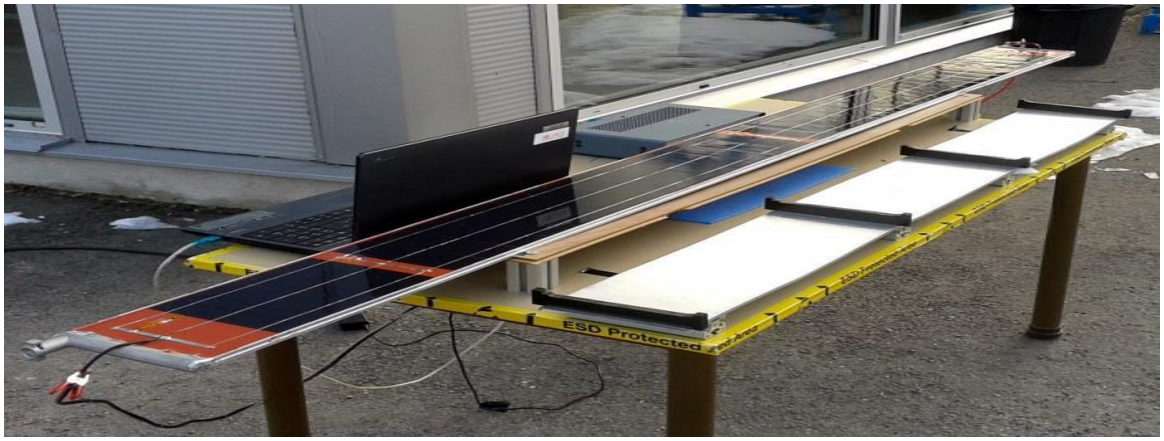

Stationary Solar Concentrating Photovoltaic-Thermal Collector Cell String Layout

Samuel Kessete Nashih

Thesis to obtain the Master of Science Degree in

Electronics Engineering

Supervisors: Prof. Carlos Alberto Ferreira Fernandes
Eng. João Santos Leite Cima Gomes

Examination Committee

Chairperson: Prof. João José Lopes da Costa Freire
Supervisor: Prof. Carlos Alberto Ferreira Fernandes
Member of the committee: Prof. José Júlio Alves Paisana

October 2015

Acknowledgement

First of all I would like to express my deepest gratitude to my advisor, Prof. Carlos Alberto Ferreira Fernandes, for his excellent guidance, caring, patience, and providing me with an excellent atmosphere for doing my research. I would also like to thank Eng. João Leite Cima Gomes and Eng. Linkesh Diwan for providing me data from Solarus and their support. I would also like to thank Prof. João Torres for being beside me all the time and Mrs. Idalina Rosa for her unconditional support.

I would never have been able to finish my dissertation without the guidance of my committee members, help from friends, and support from my family.

I would also like to thank ERASMUS MUNDUS, for giving me, the opportunity to study in the programme, the stuff of international office IST, Ana Barbosa and Graça Pereira in the Núcleo de Mobilidade e Cooperação Internacional and the stuff of the Department of Electrotechnical and Computer Engineering (DEEC) at IST-Tagus.

Last but not least, I would like to thank my family, Mr. Semere Amlesom's family and my wife Mrs. Meron Mehari. Without their support and encouragement and their prayers to GOD, it wouldn't be possible to accomplish my work.

Abstract

An adequate development of society deeply relies on the rational use of energy sources, which is crucial for sustainability of the earth's energy supply chain. Solar energy can be harvested in different ways, by choosing different technologies. Among them, the most common are solar photovoltaic (PV), solar thermal and hybrid solar photovoltaic/thermal (PVT). Despite the sharp decrease in the solar cell price, solar cells still remain today the most expensive component of any solar panel, which enhances the importance of the study concerning the optimization of the cell string layout and of the diode system.

Solarus AB[1] manufactures hybrid solar PVT using concentrating technology. This means that the solar radiation is reflected to the string of solar cells in a non-uniform distribution. Besides, the frame casts shadow on the reflector and hence on the cells. When the solar cells are connected in series, a single fully shaded cell causes the whole generated power from the string to vanish. The development of numerical models, flexible enough to take into account the various details that define the string of cells, may be seen as an important contribute in this area of research. In effect, these analysis may represent an alternative tool for the re-design of actual devices or even for new proposals without the need of the fabrication of a series of expensive prototypes.

The aim of this thesis work is to evaluate possible ways of minimizing the effect of both the longitudinal and transversal shading properties inherent to concentrating collectors that are fixed to building structures. Solarus PVT cell strings contain 38 solar cells connected in series. Solar cells in the concentrated side of the collector are shaded due to the presence of the aluminium frame of the PVT collector. This causes a serious decrease in the electrical power generated from the cells, which should be overcome. The effects of shading and of non-uniform illumination are minimized by including bypass diodes. Each string has 4 groups, each one associated to a bypass diode. The groups have not the same number of solar cells, since the cells closer to the frame are more deeply affected by shading, i.e. for a longer period of time. In this work, different combinations of string cells in the collector receiver have been simulated in a PSPICE environment, and a comparative analysis is presented at the end.

Keywords

Solar cells; longitudinal and transversal shading; concentrating collectors, bypass diodes.

[1] Swedish enterprise: (http://www.bcorporation.net/community/solarus-sunpower-sweden-ab)

Resumo

Um desenvolvimento ajustado da sociedade depende muito do uso racional das fontes de energia, uma vez que este se revela crucial para a sustentabilidade da cadeia de fornecimento de energia da Terra. A energia solar pode ser obtida de maneiras diferentes, por escolha de diferentes tecnologias. As mais comuns são a energia solar fotovoltaica (PV), solar térmica (T) e solar fotovoltaica e térmica, ou híbrida (PVT). Cada tecnologia apresenta características diferentes, que conduzem a diferentes custos associados. Este facto é determinante na seleção da tecnologia utilizada. Apesar da diminuição acentuada dos preços de células solares verificada ultimamente, estas ainda permanecem hoje o componente mais caro de qualquer painel solar. Este facto vem realçar a importância dos estudos sobre as otimizações dos traçados das cadeias de células solares no sistema elétrico.

A empresa sueca Solarus AB fabrica coletores solares híbridos. Estes usam a tecnologia de concentração. A radiação solar é refletida de uma forma não uniforme para a cadeia de células solares. Para além disso, a moldura em alumínio do coletor produz o sombreamento do conjunto refletor/células. Uma iluminação não uniforme, associada a um sombreamento longitudinal/transversal reduzem de forma significativa a eficiência dos coletores. O desenvolvimento de modelos numéricos, suficientemente flexíveis de modo a incluir os inúmeros pormenores que caraterizam a cadeia de células solares, representa uma ferramenta poderosa na investigação nesta área, permitindo o redimensionamento de dispositivos existentes no mercado ou a elaboração de propostas de novos dispositivos. Trata-se assim de uma alternativa à fabricação de uma série de protótipos em laboratório, obviamente mais onerosa.

O objetivo principal deste trabalho de dissertação de mestrado é a avaliação de possíveis formas de minimizar os efeitos simultâneos dos sombreamentos longitudinal e transversal inerentes aos coletores concentradores que são fixos em estruturas no topo dos edifícios. As cadeias de células nos coletores da Solarus contêm 38 células solares ligadas em série, estando as células solares no lado inferior do recetor sujeitas a sombreamentos com origem na moldura do coletor. Este facto provoca uma diminuição acentuada da energia elétrica gerada a partir das células que é necessário ultrapassar. Os efeitos simultâneos do sombreamento e de uma iluminação não uniforme são minimizados pela inclusão de díodos de contorno. Cada cadeia de células solares agregada a um díodo de contorno constitui um grupo. As 38 células solares estão divididas em 4 grupos mas com uma distribuição não uniforme, dado que as células mais próximas da moldura do coletor são mais fortemente

afetadas pelo sombreamento. Neste trabalho de dissertação foram analisados coletores solares com combinações distintas de díodos de contorno, usando modelos de simulação numérica enquadrados no PSPICE, e feito um estudo comparativo que é apresentado no final.

Palavras-chave

Células solares; sombreamento longitudinal e transversal; coletores de concentração, díodos de contorno.

Table of Contents

List of figures

List of tables

List of abbreviations and acronyms

α	Absorbance
β	Aperture tilt
η_{cell}	Photovoltaic cell efficiency
$\delta\eta_{el}$	Uncertainty in efficiency
δ	Declination angle
δFF	Uncertainty in FF
δP_{mp}	Uncertainty in peak power
$\lvert\Delta_{abs}\rvert$	Absolute difference between simulated and experimental results
$\lvert\Delta_{rel}\rvert\%$	Percentage deviation of measured data from simulated results
ΔT	Change in temperature from 25ºC
ΔT_{GMT}	Difference expresses in hours between Local Time (LT) and GMT
η_{th}	Thermal efficiency
Φ	Absorber inclination
τ	Transmittance
Θ	Incidence angle of beam ray
Θ_c	Acceptance angle
Θ_{diff}	Incidence angle of diffuse light
Θ_l	Incidence angle of beam ray projected to longitudinal section
Θ_{ref}	Incidence angle of reflected light
Θ_t	Incidence angle of beam ray projected to transversal section
$K_{\theta l}$	Incidence angle modifier constant, longitudinal component
$K_{\theta t}$	Incidence angle modifier constant, transversal component
$K_{\theta t,net}$	Net incidence angle modifier constant
$K_{\tau\alpha}$	Incidence angle modifier constant
AC	Alternating Current
A_{cell}	Solar cell area
AM0	Atmosphere zero
AM1.5	Atmosphere 1.5
b_o	Incidence angle modifier coefficient
C	Concentration factor

C_1	Current dependence on temperature [A m^2/ (W/K)]
$C_{circular}$	Circular Concentration factor
C_{linear}	Linear Concentration factor
C_o	Constant which depends on the solar cell area and characteristics [A/(W/m^2)]
CPC	Compound Parabolic Concentrator
CSC	Concentrating Solar Collector
CSP	Concentrating Solar Power
D	Day of the year starting from January 1st
DC	Direct Current
d_1	CPC opening
d_2	Receiver opening
E_f	Energy of photon [J]
EoT	Equation of Time [minutes]
f	Frequency of photon [Hz]
F	Ratio of current generated by shaded cell to fully illuminated cell
FF	Fill Factor
G	Global irradiance [W/m^2]
G_{beam}	Beam irradiance [W/m^2]
G_{diff}	Diffuse irradiance [W/m^2]
G_{ref}	Reflected irradiance [W/m^2]
G_{ref}	Global reference irradiance [1000W/m^2]
h	Planck's constant [J.s]
HRA	Hour Angle
I	Solar cell/module output currents [A]
IAM	Incidence Angle Modifier
IAM_l	Longitudinal incidence angle modifier
IAM_t	Transversal incidence angle modifier
I_D	Diode current [A]
I_{mp}	Current at maximum power [A]
I_{PV}	Photon generated current [A]
IR	Infrared light
I_{Rp}	Current through parallel resistor
I_s	Reverse saturation diode current [A]
I_{sc}	Short circuit current [A]

I_{sh}	Shaded cell current [A]
I_{il}	Fully illuminated cell current [A]
$I_{pv,il}$	Fully illuminated cell photo generated current [A]
J_{sc}	Short circuit current density [A/m^2]
$J_{sc,ref}$	Short circuit current density at G_{ref} [A/m^2]
K	Boltzman constant [J/K]
KWh	Kilowatt Hour
LST	Local Solar Time [hour]
LSTM	Local Standard Time Meridian [hour]
LT	Local Time [hour]
LTSPICE	Linear Technology Simulation Program with Integrated Circuit Emphasis
M	Number of solar cells bridged by single bypass diode
MPP	Maximum Power Point
MaReCo	Maximum Reflection Concentrator
n	Diode ideality factor
N	Number of solar cells
η_{el}	Electrical or photovoltaic efficiency
P	Solar module output power [W]
P_{dis}	Power dissipated by the shaded cell [W]
P_{el}	Electrical power [W]
P_{mp}	Maximum power or power at MPP [W]
P_{Rs}	Power loss due to series resistance [W]
P_{Rp}	Power loss due to shunt resistance [W]
P_{th}	Thermal power [W]
PV	Photovoltaic
PVT	Photovoltaic Thermal
q	Electronic charge [C]
R_p	Parallel resistance [Ω]
R_s	Series resistance [Ω]
STC	Standard Testing Conditions (G=1000W/m^2 and T=25ºC)
SME	Small and Medium Enterprise
SPICE	Simulated Program with Integrated Circuits Emphasis
T	Absolute temperature [K]

T_a	Ambient temperature [K]
TC	Time Correction factor [minutes]
T_{in}	Collector inlet temperature [K]
T_{mid}	Collector mean temperature [K]
T_{out}	Collector outlet temperature [K]
U_1	Linear conduction loss coefficient [W/K]
U_2	Quadratic conduction loss coefficient [W/K^2]
V	Solar cell/panel output voltage [V]
V_{bypass}	Voltage across bypass diode [V]
V_c	Reverse breakdown voltage [V]
V_{co}	Contact potential in a junction [V]
V_{cell}	Illuminated cell voltage [V]
V_{il}	Fully illuminated cell voltage [V]
V_F	Forward voltage drop of diode [V]
V_{mp}	Voltage at MPP [V]
V_{oc}	Open circuit voltage [V]
V_{sh}	Shaded solar cell voltage [V]

1. Introduction

As the effects of climate change are becoming increasingly obvious and the global oil reserves seem to have reached their peak production, an imperative change to the renewable sources paradigm is today very well established.

Improving the existing resources, on one hand, and search for alternative sources, on the other hand, appear to be the appropriate strategy. Renewable sources can play an important role in this process. Some of the renewable energy sources are wind energy, solar energy, Tidal, Geothermal, etc. Efficient and economic harnessing of clean solar power may be very significant for fulfilling today's growing energy needs and tranquilizing climate concerns. Solar power can be solar photovoltaic (PV), solar thermal or hybrid of solar photovoltaic and thermal (PVT) [1]. Solar energy has the advantage of being environmental friendly and have unlimited availability [2]. Photovoltaic energy is highly dependent on the environmental conditions, such as temperature and solar irradiation, which makes the optimization analysis rather complex [3].

Stationary solar concentrating hybrid PVT systems use reflectors which may cause non uniform distribution of light on the string of PV cells. Similarly, partial shading creates non uniform illumination and, hence, leads to the development of hot spots in solar PV module, which may cause permanent damage to the cells that are shaded. Partial shading has a larger impact on PV efficiency (electrical energy output of PVT collectors) than on thermal efficiency (thermal energy output of PVT collectors). PVT produces thermal and electrical energies [4].

1.1 Outline

The document is organized as per the following:

- Section 1 is a general introduction of the work and describes the fundamentals of solar energy;
- Section 2 describes the state of the art of concentrating solar hybrid PVT collectors;
- Section 3 describes briefly Solarus AB compound concentrating collectors;
- Section 4 describes in detail solar cell modelling and simulation for the analysis of the shading effects in string of solar cells;
- Section 5 presents the simulation results of the models described in section 4, taking into account the data obtained from Solarus AB, when different configurations of solar cell strings are considered;
- Finally, section 6 summarizes the main conclusions, recommendations and future work of the thesis work.

1.2 Work goals

Concentrating light to a solar panel creates non uniform illumination which may cause heating of some of the solar cells. Shading causes a decrease in the efficiency of solar thermal, PV and hybrid PVT collectors. The decrease in the photo generated current of the shaded cells is the worst effect of partial shading in a PV string. The cells under shade are

shunted by the illuminated cells, reversing the current that flows through the shaded cells and, hence, dissipating power instead of generating power. The power dissipated by the shaded cell causes overheating, which may cause permanent damage of the cell, by the creation of *hotspots*. Bypass diodes are used to mitigate this effect by allowing current to flow in a different path at the expense of a minor fraction of the total power. However, the inclusion of bypass diodes increases both assembly time and material cost and, therefore, leads to an increase of the overall costs. A full understanding of the impact of shading on the performance of cell strings with solar cell sizes different from standard cells is imperative. The thesis work is intended to evaluate possible alternatives for the most usual cell string layout and bypass diode configuration, in order to minimize the effects of non uniform illumination and shading inherent to stationary concentrating collectors. The simulation is carried in an LTSPICE[2] software to model the string of solar cells and bypass diodes.

1.3 Solar Radiation

The sun is a medium, yellow star, consisting primarily of hydrogen at temperatures high enough to cause nuclear fusion. Nuclear Fusion is a nuclear reaction in which hydrogen nuclei fuse together to form helium nuclei and release energy.

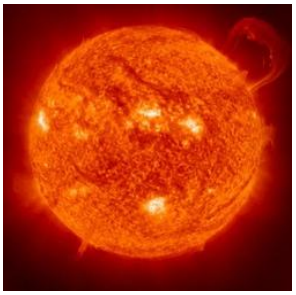

Figure 1.1: Sun [5].

Solar radiation is an electromagnetic wave emitted by the sun's surface that originates from deep inside the sun, where fusion reactions convert hydrogen atoms into helium. This nuclear energy flux is rapidly converted into thermal energy and transported toward the surface of the star, where it is released in the form of electromagnetic radiation [6].

The total power density of the solar radiation at the mean earth-sun distance on a plane perpendicular to the direction of the sun, outside the earth's atmosphere, is referred to as the *solar constant* [7]. Solar constant is the intensity of solar irradiation directly outside the earth's atmosphere on a horizontal surface; it is almost constant at around 1367 W/m^2. This value is annual averaged, as the solar radiation varies slightly over the year due to the earth's slightly elliptical orbit around the sun and to the variations in solar activity. This one varies by $\pm 3\%$ as the earth orbits the sun. The solar radiation that reaches the earth's surface is only 1000 W/m^2. This reduction is due to the presence of atmospheric gases like CO_2, water vapour and others, which absorb, reflect and scatter light.

As the latitude of the place on earth increases, the solar irradiance that falls on that particular place decreases. This is due to the increase in the angle of incidence of solar

[2] Electronic circuits simulator, *Linear Technology Simulation Program for Integrated Circuits Emphasis.*

radiation at higher latitude. Solar radiation travels longer distance in the atmosphere to reach higher latitude, which reduces its energy content by absorption, scattering and reflection before striking the ground. As a consequence, the average irradiance at high latitude is lower than in places at lower latitude (near equator). The irradiance level is also greatly affected by humidity and particle concentration in the atmosphere. Figure 1.2 indicates the irradiance levels in different parts of the world.

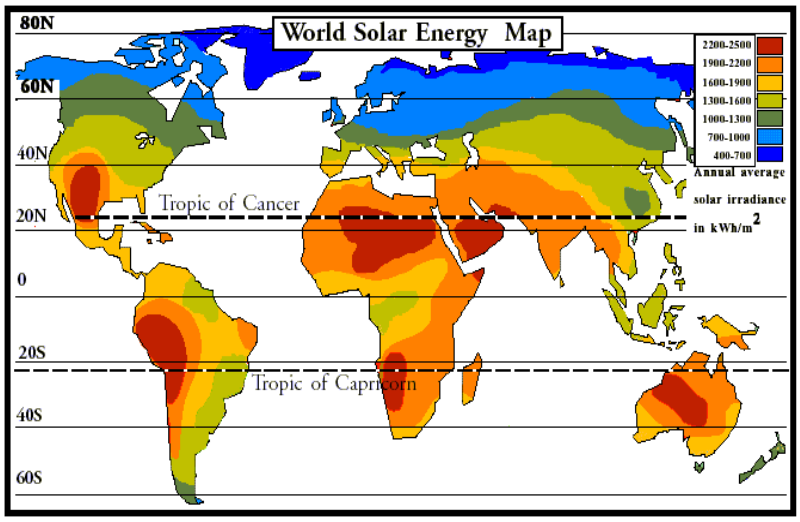

Figure 1.2: The annual global irradiation throughout the world, measured on a horizontal [8].

Solar radiation contains different wavelengths (frequencies). Each wavelength has an associated energy. Waves with short wavelengths have higher energy content than the longer waves. The following graph shows the relationship between wavelength and energy content.

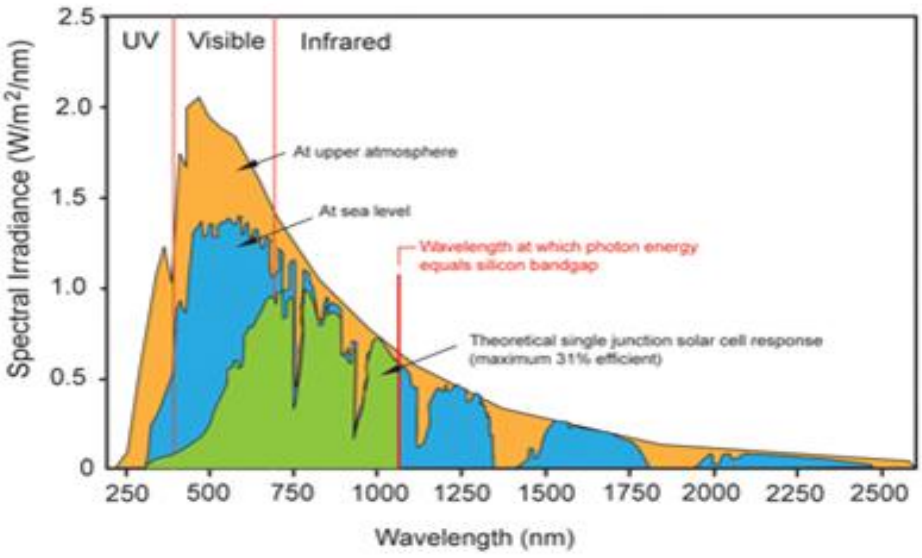

Figure 1.3: Spectral power density of sunlight.

The different spectra refer to the black-body radiation at 6000 K, the extraterrestrial AM0 radiation and the AM1.5[3] radiation.

[3] The spectrum outside the atmosphere (approximated by the 5,800 K black body) is referred to as "AM0", meaning "zero atmospheres". Solar cells used for space power applications are generally characterized using AM0. The spectrum after

The earth receives both direct and diffused sunlight. The portions of these two components depend on weather conditions at a particular instant. So, the actual amount of solar radiation that reaches a particular place on the earth is extremely variable. In addition to the regular daily and yearly variation due to the apparent motion of the earth around the sun, irregular variations are caused by local atmospheric conditions, such as clouds. These conditions influence the *direct* and *diffuse* components of solar radiation. The direct component of solar radiation is the part of the sunlight that directly reaches the earth's surface. Scattering of the sunlight in the atmosphere generates diffuse component. A part of the solar radiation that is reflected by the earth's surface, which is called *albedo*, may also be present in the total solar radiation. The term global radiation is used to refer to the total solar radiation, which is made up of these three components [7]. The direction of the target (PV, solar thermal and PVT) surface must be defined for global irradiance. For direct radiation the target surface faces the incoming beam [9]. In general, the solar radiation that strikes the earth per square meter depends on many factors. Namely, the day of the year, time of the day and latitude.

Solar energy is a term related to part of the sun's electromagnetic energy converted to useful electrical or thermal energy on earth.

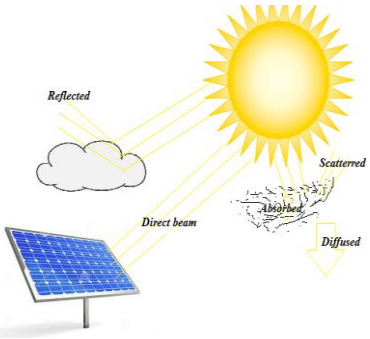

Figure 1.4: Light falling on a panel.

1.4 Photovoltaic Effect

Power generation from solar PV is a clean and renewable energy technology, which is undoubtedly an important advantage in today's world. Photovoltaic is a method of converting solar energy to electrical energy using semicondutor materials. The working principle of solar cells is based on the *photovoltaic effect*. In general, the photovoltaic effect means the generation of a potential difference at the semiconductor junction (homo or hetero-junction) in response to an adequate radiation.

The basic processes behind the photovoltaic effect are:

i. Generation of the charge carriers due to the absorption of photons of adequate wavelength in the material or materials that form the junction.
ii. Subsequent separation of the photo-generated charge carriers in the junction, before they may disappear by spontaneous recombination.
iii. Collection of the photo-generated charge carriers at the terminals of the junction.

---

travelling through the atmosphere to sea level with the sun directly overhead is referred to as "AM1". Solar panels do not generally operate under exactly one atmosphere's thickness. An effective thickness shall be used to take into account with the angle of the sun regarding the Earth's surface. Since the major population centres lie in temperature latitudes, an "AM1.5", 1.5 atmosphere thickness is much more common.

In general, a solar cell structure consists of an absorber layer, in which the photons of incident radiation are efficiently absorbed, resulting in the creation of electron-hole pairs. The presence of the built-in electric field in the vicinity of the junction in solar cells facilitates the separation of photo-generated electron-hole pair by drift. When the charge carriers are not separated from each other in a time shorter than the carrier mean-life times, they will be recombined and will not contribute to energy conversion [10].

Most PV cells are either silicon *p*-*n* junction or *p*-*i*-*n* diodes. Silicon is widely used because it is well studied, it uses mature technology, it is cheap, it is easily available, etc. The energy band gap of silicon is 1.11eV. This falls in the infrared (IR) range of light spectrum (shown in figure 1.3). The efficiency of photovoltaic conversion is limited by the relationships between the photon energies and the energy gap in the semiconductor.

The conduction and valence band types are also crucial in the generation-recombination processes within the semiconductor material. In figure 1.3, it can be seen the theoretical single junction solar cell response, referring a maximum efficiency value of 31%.

The energy E_f of a photon is given by

$$E_f = hf \tag{1}$$

where *h* is plank's constant and *f* is the frequency of the radiation.

If the photon energy is greater or equal to the energy band gap of the semiconductor material, it will give rise to the creation of an electron-hole pair. This condition determines the minimum frequency (maximum wavelength) for the light to be absorbed by the material, regardless to its intensity. When solar radiation falls on a silicon *p*-*n* junction, photons with wavelength less than 1.13 μm generate electron-hole pairs. The electric field in the depletion layer drives the electrons to the *n*-type side and the holes to the *p*-type side. This separates most of the electrons and holes before they can recombine. In figure 1.5 (a) the depletion region is the zone between $-x_{po}$ and x_{n0}.

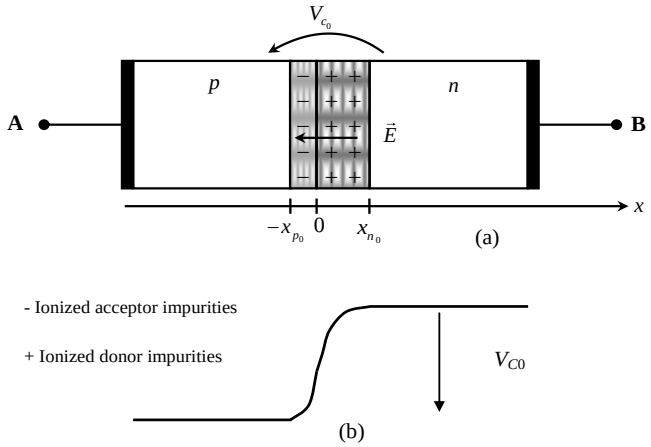

Figure 1.5: Schematic representation of diode junction (a) and of the potential distribution *V*(x) along the diode (b).

This is the zone where the built-in electric field *E* is non-null for a *p*-*n* homojunction. The potential contact V_{co} is given by the difference of the values assumed by the potential *V*(*x*) in the *n*-side and in the *p*-side of the junction (V_{co}= *V*(x_{no})-*V*(x_{po}), as represented in figure 1.5(b). A solar photovoltaic cell consists of a thick *n*-type crystal covered by a thin *p*-

type layer exposed to the sunlight. If an external load resistance *R* is connected between the terminals of the *p-n* junction, the electrons move through the external circuit and recombine with the holes, thus producing a current *I* (figure 1.6). The energy of the solar radiation is converted into electrical energy in the circuit.

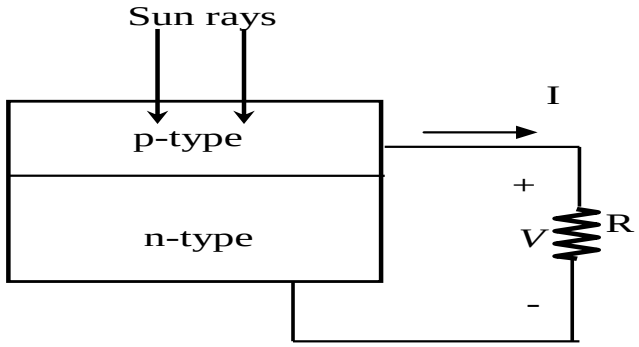

Figure 1.6: Photovoltaic solar cell circuit.

1.5 *I-V* characteristic curve and the three points of interest

A photovoltaic cell/module will produce its maximum current when there is essentially no resistance in the circuit, i.e. when shorted. This corresponds to a short circuit between its positive (*p*) and negative (*n*) terminals. The current that flows at this condition is called *short circuit current*. On the other hand, the maximum voltage produced by the photovoltaic cell/module corresponds to an infinite resistance in the external circuit and the voltage is called *open circuit voltage*. The condition where the power delivered from the solar cell is highest is called *maximum power point* (MPP).

The important points that characterize a solar cell/module (figure 1.7) are the short circuit current (I_{sc}), the open circuit voltage (V_{oc}) and MPP. V_{mp} and I_{mp} are the voltage and current respectively at MPP. These points are discussed in detail in section 4.2. These three points can be found in the data sheet of the solar cell/module.

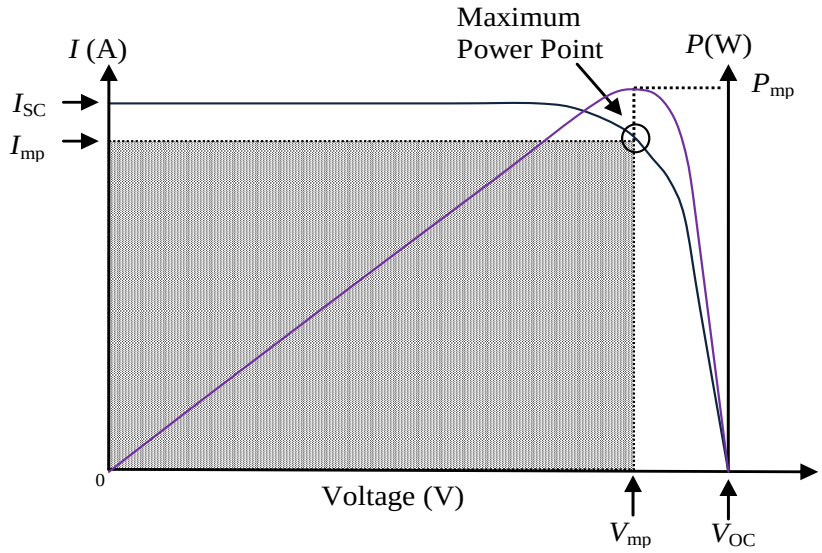

Figure 1.7: *I-V* and *P-V* curves of a photovoltaic cell/module [11].

1.6 Solarus AB

1.6.1 Company Description:

Solarus AB is a Swedish small and medium enterprise (SME) that produces asymmetric concentrating solar collectors (CSC). Solarus has a modular collector box in which different types of absorbers can be inserted in order to create different products, such as the asymmetric concentrating PVT collector, solar thermal and solar PV. Company logo is shown figure 1.8

Figure 1.8: Company logo [4].

Solarus AB was founded by Niclas Stenlund and Stefan Larsson as a private limited company in Norrtäljie, Sweden, in 2006. "The company's mission is the development, production and marketing of concentrated solar technology to the world market". Solarus provides solar energy technology to professional users. In figure 1.9 it is shown the Solarus evolution in the last decade.

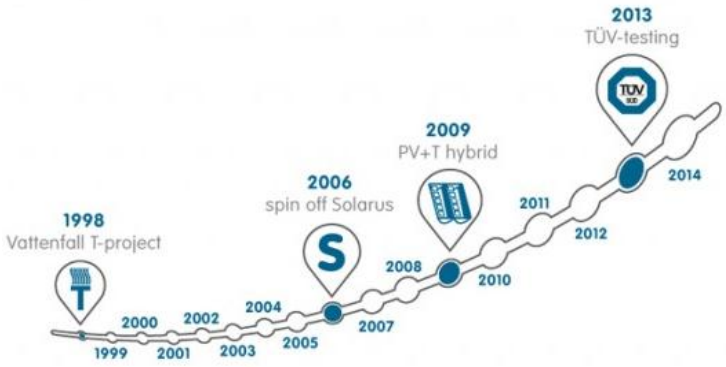

Figure 1.9: Solarus AB timeline [4].

1.6.2 Solarus Products

The Swedish start-up Solarus develops and markets three types of solar energy systems namely, thermal, PV, and hybrid PVT solar collectors (figure 1.10), namely,

A) **Bifacial PV**: Converts the solar energy to electrical energy.
B) **Solar Thermal Collector**: Converts the incoming solar energy to thermal energy.
C) **PVT Collector**: Produces both electrical and thermal energy from a single collector.

The Maximum Reflection Concentrator (MaReCo) collectors are seasonal adapted, which implies that a larger tribute of the annual energy demand can be met. The reflector used by Solarus is made of aluminium, one of the pioneers among the maximum concentrating reflector and solar concentrating technology. Despite its low weight and low material content (thin), Solarus collector is able to concentrate sunlight up to 3.5 times [13].

PV System Thermal System PVT Collector

Figure 1.10: Solarus products.

Solarus' technical team pioneered MaReCo technology in a joint research and development project accomplished by Swedish research institutions and companies, namely Uppsala and Lund Universities, Vattenfall and the Swedish Energy Agency [14].

2. State of the Art

The state of the art on solar concentrating collectors is introduced in this section. Collectors can be classified as non concentrating or concentrating type. The non concentrating solar collectors have no means to concentrate light; they use the light which falls from the sun without concentrating. On the contrary, concentrating collectors use optical devices such as mirrors/aluminium or lenses to concentrate light to the receiver in order to increase the light collected by the device. By increasing the concentration of light, high temperatures and higher energy can be collected, depending on the application.

An overview of shading and incidence angle modifier (IAM) are also presented. The two aspects have a considerable effect on the performance of solar collectors. Thus, their analysis is crucial to improve better energy harvesting.

2.1 Concentrating Collectors

2.1.1 Types of concentrators

Different concentrating solar power (CSP) technologies may be used to concentrate and collect direct solar radiation to provide medium to high temperature heat. The heat can be used to generate steam to run a steam turbine connected to an electric generator or can be stored in liquid, solid or phase changing media like molten salts, ceramics, concrete, etc. At night, it can be extracted from the storage medium to run the steam turbine [15].

Concentrating collectors can be categorized in to line focus (parabolic trough and linear Fresnel), point focus with central receiver (power towers, dish collectors) and point focus with a distributed receiver (solar driven Stirling engines). They produce true image of the sun in the receiver. The concentration of solar radiation to the receiver increases the intensity of radiation and thus the collected power. Different types of collectors are shown in figure 2.1 below.

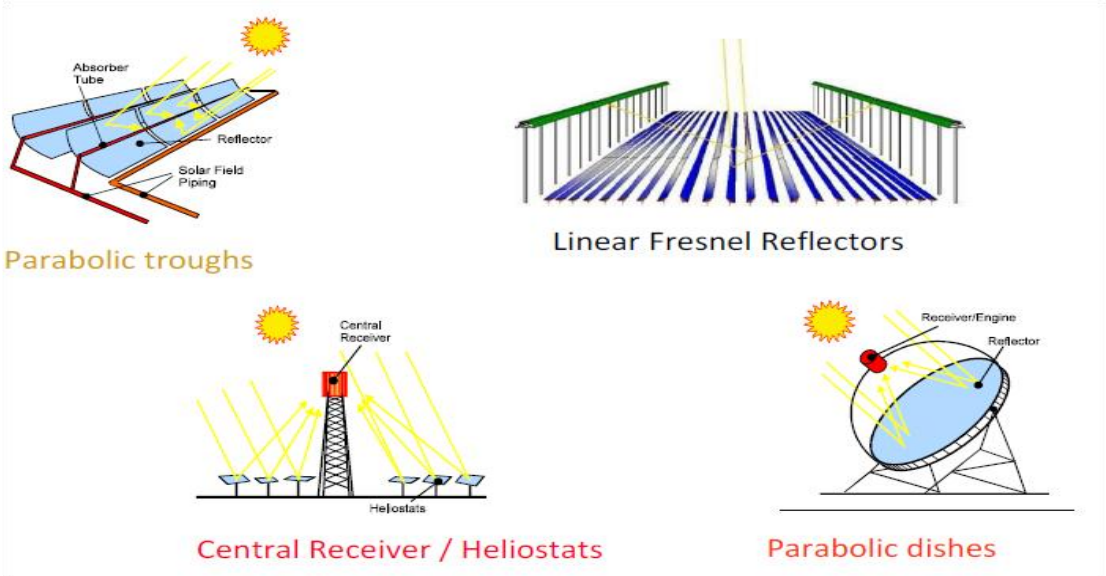

Figure 2.1: Concentrating solar energy source [15-16].

2.1.2 Solarus Compound Parabolic Collectors (CPC)

Solarus CPC is a non imaging concentrating collector. The name CPC is derived from the fact that these systems are composed of two parabolic reflectors with different focal points. The basic shape is shown in figure 2.2 [17]. These collectors can operate without tracking system. This minimizes the mechanical failure issues and the control mechanism associated with it. However, in order to maximize output, the collectors must be oriented properly to south in northern hemisphere.

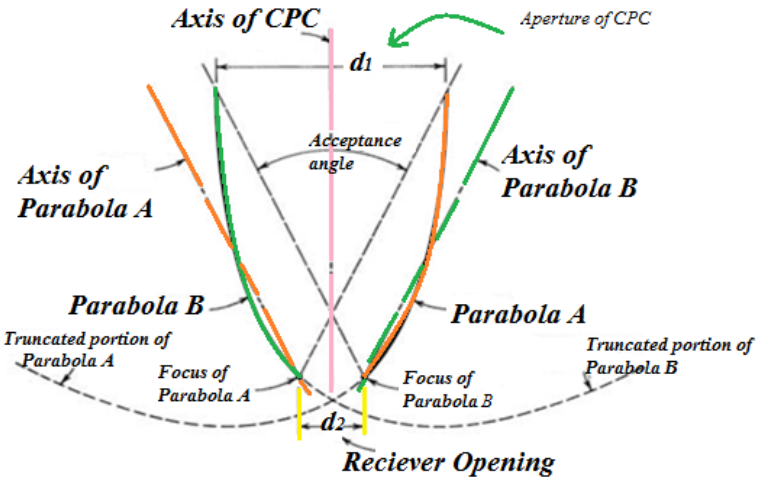

Figure 2.2: Basic shape of symetric CPC.

The receiver is placed between the focus of parabolas A and B, whose distance is called *receiver openning*. Both parabolas reflect the incoming solar radiation on to the reciever. The focal point of each parabola lies on the other parabola and are symmetric with the axis of the CPC.The optical axis determines the upper and lower acceptance angles. The acceptance angle determines the amount of light that can be reflected to reach the receiver. If an incident ray is in the range of the acceptance angle it will be reflected to the receiver by one of the parabolic reflectors. If it falls outside the acceptance angle, it will not be reflected to the receiver but will be reflected back and goes out through the aperture of the CPC without contributing to the amount of energy collected in the receiver [17].

2.1.3 The Maximum Reflector Collector (MaReCo)

The PV and thermal absorbers are costly in the electrical or thermal energy collection from solar energy. The use of concentrating collectors to minimize the collector area allows the replacement of costly absorbers by inexpensive reflective materials, thus reducing the costs. Concentrating irradiance increases the solar input for PV cells increasing the electrical output, but this increase in irradiance level can cause an increase in cell temperature which causes decrease in PV cell efficiency. For concentrated PV solutions, it is necessary to remove the built up heat from the PV cell, which is usually accomplished by running cooling water, with the added benefit of warm water. Thus, the hybrid concentrating collectors have an advantage of collecting both thermal and electrical energy from the same collector.

According to Gomes *et. al* [18], the main advantages of PVT collectors as compared to PV and solar thermal collectors are:

i. PV cells operate at higher efficiency when operating at low temperature, cooling water should be extracted at low temperature unless increase in temperature causes decrease in PV cell efficiencies.
ii. The production of one unit of PVT uses fewer expensive raw materials than an equivalent area of thermal and PV panels. This can reduce the production cost per KWh of annual energy produced heat and electricity [18].
iii. The life time of the PV cells is longer.
iv. The installation area is reduced, if limited space is available like roof.

At the most basic level, the MaReCo consists of an asymmetrical truncated CPC with a flat receiver, preferably bi-facial absorbers in order to minimize the absorber area. The main purpose of the MaReCo is to maximize the annual performance for a given reflector area by reducing the expensive absorber area by less expensive reflectors and thus minimizing the heat losses. The reduction in absorber area eliminates the need of larger insulating material. The collector consists basically on an asymmetric reflector and a trough with a single absorber fin that runs along it [19, 25].

The MaReCo design (shown in figure 2.3) is the product of research activities at Vattenfall Utveckling. The MaReCo is a heavily truncated asymmetric CPC-collector specially designed for high latitudes. It is usually extended in the east-west direction and has a bi-facial absorber. The aim of the MaReCo concept is to create inexpensive and flexible concentrating collectors without reducing the annual output when compared to flat plate collectors. This design concept can be used for various conditions, namely roof, wall or stand-alone installations [20].

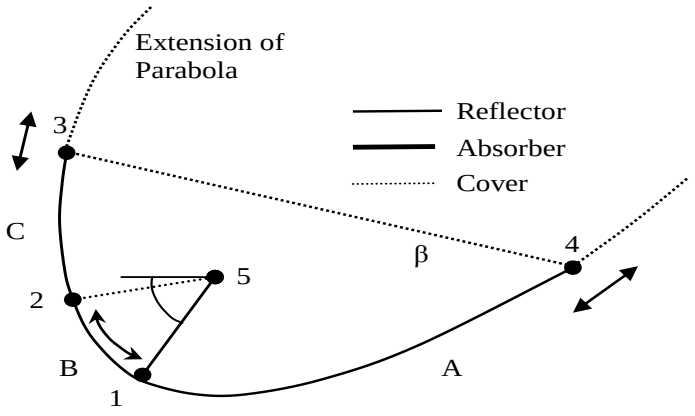

Figure 2.3: The basic MaReCo design.

For simplicity, the MaReCo design is divided in to three parts (A, B and C in the figure 2.3) [20-22]. These are:

i. **Part A**: it is the lower parabolic reflector and corresponds to section 1–4.
ii. **Part B**: It is a circular reflector directing light to the absorber (section 1–2).
iii. **Part C**: It is the upper parabolic reflector (section 2–3).

The aperture 3–4 is covered by glass. Points 3 and 4 can vary along the extensions of the parabola, depending on the desired truncation. The absorber (1–5) makes an angle φ with the horizontal, called the *absorber inclination angle*, and the aperture (3–4) makes an angle β with the horizontal, called the *aperture tilt* [22].

There are various types of MaReCo designs. The most common are stand alone, roof integrated and wall mounted.

The Stand-Alone MaReCo

The stand-alone MaReCo design follows the general design pattern, and it is dimensioned using simulation software to determine the right configuration for the desired annual yield. Figure 2.4 shows a schematic section of a stand-alone MaReCo designed for maximum annual power production in Stockholm, Sweden. The design facilitates the use of a single-axis tracking system. The acceptance angle range when the collector is fixed without tracking is from 20° to 65°. The optical axes 20° and 65° are defined from the horizon [22].

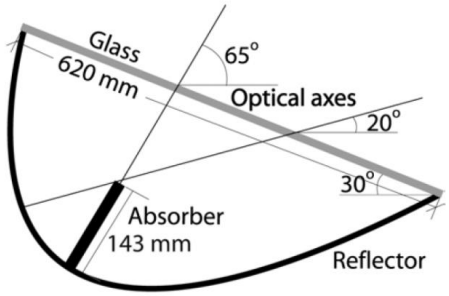

Figure 2.4: The stand-alone MaReCo collector.

The Roof-Integrated MaReCo

The roof-integrated MaReCo is designed to be mounted directly on south-facing roofs in northern hemisphere and north facing roofs in southern hemisphere, with the glass parallel to the roof surface, and the trough axis parallel to the ground. It is designed to be mounted passively on the roof without tracking. The yearly power production profile is load-adapted to the domestic heating requirements in higher latitudes, reducing production in the summer when heat is not so needed. All radiation falling within the range 0° to 60° (when oriented as shown in figure 2.5 i.e. 90^{o}-tilt angle) is accepted by the reflector [22].

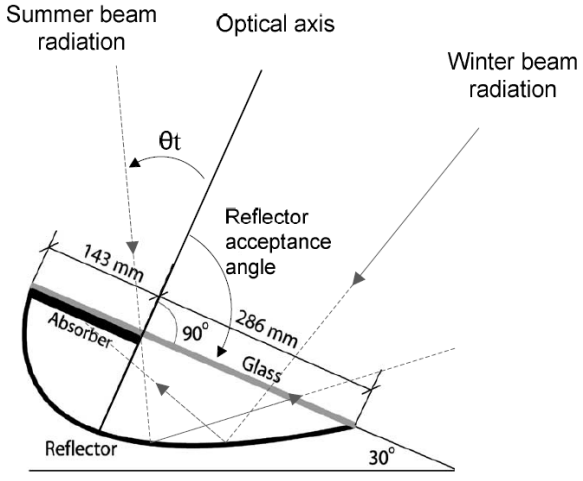

Figure 2.5: The roof-integrated MaReCo collector.

Like the stand-alone collector, the roof-integrated collector is designed according to the specifics of the locality. Figure 2.5 shows a collector designed for Stockholm, Sweden, on a roof with a 30° angle facing south. The Solarus CPC module (described in chapter 3) is based on the roof-integrated MaReCo and dimensioned to be generally applicable to a wide variety of roofs.

Other MaReCo Designs

The MaReCo reference design has also been optimized for integration with east or west facing roofs and in south facing walls. A further special case has been developed for spring and fall of higher latitudes, designed to maximize the solar fraction in a domestic heating system. This is achieved by optimising the angles and extent of the parabola to maximise the production of heat during the spring and fall, when demand is high and solar availability is average.

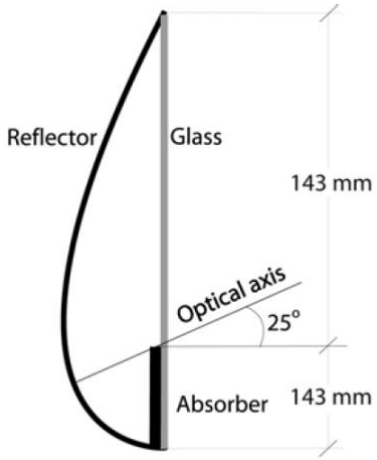

Figure 2.6: Wall integrated MaReCo [20-22].

2.1.4 Concentration Factor (*C*)

Concentration factor represents the ratio of concentrated light to non-concentrated light. The concentration factor depends on whether the concentrating system is a two-dimensional concentrator (linear), such as parabolic trough collector, or a three dimensional concentrator (circular) concentrator, like parabolic dish. The ideal concentration factor for a CPC with an acceptance half angle of $\frac{\theta_c}{2}$ is given by the formula

$$C_{linear} = \frac{1}{\sin\left(\frac{\theta_c}{2}\right)} \tag{2}$$

$$C_{circular} = \frac{1}{\left(\sin\left(\frac{\theta_c}{2}\right)\right)^2} \tag{3}$$

where Θ_c is the acceptance angle of the collector

For roof integrated MaReCo, the acceptance angle is 90^o, so C = 1.414. Equation (2 and 3) is difficult to apply for anisotropic light sources, which have a combination of beam and diffuse light. Therefore, as in L.R. Bernardo et al. [2011], the geometric concentration ratio has been used as it is easy to measure. the concentration ratio is then given by

$$C = \frac{\text{Aperture area}}{\text{Receiver area}} = \frac{d_1}{d_2} \tag{4}$$

where d_1 is the CPC opening length and d_2 is the receiver opening length.

According to the sizes of figure 3.4 (Solarus PVT dimensions), the area concentration ratio of the Solarus PVT collector for the lower part of the receiver is given by

$$C = \frac{\text{Aperture area}}{\text{Receiver area}} = \frac{0.273 \times 2.31}{0.158 \times 2.31} = 1.728$$

or

$$C = \frac{d_1}{d_2} = \frac{0.273m}{0.158m} = 1.728$$

The concentration factor of the studied PVT collector is low. At peak sun, the absorber side with the concentration is exposed to about 1.8 suns, while the upper or flat side has no concentration. This gives an average concentration factor of 1.4 to 1.5 suns for the whole collector.

2.2 Shading of the PVT

The Solarus hybrid concentrating PVT collector has two troughs. Each trough has two sides, the top/front side, similar to a flat plate receiver that receives non-concentrated light, and the back/bottom/concentrated side, which receives concentrated light from the reflector. The concentrated side of the receiver has two strings of cells per trough if the cells are 1/6[4] cell type or one string of 38 solar cells if they are 1/3 cell type. The two strings are identical, each containing 38 solar cells. In case of 1/3 cells there is only one string of solar cells and it is the case considered in this thesis.

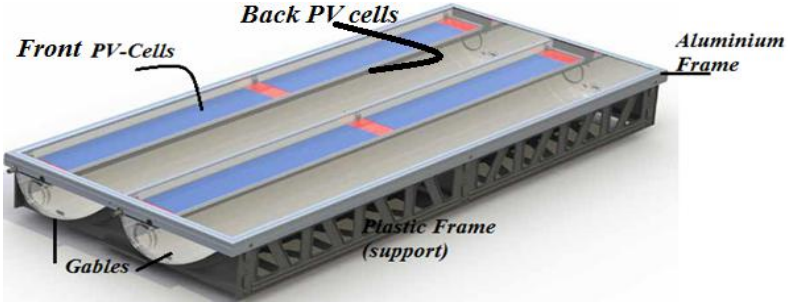

Figure 2.7: Solarus PVT.

At the beginning of the day, the whole concentrated side string does not receive reflected light and the electrical power generated is proportional to the diffuse radiation received. The shade from the frame falls on the reflector and is the main source of shade for the concentrated side of the trough. As the sun rises it starts to unshade progressively the solar cells of the string and the power starts to increase in a similar manner as the increase of global irradiation received. Thus, the power generation increases until all cells of the string are illuminated and produces peak power for a longer period of time. Shading starts again

[4] Standard cell has a size of 156mm×156mm. The cell is cut to 148mm×156mm to fit the receiver and then the longer dimension is cut in to 3 equal solar cells, which are called 1/3 solar cell with a dimension of 52mm×148mm. If these cells are again cut in to two halves they form a cell called 1/6, with dimension 26mm×148mm.

during the afternoon until the whole string is shaded at sunset. It should be referred that in the afternoon the situation is similar but opposite to the one in the morning: it starts to gradually shade the solar cells one by one in a progressive way with a decrease in the power produced. Figure 2.8 illustrates the shading from the frame.

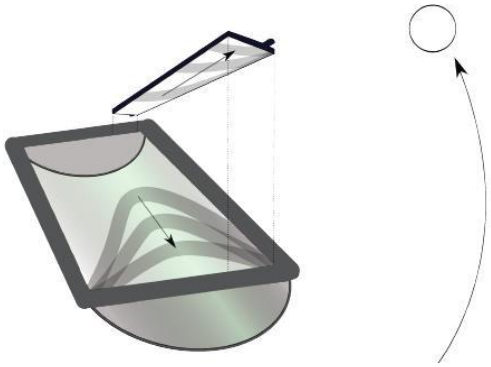

Figure 2.8: Shading from the frame of PVT.

The arrows show the movement of the shade produced by the frame on the reflector trough and on the underside of the receiver, as the sun rises from the horizon to zenith.

Shading has different impact on PV panels and on thermal collectors. In PV modules, the solar cells are often connected in series. This way, one fully shaded solar cell will reduce the output of the whole string to vanish. In industry, this is known as the *Christmas-lights effect*, an obvious reference to the way an entire string of series-strung Christmas tree lights will fail if a single bulb fails. Bypass diodes can be used to mitigate this effect by allowing current to flow in a different path at the expense of a minor fraction of the total power [18]. On the other hand, bypass diodes also prevent hotspots that can destroy PV panels. However, the introduction of diodes increases both assembly time and material cost and may also cause losses due to leakage current.

In thermal collectors, the decrease in power produced due to shading is approximately proportional to the shaded area. Thus, shading clearly has a much bigger impact on PV panels than thermal collectors. Similarly, the effect on PV cell performance is immediate, that is the shade instance and electrical power decrease happens at the same time. In thermal collectors the effect of shading is visible after some time (have some delay).

2.3 Incidence Angle Modifiers (IAM)

The transmittance (τ) of the collector glazing varies with the incidence angle of radiation. Usually the transmittance is highest when the incident radiation is normal to the glazing surface. Test conditions determine the efficiency coefficients for normal incidence. If the angle of incidence is different from normal, the performance varies considerably. This can be explained by angular effects, such as decrease of transmittance in the glazing, decrease of absorption (α) of the receiver at large incidence angles, shading effects caused by collectors frame, etc [18].

For off-normal angles, the transmittance of the glazing is modified by an incidence angle modifier coefficient ($K_{\tau\alpha}$). Thus, the incidence angle modifier constant is the ratio of the efficiency at off normal angles to the efficiency at normal incidence and is given by

$$K_{\tau\alpha} = \frac{\tau\alpha}{(\tau\alpha)_n} \tag{5}$$

where *n* stands for normal incidence.

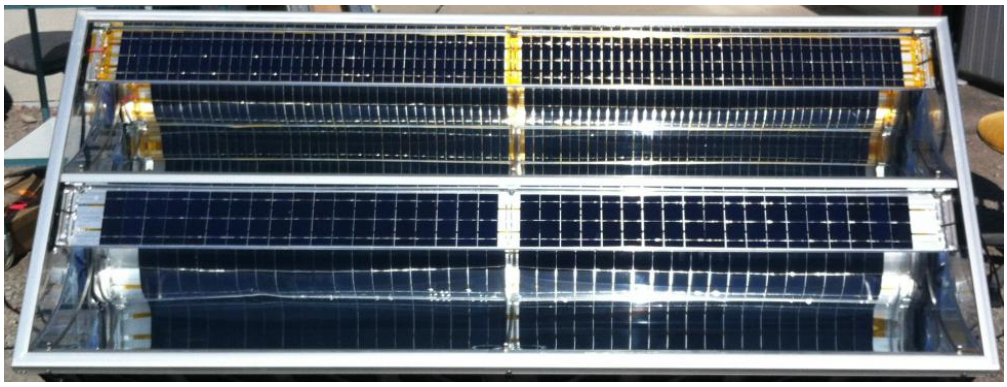

Figure 2.9: Solarus PVT.

The incidence angle modifier coefficient is calculated from experimental data as a function of the incident angle. Commonly, it is given by the following first order function

$$K_{\tau\alpha} = 1 + b_o\left(\frac{1}{\cos(\theta)} - 1\right) \tag{6}$$

The incidence angle modifier coefficient b_o is a constant that is generally negative. Normally b_o ranges from -0.11 to -0.1 for single glazed collector and -0.17 for double glazed collector [24]. Θ is the incidence angle of the ray.

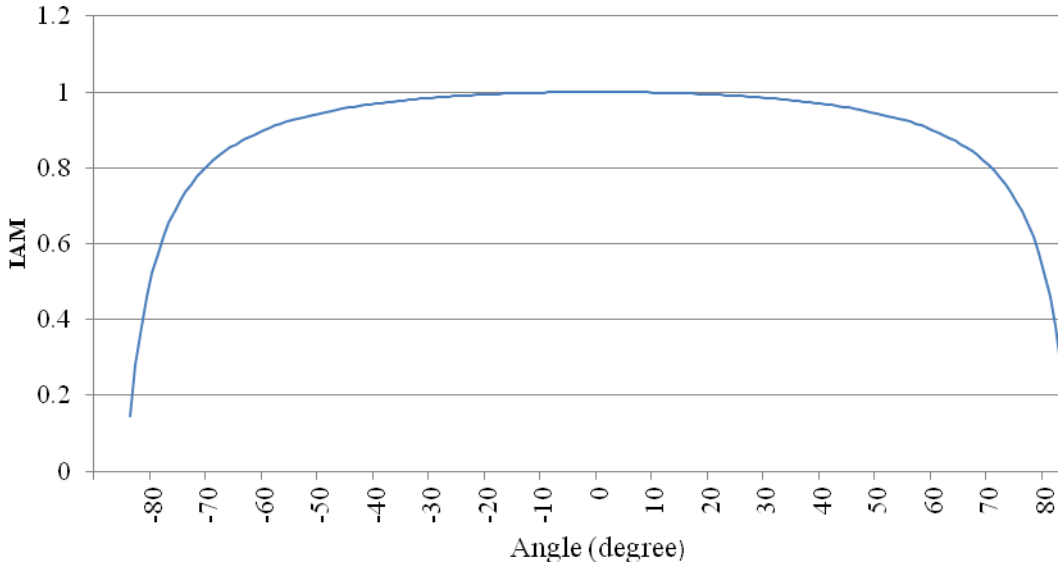

Figure 2.10: Incidence angle modifier (IAM).

The incident angle modifier equation coefficient (equation 6) is only valid for incident angles of 60° or less. For angles greater than 60°, the coefficient is given by,

$$K_{\tau\alpha} = 2\left(1+b_o\right)\cos(\theta) \tag{7}$$

For flat-plate collectors, the incident angle modifier is generally symmetrical. However, for tubular collectors the incident angle modifier is different, depending on whether the incident angle is parallel or perpendicular to the tubes. These are called *bi-axial modifiers*, either longitudinal (parallel to the length) or transversal (perpendicular to length) incidence angle modifiers. The *longitudinal angle of incidence* (Θ_l) is the angle between the collector aperture normal and the incident sun beam projected into the longitudinal plane. The *transversal angle of incidence* (Θ_t) is the angle between the collector aperture normal and the incident sun beam projected into the transversal plane [24].

The *Transverse Incidence Angle Modifier* (IAM_t) is defined by the reduction in electrical efficiency for a given irradiation caused by the increase of the incidence angle between the sun and the normal to the collector in the transverse direction (Θ_t)**.** This is shown in figure 2.11A. From 0 to $+90^o$, the sun's direct beam direction is inside the acceptance angle of the reflector, and outside from 0 to -90^o. IAM measurements are a combination of all angular effects, such as the decrease of transmission in the glazing for high incidence angles and the shading effects from the frame of the collector.

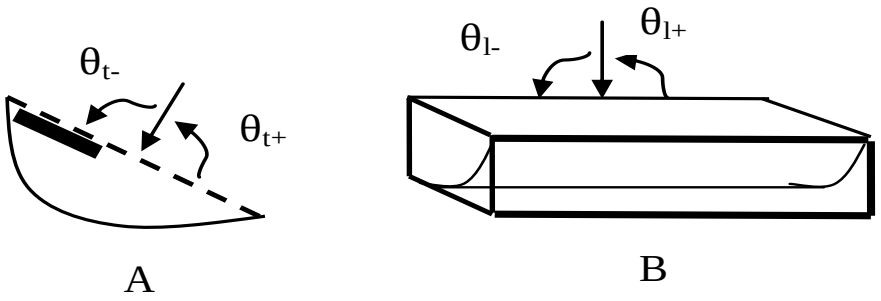

Figure 2.11: Transversal incidence angle (A) and longitudinal incidence angle (B).

To be able to measure IAM_t for different transverse angles, the longitudinal angle had to be kept equal to zero. This was measured by facing the collector towards the solar azimuth for various tilt angles [26]. The IAM_l is calculated similarly by keeping transversal angle at zero.

The IAM is only applied for the direct beam. But normally, even during clear days, there is a percentage of diffuse light that contributes towards electricity production from PV cells. The equations used to calculate the longitudinal and transversal angle modifiers is the same equation as referred above, replacing the angle by Θ_l for longitudinal and by Θ_t for transversal incidence angle modifier. The overall incidence angle modifier is given by the product of the longitudinal and transversal incidence angle modifiers, $K_{\theta l}$ and $K_{\theta t}$, respectively

$$K_{\tau\alpha} = K_{\theta l} \times K_{\theta t} \tag{8}$$

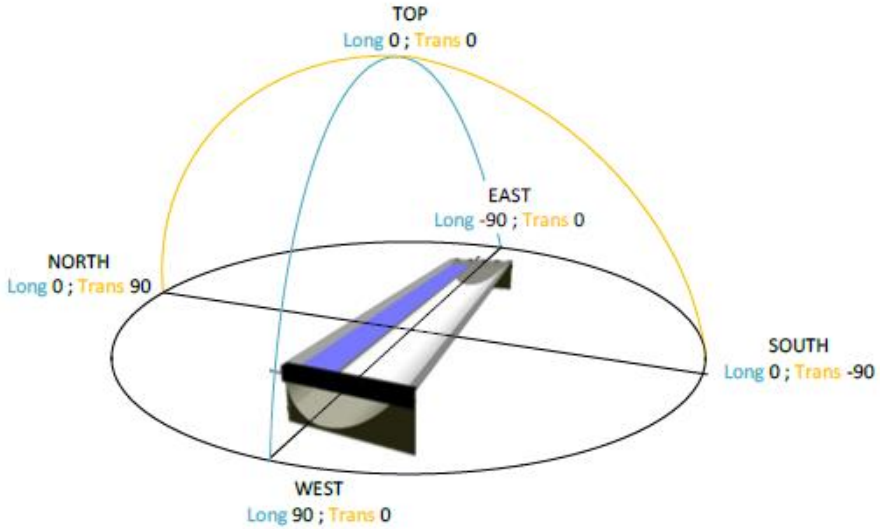

Figure 2.12: Representation of the longitudinal and transversal directions.

The incidence angle modifier can also be calculated for all types of rays separately, i.e. for beam (G_{beam}), reflected (G_{ref}) and diffused (G_{diff}) and then can be calculated as net incidence angle modifier as a weighted average of all.

$$K_{\tau\alpha,\text{net}} = \frac{G_{\text{beam}} \cdot K_{\tau\alpha,\text{beam}} + G_{\text{diff}} \cdot K_{\tau\alpha,\text{diff}} + G_{\text{ref}} \cdot K_{\tau\alpha,\text{ref}}}{G_{\text{beam}} + G_{\text{diff}} + G_{\text{ref}}} \tag{9}$$

Diffused and reflected light incidence angle is not easy to measure. So, for these radiations, the incident angle is approximated by using Brandemuehl and Beckman's equations given, respectively, by

$$\theta_{\text{dif}} = 59.68 - 0.1388\phi + 0.001497\phi^2 \tag{10}$$

$$\theta_{\text{ref}} = 90 - 0.5788\phi + 0.002693\phi^2 \tag{11}$$

where Φ is the tilt angle of the collector in degrees, Θ_{diff} is the angle for diffused light and Θ_{ref} is the angle for reflected light.

The variation in IAM can also be studied in a different way, by the position of the sun with respect to the earth. Due to the rotation of the earth along its axis, a change in the angle of incidence of beam radiation is seen. For a specific location on Earth, the sun appears to move from east to west. The position of the sun depends on the location of a point on Earth, the time of the day and time of year. The sun light is defined by the sun position, i.e. the elevation and the azimuth. These two parameters can also be calculated as a function of the day, the hour, the latitude and the longitude.

i. *Latitude* is the angular distance of a location north or south of the equator. North latitudes are positive while south latitudes are negative.
ii. *Hour Angle* (HRA) is a measure from local noon, being positive in the morning and negative in the afternoon. One hour of time is represented by 360/24 =15 degrees of hour angle.
iii. *Declination Angle* δ (figure 2.13) is the angular distance of a sun's ray north or south of the equator. It is the angle between a line extending from the centre of the sun to the

centre of earth and the projection of this line upon the earth's equatorial plane. Declination angle is positive when the sun is in the north of the equator and negative when it is in the south of the equator. Declination angle exists due to the tilt of the earth on its rotation. The declination angle throughout a year can be approximated by a sine function and is always in the range $-23.45 \le \delta \le +23.45$,

$$\delta = 23.45 \times \sin\left[\frac{360}{365}(284 + D)\right] \tag{12}$$

where D is the day of the year, starting at 1 in January 1st.

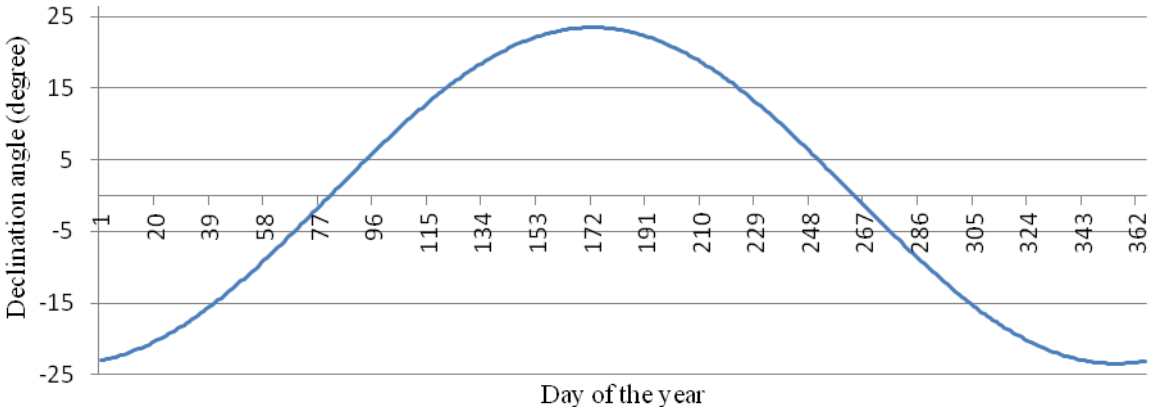

Figure 2.13: Declination angle variation throughout the year.

The net *Time Correction Factor* (TC), expressed in minutes, accounts for the variation of the *Local Solar Time* (LST) within a given time zone due to the longitude variations within the time zone and also incorporates the *Equation of Time* (EoT),

$$\text{TC} = 4(\text{Longitude-LSTM}) + \text{EoT} \tag{13}$$

where, the *Local Standard Time Meridian* (LSTM) is a reference meridian used for a particular time zone and is similar to the Prime Meridian, which is used for Greenwich Mean Time.

The LSTM in degree is calculated according to the equation

$$\text{LSTM} = 15^{\circ}\left(\Delta T_{GMT}\right) \tag{14}$$

where ΔT_{GMT} is the difference between Local Time (LT) and GMT in hours.

The factor of 4 minutes comes from the fact that the Earth rotates 1° every 4 minutes. Finally, EoT (figure 2.14), expressed in minutes, is calculated by

$$\text{EoT} = 60\{0.165\sin(2B) - 0.126\cos(B) - 0.025\sin(B)\} \tag{15}$$

where B, in degrees, is given by

$$B = \left[\frac{360}{364}(D - 81)\right] \tag{16}$$

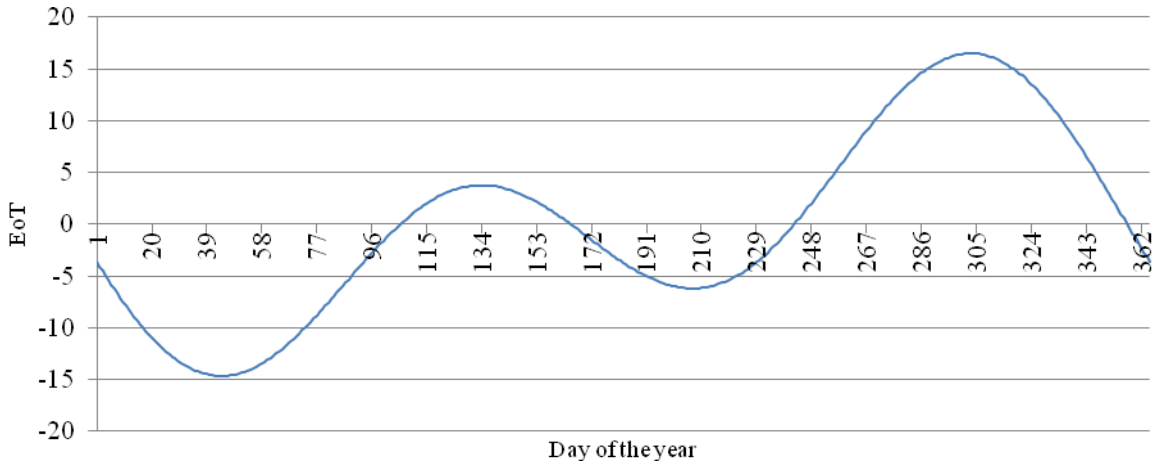

Figure 2.14: Equation of time variation throughout the year.

The *Local Solar Time* (LST) can be found by using the previous two corrections to adjust the local time (LT)

$$\text{LST} = \text{LT} + \frac{\text{TC}}{60} \tag{17}$$

The Hour Angle (HRA) converts LST into the number of degrees the sun moves across the sky. Once LST is established, HRA can be determined. Hour angle varies at the rate of 15 degrees per hour. At solar noon, HRA=0, negative before solar noon and positive after solar noon. Solar angle, expressed in degrees, is given by

$$\text{HRA} = 15^{\circ}(\text{LST}-12) \tag{18}$$

In addition to latitude, hour angle and sun's declination, there are other angles useful in solar radiation calculations. Some of the angles are sun's zenith angle, altitude angle and azimuth angle.

3. Solarus PVT Collectors

3.1 General Description

Solarus PVT Collector (figure 3.1) is a compound parabolic collector (CPC).The receiver is placed in one side of the concentration trough instead of in the centre, as in symmetric collectors. The receiver is a bi-facial PV pasted in a thermal absorber with pipes in the absorber. The solar radiation is concentrated onto thermal absorber from an aluminium reflector. A highly transparent and electrically insulating silicone is used to laminate the PV cells to the thermal absorber on both the upper and lower sides of the absorber. The upper side works like a standard PV module without concentration, while the lower side receives the concentrated solar radiation from the compound reflector (parabolic and circular).

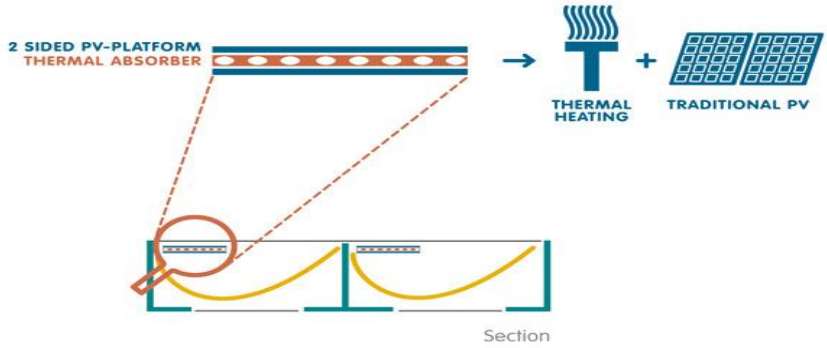

Figure 3.1: Solarus PVT collector (side view) [4].

The Solarus PVT collector is shown in figure 2.7. The collector has glazed protection made from low iron content glass for high transmittance. The supporting structure is made of plastic and metal [26]. The sides of the collector are made of transparent end gables. This type of collectors operates without tracking the sun, which represents an obvious advantage, as it makes less complex their mechanical issues and, simultaneously, minimizes the difficulties associated with multi-element systems. However, to maximize their output, they have to be properly oriented for global irradiance (sun).

The concentration factor of the studied PVT collector is low. At peak sun light the concentrated side receives approximately 1.8 suns while the flat side receives 1 sun. Thus the average concentration for the whole hybrid concentrating PVT is 1.4 suns [23]. Though the concentration factor of the PVT collector is low, the PV cells can still reach high temperatures. Since mono-crystalline solar cells exhibit a reduction in power output at elevated temperatures, cooling is needed to maintain the electrical efficiency. Cooling is accomplished by running a fluid (normally water, with antifreeze in cold climate) through the channels of the thermal absorber. Thus the PVT collector produces electricity and heat from the same area. In northern hemisphere, the solar radiation is high in the summer and low in the winter, while the domestic hot water demand is almost constant throughout the year. So, in winter there may be a need of auxiliary hot water source and an overproduction in the summer. Therefore, the design of the collector area should be in such a way that the summer production is without overproduction in order to increase the annual solar fraction contribution of energy. This can be accomplished by designing the collector with an optimal

tilt, collector area and flow rate. The optical axis for the reflector geometry is normal to the glass of the collector, which defines the acceptance angles for an effective radiation. If the radiation falls outside this angle, the reflector does not redirect the incoming beam radiation to the lower side of the absorber and the optical efficiency of the collector is greatly reduced [27].

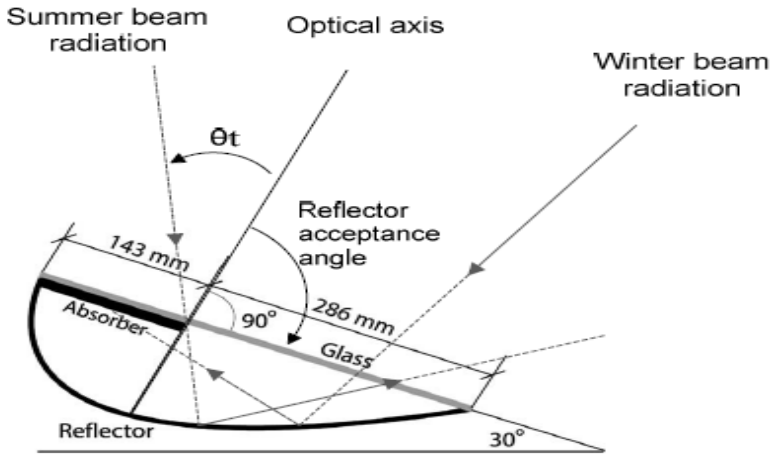

Figure 3.2: Cross section of CPC collector.

The collector's optical efficiency changes throughout the year depending on the projected solar altitude. The tilt determines the amount of total annual irradiation kept within the acceptance angle interval [25, 33]. As a result, by varying the tilt, it is possible to increase the effective collector area without causing overproduction in the summer when the collector has lower optical efficiency. The acceptance angle for roof integrated is given by (90^o-Θ_t), or 60^o, as it is shown in figure 3.2.

3.2 Solarus Receiver (Trough)

Figure 3.3 shows the collector plan view. The PVT collector has two troughs. The water connections for extracting the heat are represented in blue and the electrical arrangements of the solar cells are shown in red.

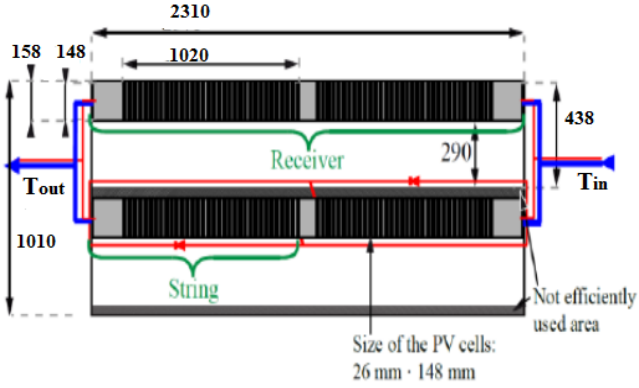

Figure 3.3: Top view of Solarus CPC [18] (all dimensions are in mm).

Since both troughs are similar, most tests need only the investigation of a single trough. The lower part of the receiver, i.e. the part that receives concentrated light, has exactly the same hydraulic arrangement and similar electrical configuration as the upper, except the

number of bypass diode connected. The electrical part of each PVT collector consists of strings of PV cells, each one with 38 series-connected cells of 1/6 type. The total number of PV cells is 152 cells per trough. The concentrated side of the trough has two strings of solar cells each with 38 cells of 1/6 type. In this thesis work the test is carried for a single string with four bypass diodes in the string of 38 cells of 1/3 type.

Solarus uses solar cells from Big Sun Energy with a physical size of 156mm×156mm and thickness of nearly 200µm monocrystalline cells with an efficiency of 18.6%. The cells are first cut in to 148mm×156mm to fit the width of the absorber. Concentration of irradiation on the collector may cause current capacity losses. Thus, the solar cells are cut in to three or six cells. One trough has cells one third (1/3) of the standard cell size (52mm×148mm) and the other trough has cells one sixth (1/6) of the size of a standard cell (26mm×148mm). The objective is to increase the voltage and to reduce the current at high irradiation levels and thus decreasing the current capability constraints due to increased concentration.

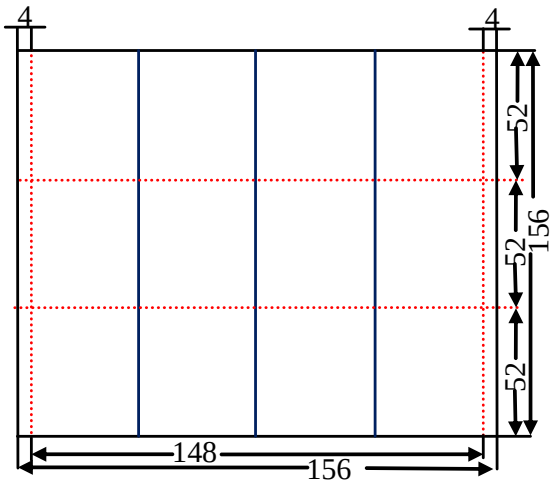

Figure 3.4: 1/3 cell size and cutting (all dimensions in mm).

Solar cells are laminated in both sides of the thermal absorber, which is electrically insulating. This thermal absorber acts as a support for the PV cells and as a heat sink. Eight elliptical pipes/channels for passage of heat transport fluid (water, water + antifreeze) pass through the absorber to extract heat from the solar cells.

The total area of PV cells on a receiver is approximately 0.58 m² and the active glazed area[5] is approximately 0.87 m² per receiver. T_{in} and T_{out} represent the temperature reading of the sensors placed at the inlet and outlet of the water running inside the collector, respectively. The temperature of water at the middle of the receiver (T_{mid}) is taken as the average of T_{in} and T_{out}.

Procedures regarding performance testing of solar collectors are defined and published by standard institutions. There is no standard detailing for the procedures to be adopted for simultaneous electrical and thermal performance testing of PVT collectors. According to the

[5] Active glazed area is defined as the glazed area where the incident radiation can contribute to electricity production, i.e. the area on top of the cells and the area on top of the reflector in front of the cells, excluding edges, spaces between cells and parts where there was no reflector [20]

collector model proposed in ASHRAE[6] [28], the electric (P_{el} in W) and thermal (P_{th} in KWh) powers respectively are given by:

$$P_{el} = G\eta_{el} \tag{19}$$

$$P_{th} = G\eta_{th} - U_1\Delta T - U_2\left(\Delta T\right)^2 \tag{20}$$

where $\Delta T=T_{mid}-T_a$, T_a is the ambient temperature, G is the global solar irradiance[7], η_{el} is the PV electrical efficiency, η_{th} is the thermal efficiency, U_1 and U_2 are heat loss coefficients.

In this model, only the main factors are taken in consideration. In reality, there are more factors to be considered, such as the increase of the temperature of the solar cells due to the solar radiation, which will lead to a decrease in solar cell efficiency by increasing contact losses. The increase in contact resistance due to irradiation is not easy to be represented in the mathematical model, but can be estimated by series experimental tests. Power generated by solar cells decreases with temperature, following a coefficient of around 0.34%/ºK for mono crystalline solar cells.

3.3 Applications

The hybrid PVT produces both electricity and heat from the same area. It is called hybrid due to simultaneous generation of electrical energy and thermal energy. Some of the applications are presented in the figure 3.5.

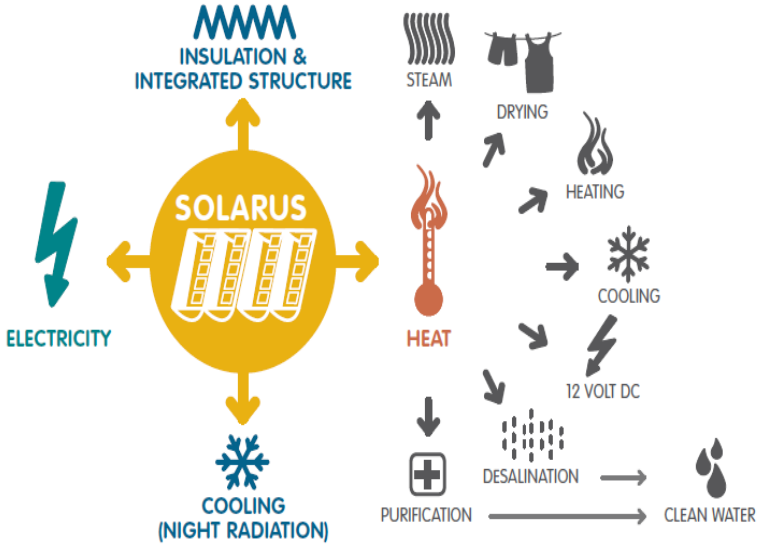

Figure 3.5: Hybrid PVT applications [4].

3.4 Nomination of Solar Cell String Configurations

The evaluation of hybrid Solarus PVT Collector has two components, namely electrical and thermal. The thermal part was previously evaluated in [29]. The front side of the receiver

[6] *ASHRAE* was founded in 1894. It writes standards for the purpose of establishing consensus. These are developed and published to define minimum values or acceptable performance.

[7] *Irradiance* is the power of electromagnetic radiation per unit area (radiative flux) incident on a surface. The SI unit for irradiance is watt per square meter (W/m2).

is only slightly affected by shading from the frame of the receiver; hence the shading effect is omitted for the front side. Shading and non-uniform illumination due to concentration is more pronounced on the concentrated side of the PVT solar cells. So, this thesis work is evaluating possible cell string layout for better performance in terms of the electrical output generated from the PVT. There are 38 cells in a string grouped in to 4 groups, each group bridged by (in parallel with) a single bypass diode. Hereafter, the following nomination is used in this thesis work

- **3-16-16-3:** The solar cell string layout is represented in figure 3.6. The cells are arranged as shown, where the first bypass diode is in parallel to three (3) solar cells, second bypass diode in parallel with sixteen (16) solar cells, third bypass diode in parallel with sixteen (16) cells and the fourth bypass diode with three (3) solar cells.

Figure 3.6: 3-16-16-3 string of solar cells.

- **4-15-15-4:** The solar cell string layout is is shown in figure 3.7. The cells are arranged as follows: the first bypass diode is in parallel to four (4) solar cells, the second bypass diode is in parallel with fifteen (15) solar cells, the third bypass diode is in parallel with fifteen (15) cells and the fourth bypass diode with four (4) solar cells.

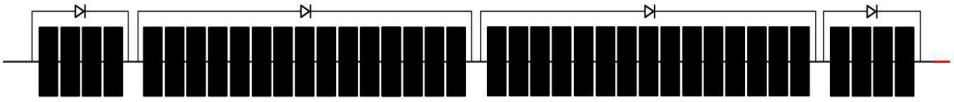

Figure 3.7: 4-15-15-4 string of solar cells.

- **5-14-14-5:** The solar cell string layout is is represented in figure 3.8. The cells are arranged as shown, where the first bypass diode is in parallel to five (5) solar cells, the second bypass diode in parallel with fourteen (14) solar cells, the third bypass diode in parallel with fourteen (14) cells and the fourth bypass diode with five (5) solar cells.

Figure 3.8: 5-14-14-5 string of solar cells.

4. Theoretical Analysis

4.1 PSPICE

SPICE (***S**imulated **P**rogram for **I**ntegrated **C**ircuit **E**mphasis*) is a general purpose open source software that simulates different circuits and can perform various analysis of electrical and electronic circuits, including time domain response, small signal frequency response, total power dissipation, determination of nodal voltages and branch current in a circuit, transient analysis, determination of operating point of transistors, determinations of transfer functions, etc. This software is designed in such a way, so that it can simulate different circuit operations involving transistors, operational amplifiers (Op-Amp), etc. It contains models for circuit passive and active elements.

4.2 PV cell model

Photovoltaic energy is highly dependent on the environmental conditions, such as temperature and solar irradiation. The optimization of the energy conversion system is not a trivial problem. Solar cell modelling represents a current task [1].

The analytical method to model the behaviour, the load current *I* and terminal voltage *V* of a solar photovoltaic cell is based on the use of the equivalent circuit for a photodiode. There are two model types for a solar cell. The *single diode* model and *two diode* model equivalent circuit approximation. The single diode model is widely used and the results obtained are generally acceptable [25]. For an ideal model, a PV device can be simply modelled by a *p-n* junction in parallel with a current source (I_{PV}) that is associated to the photo generated carriers (Figure 4.1a). A more accurate model would take into account the influence of contact and the leakage, using series R_s and parallel R_p resistors, respectively (Figure 4.1b).

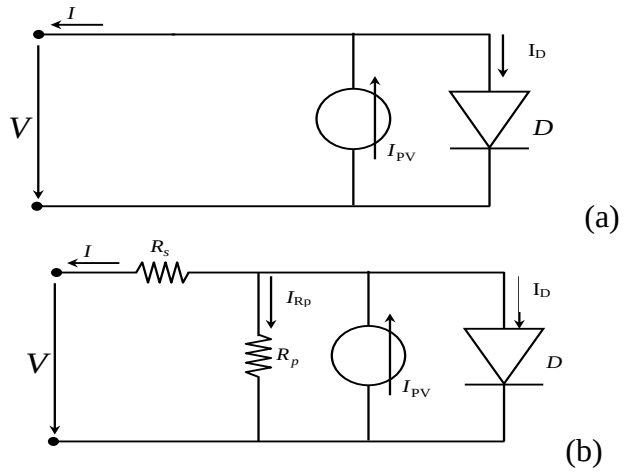

Figure 4.1: Single diode model of solar cell.
a) Ideal PV cell model; (b) Real PV cell model.

For an ideal PV cell:

$$I_{pv} = I_D + I \tag{21}$$

$$I_D = I_s \left\{ \exp\left(\frac{qV}{nKT} \right) - 1 \right\} \tag{22}$$

$$I = I_{pv} - I_s \left\{ \exp\left(\frac{qV}{nKT} \right) - 1 \right\} \tag{23}$$

$$I_{pv} = \left(C_o + C_1 \Delta T \right) G \tag{24}$$

Figure 4.2 shows the stationary $I(V)$ characteristic for a typical PV cell under illumination associated to different irradiance levels G. It corresponds to the graphic representation of equations (23) and (24). The shaded area corresponds to the PV region.

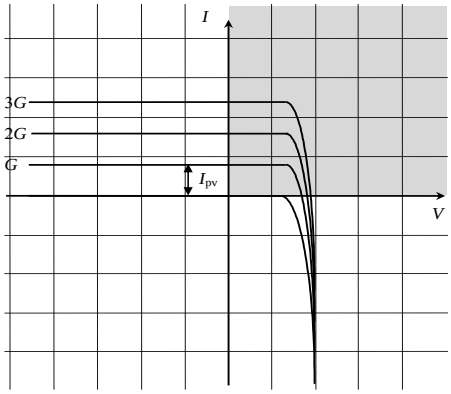

Figure 4.2: Stationary $I(V,G)$ characteristic
of a PV cell under different illumination levels..

For a real PV cell, taking the effects of contact resistance and leakage resistance, the above equations are modified to the following

$$I_{pv} = I + I_D + I_{Rp} \tag{25}$$

$$I_D = I_s \left\{ \exp\left(\frac{q(V + IR_s)}{nKT} \right) - 1 \right\} \tag{26}$$

$$I_{Rp} = \frac{V + IR_s}{R_p} \tag{27}$$

$$I = I_{pv} - I_S \left\{ \exp\left(\frac{q\left(V + IR_S\right)}{nKT} \right) - 1 \right\} - \left(\frac{V + IR_S}{R_p} \right) \tag{28}$$

$$I_{pv} = \left(C_o + C_1 \Delta T \right) G \tag{29}$$

where, I represents the current through, V is the voltage across the load, I_{PV} is the light generated current, I_s is the diode leakage current in the absence of light, n is the ideality factor of the diode, q is the absolute value of the electronic charge, K is the Boltzmann constant, T is the absolute temperature, ΔT is the deviation of temperature from 25ºC, R_s is the cell series resistance associated with the contact losses, R_{sh} is the shunt resistance related to the leakage current of the device, C_o is a constant which depends on the solar cell area and characteristics, C_1 is the current dependence on temperature and G is global irradiance.

$$G = G_{\text{beam}} \cos(\theta) + G_{\text{diff}} \tag{30}$$

where, G_{diff} is the diffuse radiation, G_{beam} is the beam radiation and the angle θ is the angle made by direction of beam with the normal (noon), assuming reflected light as zero.

For a given irradiance and *p-n* junction temperature conditions, the presence of series resistance in the model implies the use of a recurrent equation to determine the output current as a function of the terminal voltage. MATLAB or circuit simulators can be employed to determine the *short circuit current*, (i.e., the current that flows when V=0V). From equation (28) by setting V=0,

$$I_{sc} = I_{pv} - I_s \left\{ \exp\left(\frac{q(I_{sc}R_s)}{nKT} \right) - 1 \right\} - \left(\frac{I_{sc}R_s}{R_p} \right) \tag{31}$$

Normally $R_P >> R_S$. Therefore, the last term in (24) can be neglected and the short circuit current can be approximated by

$$I_{sc} \approx I_{pv} - I_s \left\{ \exp\left(\frac{q(I_{sc}R_s)}{nKT} \right) - 1 \right\} \tag{32}$$

In the ideal PV cell model R_s=0 and, obviously, I_{sc}=I_{pv}.

The open circuit voltage V_{oc} is the voltage across the diode when the load current, I =0A. Substituting I = 0 in equation (28),

$$0 = I_{pv} - I_s \left\{ \exp\left(\frac{q(V_{oc})}{nKT} \right) - 1 \right\} - \left(\frac{V_{oc}}{R_p} \right) \tag{33}$$

The leakage resistance R_p is large and, as a result, the last term in equation 26 can be neglected. Hence, the open circuit voltage V_{oc} is approximated by

$$V_{oc} \approx \frac{nKT}{q} \ln\left(\frac{I_{pv}}{I_s} + 1 \right) \tag{34}$$

According to the power convention, the power related with the diode is P = - $V \times I$. In the PV quadrant of the characteristic, shown in figure 4.2, this value is negative, meaning that this power is delivered by the solar cell. It is given by

$$P = V \left\{ I_{\text{PV}} - I_S \left(\exp\left(\frac{q(V + IR_s)}{nKT} \right) - 1 \right) - \frac{V + IR_s}{R_p} \right\} \tag{35}$$

The expression of electrical power output at peak power (P_{mp}) is given by

$$P_{mp} = I_{mp} \times V_{mp} \tag{36}$$

where, V_{mp} and I_{mp} are the voltage and current at MPP, respectively.

Fill Factor (*FF*)

Fill factor describes how close the *I-V* characteristic of solar cell is to the ideal characteristics. Normally, it is expressed as percentage.

$$FF = \frac{I_{mp} \times V_{mp}}{I_{sc} \times V_{oc}} \tag{37}$$

Efficiency (η)

Solar cell electrical efficiency is given by

$$\eta_{el} = \frac{I_{mp} \times V_{mp}}{G \times A_{cell} \times N} \tag{38}$$

where A_{cell} is cell area, N number of solar cells and G is the global solar irradiance.

Power losses exists due to the series and shunt resistors and are given by

$$P_{Rs} = R_s \times I_{mp}^2 \tag{39}$$

$$P_{Rp} = \frac{\left(V_{mp} + I_{mp} R_s\right)^2}{R_p} \tag{40}$$

where P_{Rs} and P_{Rp} are power losses due to series and shunt resistances, respectively [30].

Figure 4.3 shows the stationary characteristics *I-V* and *P-V* for a module of 38 solar cells connected in series for G=1000W/m^2.

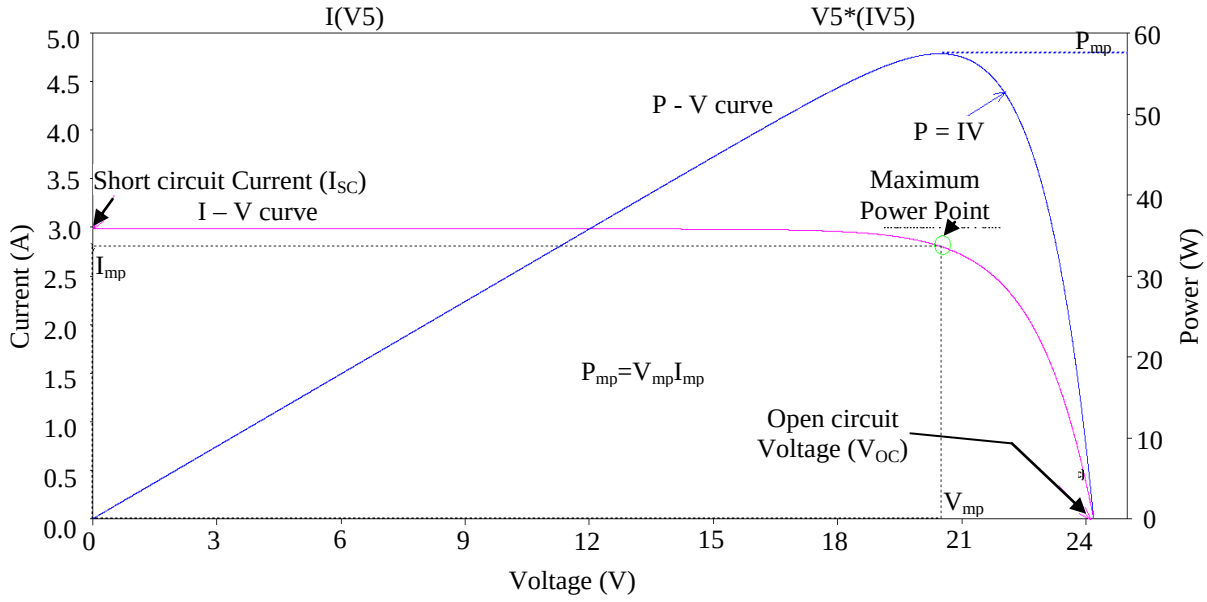

Figure 4.3: *I-V* and *P-V* curves of a photovoltaic module of 38 solar cells.

4.3 Shading in solar cells

The power generated by photovoltaic cells depends on many factors. Some of them include, but are not limited, to solar irradiance, solar cell active area, solar cell short circuit, current density at standard test conditions (STC) and its conversion efficiency, temperature, etc. In a string of cells, the power reduction may be attributed to shading, mismatch effects, etc [30-32]. Mismatch can be current or voltage mismatch. Current mismatch exists in series connected PV cells when the cells are not uniformly illuminated. In this case, the current that flows through the string of solar cells will be limited by the PV cell that generates lowest current. For parallel connected cells, the voltage across them should be equal or at least close to each other, unless a voltage mismatch is created.

Partial shading greatly reduces the electrical energy generated from solar cells connected in series. The decrease in power is not directly proportional to the shaded area of the cell. The current in a series connected cell should be the same. If some of the cells are

partially shaded while others are illuminated, the current of the string will be limited by the worst performing cell, thus limiting the power generated by the string of cells. As per study carried in [26], the indoor solar laboratory tests showed that shading a cell parallel or perpendicular to the cell bus bar had a similar impact in terms of power reduction. In terms of shading, for example when 25% of a single solar cell is covered, the power decrease is higher for the whole string than for a single cell. It is interesting to notice that 75% shading in a string or 75% shading of one single solar cell have similar consequences, that is, they resulted in a similar decrease in power. As expected, shading one whole cell or string yields to an almost vanishing of the power output. The cell with shade will be reverse biased and dissipates power in the form of heat instead of generating. In addition to reducing the power, it may also create *hot spots* on the shaded cell. If the power dissipated by the solar cell in hot spot conditions exceeds the maximum power that can be sustained by the cell, it will be permanently damaged: an open circuit appears in the string. To prevent hotspot formation during partial shading conditions, manufacturers of solar PV panels include bypass diodes (figure 4.4).

The PV array design and the adequate configurations of bypass diodes used on the PV module forming part of the array have an important role in reducing the possibility of forming hot spots due to partial shading.

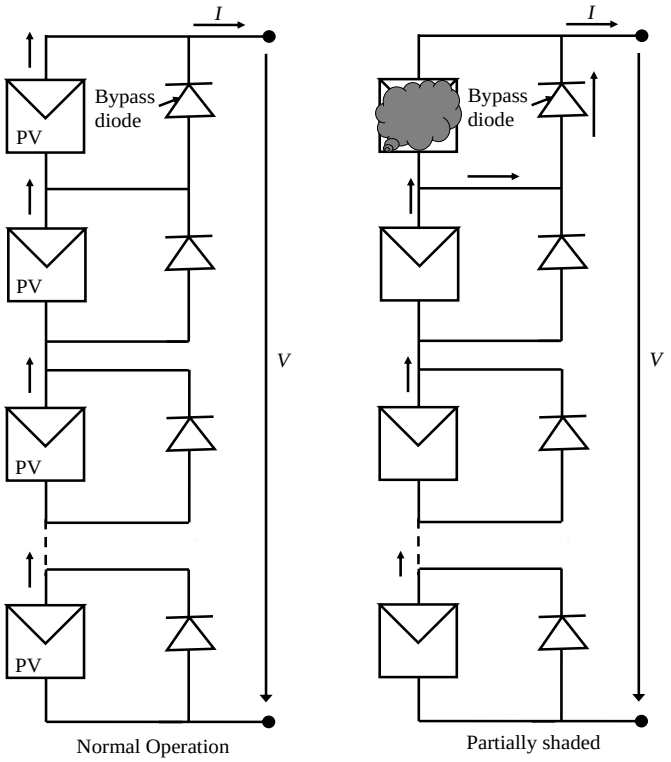

Figure 4.4: String of cells with bypass diode.

Shading can be classified as *hard* and *soft* shade. Hard shade occurs when a solid object is placed in front of the array, blocking the sunlight in a clear and definable shape. Soft shade occurs when the overall intensity of the light is reduced, such as haze or smog in the atmosphere above. It is important to note the difference in shading types, because each causes a different effect on a PV array. Hard shade reduces the current generated by the PV to zero.

In case of soft shade the current generated is directly proportional to the irradiation, so it reduces the current proportionally. The open circuit voltage is proportional to the short circuit current (and hence, to the irradiance) in a logarithmic scale. Therefore, it should be lightly affected by soft shade. The voltage across a PV cell depends more on temperature and on the electron band-gap of the semiconductor materials used in the solar cell than on the light itself.

PV systems with the same nominal power generate with quite different energy yields due to different shading patterns. The typical problems are:

i. Reduction of power generated: the irradiation level is reduced due to shading, decreasing the photo current. For series connected solar cells, the current of the string is reduced.
ii. Thermal stress on the module: depending on the level of shading, number of solar cells in the string and the load, the voltage of shaded cells may be reverse biased and reach its reverse breakdown voltage.

If shaded, solar cells may operate in the blocking state as a resistive load. The losses in the individual cell can increase the cell temperature dramatically and overheating may occur. Inhomogenities of the cell current density may result in hot spots, local defects due to high temperatures. In order to overcome some of the problems related to shading, by-pass-diodes are connected in parallel to a number of solar cells. Under normal operating conditions, the diodes are blocked. When shading occurs, the voltage in that specific section can be reversed, activating the bypass diode in parallel with shaded cells. The main consequences are:

i. The current of the unshaded section flows through the bypass diode and the *P*-*V* characteristics shows a second local maximum.
ii. The power is only generated by the unshaded solar cells of the bridged group associated to the same bypass diode.

If the number of solar cells bridged by a by-pass diode is small, the level of breakdown voltage will not be reached. This reduces the possibility of hot spot formation, but introduces some limitations, namely

i. Higher cost for the module production and assembly problems associated to the by-pass diodes.
ii. Additional losses in the by-pass diode in case of shading.

The number of bypass diodes per string should be carefully calculated in order to prevent damage (figure 4.5).

For a fully illuminated string of cells, the current/voltage generated by individual cells is nearly equal.Non-uniformly illuminated solar cells, generate different currents and voltages and, hence, create mismatch.

$$V_{bypass} = -M \times V_{cell} \tag{41}$$

where M is the number of solar cells in parallel to single bypass diode, V_{cell} is the illuminated PV cell voltage and V_{bypass} is voltage across the bypass diode.

In the presence of shading, the shaded cell generates low current/voltage and becomes reverse biased by the illuminated cells. As a consequence the bypass diode becomes forward biased and provides a bypass path for the current generated from other strings. The voltage drop across the bypass diode becomes the forward voltage drop (V_{F}) of a forward biased

diode, which is normally 0.5 to 0.7V in silicon diodes. To minimize power losses during shading, the bypass diode must have low forward voltage drop.

The forward voltage drop in the bypass diode is the difference between shaded and illuminated cells voltages. Assuming only one solar cell is shaded

$$V_F = V_{sh} - (M-1)V_{cell} \tag{42}$$

where V_{sh} shaded cell voltage.

The maximum number of solar cells to be bridged by a single bypass diode is determined by the reverse breakdown voltage V_c of the solar cells in the string. Typical values for reverse breakdown voltage are between -12V and -20V, for poly-silicon, and -30V, for mono-crystalline solar cells.

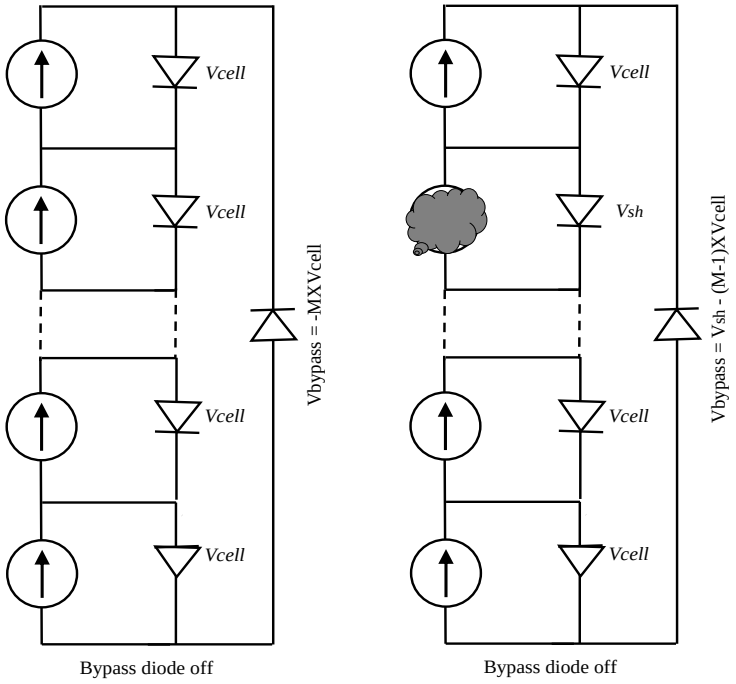

Figure 4.5: Number of solar cells bridged by bypass diode.

For an efficient operation, two conditions need to be fulfilled

1. The bypass diode has to conduct when at least one cell is shadowed.
2. The shaded cell voltage (V_{sh}) must be lower in modulus than the modulus of the reverse breakdown voltage (V_c).

Using the two previous conditions, the maximum number M of solar cells to be bridged by a single bypass diode can be calculated.

$$\begin{aligned} V_{bypass} &= V_{sh} - (M-1)V_{cell} \\ V_{sh} &\le V_c \\ V_{bypass} + (M-1)V_{cell} &\le V_c \end{aligned} \tag{43}$$

During shading the bypass diode is forward biased and the voltage across it is V_F.

$$M \le \frac{V_c - V_F}{V_{cell}} + 1 \tag{44}$$

Assuming V_F=0.5V, V_{cell} = 0.636V and V_c=15V, then $M \leq 24$. Normally, a safety margin is included, in order that the reverse voltage should not be greater than 80% of V_c. So, the number of cells reduces to

$$M \leq \frac{0.8 \times V_c - V_F}{V_{cell}} + 1 \tag{45}$$

$$M \leq 19$$

The solar cells used by Solarus are mono-crystalline solar cells with reverse breakdown voltage V_c =30V. Therefore, the number of cells bridged by a bypass diode may be higher.

Temperature effects must also be considered to estimate the number of bypass diodes to be included in the PV module. Under bad conditions, the temperature of the shaded cell increases, causing irreversible damages of the cell or its encapsulation [32]. Dissipated power by the shaded cell is given by

$$P_{dis} = V_{sh} \times I_{sh} \tag{46}$$

where I_{sh} is the current that flows through the shaded cell.

Power dissipated by the shaded cells is calculated by observing the maximum negative voltage appearing across the shaded cells multiplied by the current that flows through the shaded cell. Power dissipation in the shaded solar cell may be substantial, leading to an increase in its temperature. Due to this fact, the current gets concentrated in an increasingly small region of the cell, producing hot spot. This may damage the solar cell permanently.

Solarus PVT have a string of cells with bypass diodes. The number of bypass diodes on the concentrated side string is 4, for a string of 38 solar cells. They are not uniformly distributed by the solar cells. The number of solar cells bridged by each bypass diode should be in such a way that the generated power is affected as low as possible. The choice of the more adequate configuration represents in fact the main goal of this work.

In Solarus hybrid PVT, the concentrated side of the trough has 38 solar cells with 1/3 of the standard solar cell. The frame of the trough creates shadow on the reflector and, hence, on the solar cells. For example, if one solar cell is fully shaded and the others are illuminated, the current through the string will be practically zero. To mitigate this effect, diodes are employed to bypass the shaded cell and, as a result, there will be a minor reduction in power generated from the string of cells. In case of non-uniform illumination, the use of bypass diodes in cell strings introduces multiple steps in the *I-V* curve and new local (multiple) peak power points in the *P-V* curve. In this thesis work, different type of solar cells bypass diode arrangements are simulated for different shading levels for the same number (38) of solar cells of a single string. The configuration of bypass diodes in cell string layout of the Solarus PVT has a deep influence on the probability and severity of hot spot formation in any one of the solar cells of the string. The presented model and simulation procedure can help to a better understanding of the PV strings behaviour as function of the configuration of bypass diodes included in the design [32]. The 38 cells are normally associated with 4 bypass diodes as per the requirement of Solarus. Three different configurations of the bypass diode-number of solar cells bridged are simulated. As the shade arising from the frame lasts longer time near the edges, the number of solar cells near the frame should be as low as possible. Hence, the cell string will be grouped as 3-16-16-3, 4-15-15-4 or 5-14-14-5. Each possible configuration is simulated and is presented in the next section.

5. Simulation Procedure and Results

5.1 Simulation procedure

To achieve an easy manipulation of basic cell parameters and investigate their effect on the electrical characteristics of PV system, an efficient modelling of the solar cell is proposed using PSPICE simulator [33]. The simulation is carried out in LTSPICE, which is family of PSPICE simulation software. SPICE is a simulator program for the project of electronic circuits. SPICE is the acronym of *Simulation Program with Integrated Circuits Emphasis*".
In its 1st version, SPICE was presented by Laurence W. Nagel in his PhD thesis in Berkeley University (California) in 1972.

PSPICE is commonly used to model and simulate PV cells and modules under environmental conditions. A single solar cell model is shown in figure 5.1. This one is used as the basic model to simulate string of cells. Such sub-circuits are connected in series-parallel combination to form solar module.

For simulation purposes some solar cell parameters are used as a starting point. The most important parameters are V_{oc}, I_{sc} and P_{mp}, which can be found from data sheet of solar cells. For an ideal solar cell the series resistance is zero and thus neglected and parallel resistance is considered infinite, hence its effect is neglected [34]. In real one-diode solar cell models, there are five parameters which are used to characterize the diode. These are: the diode ideality factor (n), the reverse saturation current (I_s), the series resistance (R_s), the parallel resistance (R_p) and the photo-generated current (I_{pv}). The values of R_s and R_p are assumed constant for a specific value of illumination. This assumption will not substantially affect the conclusions [35].

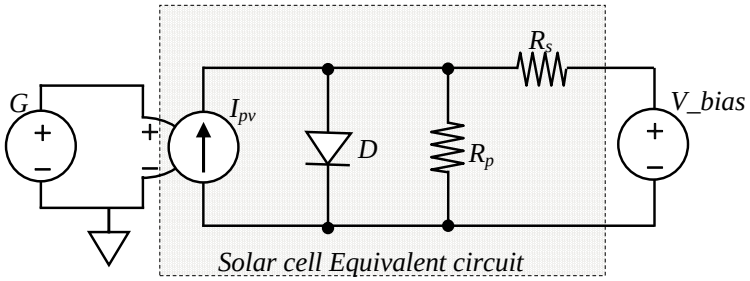

Figure 5.1: Equivalent circuit of solar cell in LTSPICE.

The circuit shown in figure 5.1 is simulated using LTSPICE. The characteristic parameters of the solar cell are self-consistently obtained in order to match the characteristics of the LTSPICE model with those obtained for a realistic solar cell specifications supplied by the manufacturer (BIG SUN).

In order to characterize the basic unit of a photovoltaic cell, a SPICE sub-circuit is adopted. The sub circuit model introduced specifies the photo generated current at a global irradiance G by

$$I_{pv} = \frac{\left(J_{sc,ref} \cdot A_{cell} + C_1 \cdot \Delta T\right)}{G_{ref}} \times G \qquad (47)$$

where $J_{sc,ref}$ is the current density and G_{ref} is the solar irradiation at STC (1000W/m^2 and temperature 25^{o}C), G is the solar irradiation at any instant, A_{cell} is the active area of a solar cell, C_1 is the current dependence on temperature and ΔT is the deviation of temperature from 25^{o}C.

In order to apply the concepts and generate an efficient SPICE-net list, the specification of solar cell used by Solarus is taken from data sheet shown in Table 5.1.

Company	BIG SUN technology
Cell type	Mono-crystalline Si solar cell
Size	156mm×156mm
Short circuit Current (I_{sc})	9.4A
Open Circuit Voltage (V_{oc})	0.636V
Maximum Power (P_{mp})	4.7W
Current at maximum Power (I_{mp})	8.9A
Voltage at maximum Power (V_{mp})	0.534V
Temperature coefficient of current I_{sc} (C_1)	5mA/K

Table 5.1 Solar cell data sheet.

$$J_{sc} = \frac{I_{sc}}{A_{cell}} \tag{48}$$

$$J_{sc,ref} = \frac{9.4\text{A}}{0.156\text{m}\times 0.156\text{m}} \approx 390\text{A/m}^2$$

For a 1/3 cell size (52mm×148mm) the short circuit current at STC is

$$I_{sc} = J_{sc,ref} \times A_{cell}$$

$$I_{sc} = (390A/m^2)\times(0.052m\times 0.148m) \approx 3A$$

The current generated by a single string depends on the solar irradiation, temperature and properties of individual single cells. If PV cells in a string are not uniformly illuminated, they will generate different currents. Taken into account that:

- The current of the string is limited by the solar cell that generates the lowest current;
- the total open circuit voltage of a string is the sum of individual open circuit voltages of all cells in the string;
- the string has 38 cells in a string,

the open circuit voltage for a uniformly illuminated string is approximately given by $V_{oc} = 38 \times 0.636\text{V} \approx 24.2\text{V}$.

Effect of Shading

Shade that falls on a group of cells will reduce the total generated power output by two reasons: it reduces the input energy and it increases losses in the shaded cells [44]. Let us consider the situation of Figure 5.2, which represents a string with two solar cells.

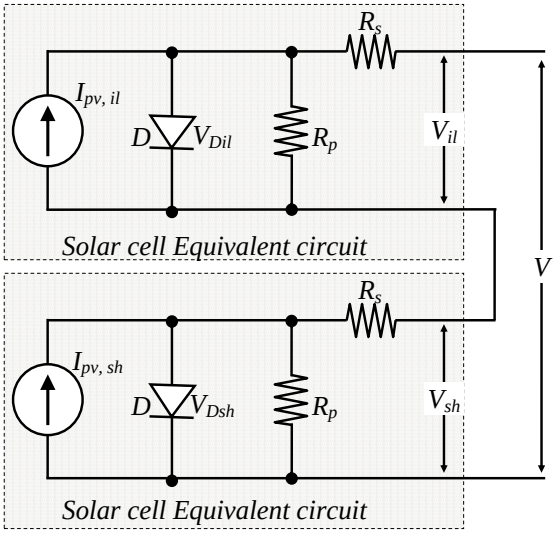

Figure 5.2: 2 Series connected PV cells.

One cell is under full illumination and the second is partially shaded. The photon current generated under full illumination is $I_{pv,il}$ and the photon current generated under partial illumination is $I_{pv,sh}$.

If the ratio of current generated by shaded cell to fully illuminated cell is represented by F, then $F = 0$ means fully shaded and $F = 1$ means fully illuminated.

Assuming a cell partially shaded and that the contact and leakage resistance values are not much affected due to partial shading and illumination [43],

$$I_{sh} = FI_{pv,il} - I_s \left\{ \exp\left(\frac{q(V_{sh} + I_{sh}R_s)}{nKT} \right) - 1 \right\} - \frac{V_{sh} + I_{sh}R_s}{R_p} \tag{49}$$

where V_{sh} and I_{sh} are the voltage and current of the shaded solar cell.

In a similar way, for the fully illuminated cell

$$I_{il} = I_{pv,il} - I_s \left\{ \exp\left(\frac{q(V_{il} + I_{il}R_s)}{nKT} \right) - 1 \right\} - \frac{V_{il} + I_{il}R_s}{R_p} \tag{50}$$

where V_{il} and I_{il} are the voltage and current of the fully illuminated cell.

The cells are connected in series. Therefore, the same current flows through both cells, i.e, $I_{sh}=I_{il}$. Then

$$I = FI_{pv,il} - I_s \left\{ \exp\left(\frac{q(V_{sh} + I_{sh}R_s)}{nKT} \right) - 1 \right\} - \frac{V_{sh} + I_{sh}R_s}{R_p}$$

$$I = I_{pv,il} - I_s \left\{ \exp\left(\frac{q(V_{il} + I_{il}R_s)}{nKT} \right) - 1 \right\} - \frac{V_{il} + I_{il}R_s}{R_p}$$

As the extent of shading increases, the exponential term tends to zero, and hence, the shaded cell voltage can be approximated to

$$V_{sh} = \left(FI_{pv,il} - I \right) R_p + IR_s \tag{51}$$

$$V = V_{il} + V_{sh} \tag{52}$$

The power dissipated by the shaded cell is

$$P_{dis} = I \left\{ \left(FI_{pv,il} - I \right) R_p + IR_s \right\} \tag{53}$$

Figure 5.3 shows the *I-V* and *P-V* characteristics for two solar cells as a function of the illumination (*F* varies from 0 to 1 in steps of 0.25).

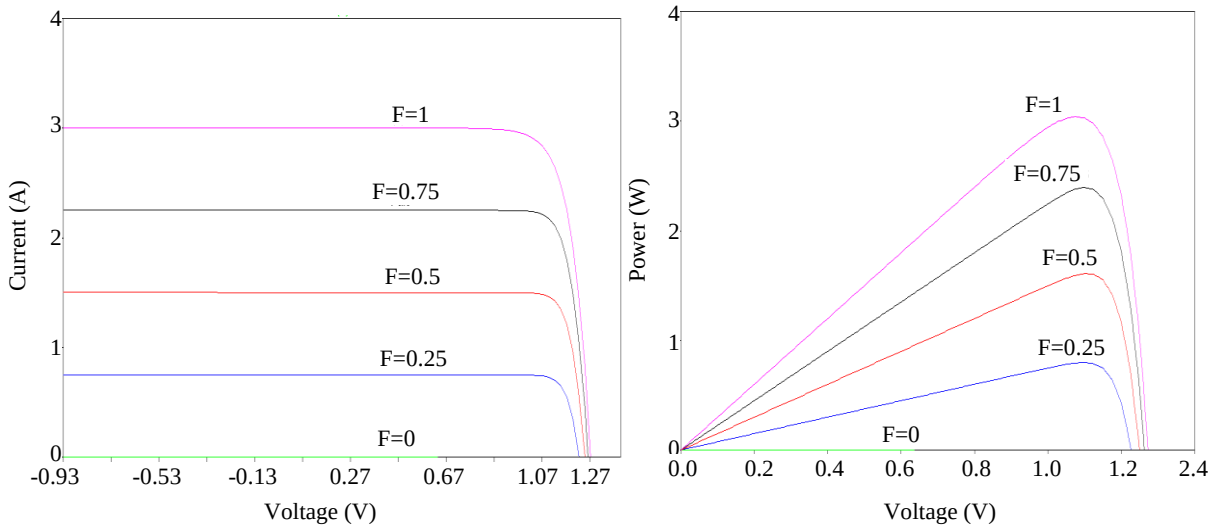

Figure 5.3: *I-V* and *P-V* curves for the solar cell circuit of figure 5.2 (without bypass).

As it is apparent from figure 5.3, the short circuit current is highly dependent on the shading, but the open circuit voltage is slightly affected.

If a bypass diode is included in parallel with each solar cell, the *I-V* and *P-V* curves are modified accordingly and the effects of partially shaded solar cell on the stationary *I-V* and *P-V* characteristics are shown in the figure 5.4 for different levels of shading.

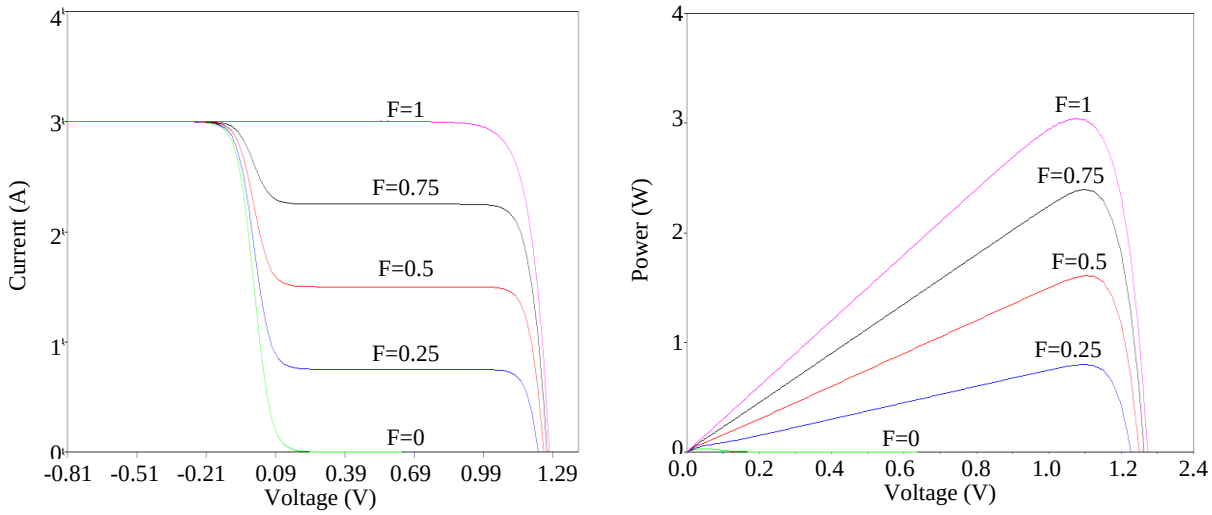

Figure 5.4: *I-V* and *P-V* curves for the solar cell circuit of figure 5.2 (with bypass).

It is worth noticing the presence of steps in the *I-V* stationary characteristics for the case the partially shades solar cells are bridged by bypass diodes. This analysis can be straightforward extended to more cells, the conclusions being qualitatively similar.

5.2 Comparison of simulation and experimental results

Solarus AB strings have 38 solar cells and 4 bypass diodes. Solarus has provided the results obtained for two types of tests: the outdoor and solar simulator tests. For comparison and validation reasons, a simulation was carried out using LTSPICE simulation.

Outdoor test

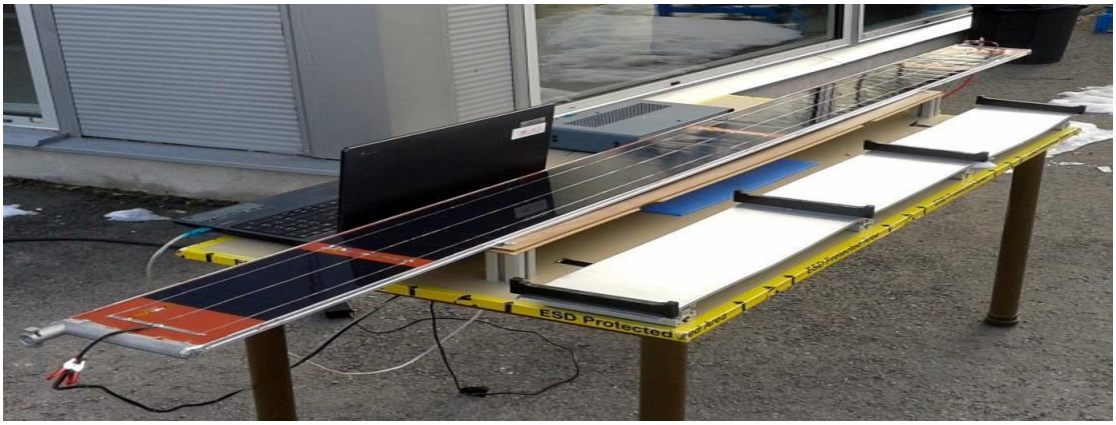

(a)

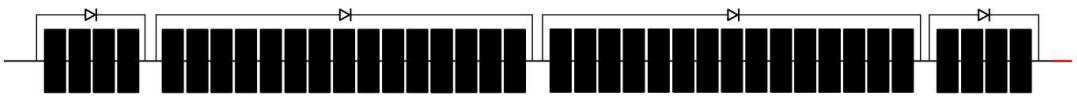

(b)

Figure 5.5: (a) Outdoor test receiver; (b) 4-15-15-4 PV-cell string.

Tables 5.2 and 5.3 show the data provided by Solarus at outdoor test conditions of 5°C temperature and global irradiances G of 800 and 780 W/m^2 for the test receiver of 4-15-15-4 shown in the figure 5.5. The simulation results are also presented.

	Data from Solarus	Simulation	$\lvert\Delta_{abs}\rvert$	$\lvert\Delta_{rel}\rvert$%
G(W/m^2)	800	800	0	0
I_{sc} (A)	2.40	2.38	0.02	0.84
V_{oc} (V)	24.40	25.45	1.05	4.13
I_{mp} (A)	2.20	2.25	0.05	2.22
V_{mp} (V)	20.60	21.89	1.29	5.89
P_{mp} (W)	45.60	49.29	3.69	8.03
FF(%)	77.90	81.38	3.48	4.28
$\eta_{cell} = \frac{P_{mp}}{G \cdot A_{cell} \cdot N}(\%)$	20.30	21.07	0.77	3.66

Table 5.2: Comparison of simulation and outdoor test results for G=800W/m^2.

	Data from Solarus	Simulation	$\lvert\Delta_{abs}\rvert$	$\lvert\Delta_{rel}\rvert$%
G(W/m^2)	780	780	0	0
I_{sc} (A)	2.20	2.32	0.12	5.17
V_{oc} (V)	24.20	25.41	1.21	4.76
I_{mp} (A)	2.00	2.20	0.20	9.1
V_{mp} (V)	20.70	21.81	1.11	5.09
P_{mp} (W)	41.50	47.95	6.45	13.45
FF (%)	77.10	81.34	4.24	5.21
η_{cell}(%)	18.90	21.02	2.12	10.09

Table 5.3: Comparison of simulation and outdoor test results for G=780W/m^2.

In Tables 5.2 and 5.3

- $\lvert\Delta_{abs}\rvert$ is the absolute difference between the simulated and outdoor test results;
- $\lvert\Delta_{rel}\rvert$% is the percentage deviation of measured data from simulated results.

The results from Solarus outdoor test and the simulation results show a good agreement. The deviations may be due to the accuracy related to the radiation meter used for the outdoor test.

Solar simulator

The Solar simulator tests were carried out for different cell sizes and configurations. The solar simulator results provided by Solarus were carried at nearly a temperature of 5^{o}C.

A comparison of the results from solar simulator (Solarus) and our simulation model is summarized and can be shown for 1/6 size solar cells of 38||38 (Table 5.4), 1/3 size Solar cells of 19||19 (Table 5.5) and 1/3 test receiver with 38 Solar cells 4-15-15-4 (Table 5.6).

	Data from Solarus	Simulation	$\lvert\Delta_{abs}\rvert$	$\lvert\Delta_{rel}\rvert$%
G(W/m^2)	1345	1345	0	0
I_{sc} (A)	4.00	4.01	0.01	0.25
V_{oc} (V)	24.4	25.25	0.85	3.37
I_{mp} (A)	3.8	3.81	0.01	0.26
V_{mp} (V)	21.8	21.67	0.13	0.6
P_{mp} (W)	82.4	82.46	0.06	0.07
FF (%)	85.5	81.44	4.06	4.99
η_{cell}(%)	-	20.96	-	-

Table 5.4: Comparison of simulation and solar simulator test results for 1/6 solar cells.

	Data from Solarus	Simulated	$\lvert\Delta_{abs}\rvert$	$\lvert\Delta_{rel}\rvert$%
G(W/m^2)	1396	1396	0	0
I_{sc} (A)	8.3	8.31	0.01	0.12
V_{oc} (V)	12.4	13.05	0.65	5
I_{mp} (A)	8.1	7.88	0.22	2.79
V_{mp} (V)	10.9	11.2	0.3	2.68
P_{mp} (W)	88.5	88.4	0.1	0.11
FF (%)	85.7	81.52	4.18	5.13
η_{cell}(%)	-	21.65	-	-

Table 5.5: Comparison of simulation and solar simulator test results for 1/3 solar cells.

	Data from Solarus	Simulation	$\lvert\Delta_{abs}\rvert$	$\lvert\Delta_{rel}\rvert$%
G(W/m^2)	1889#	1889#	0	0
I_{sc} (A)	6.6	6.6	0	0
V_{oc} (V)	24.9	25.01	0.11	0.44
I_{mp} (A)	4.3	4.01	0.29	7.23
V_{mp} (V)	20.7	22.63	1.93	8.53
P_{mp} (W)	87.9	90.91	3.01	3.31
FF (%)	54.0	55.08	1.08	1.96
η_{cell} (%)	-	16.46	-	-

Table 5.6: Comparison of simulation and solar simulator test results for 1/3 test receiver.
#: weighted average of the Global irradiance G_{av}.

In figure 5.6 are reproduced the stationary *I-V* and *P-V* characteristics obtained from a netlist of LTSPICE that took into account the *I-V* curve provided by Solarus for the 1/3 test receiver of 4-15-15-4. A more detailed analysis can be shown in section 5.4.

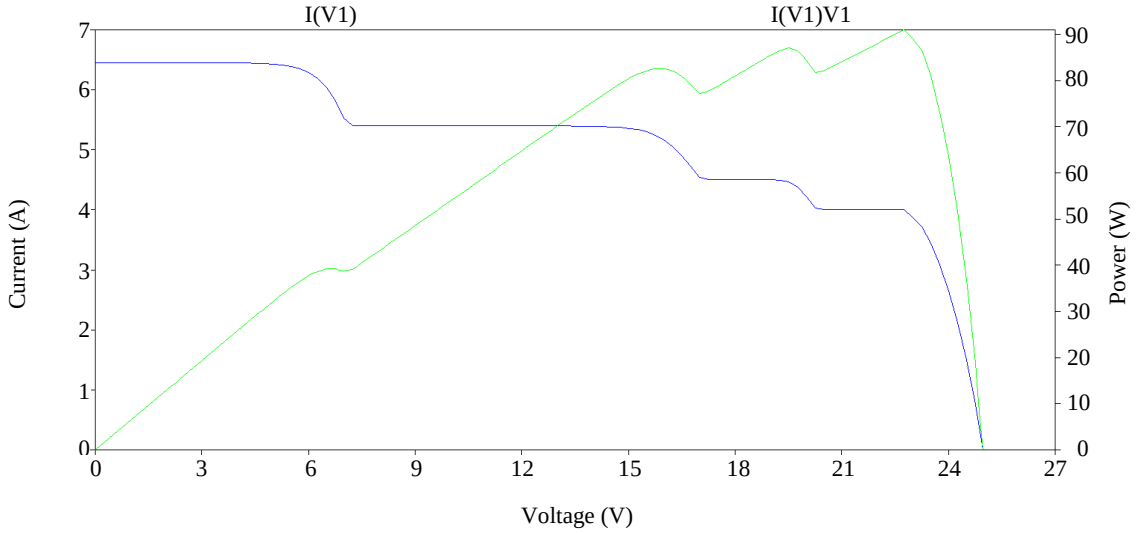

Figure 5.6: *I-V* and *P-V* curve of the 1/3 test receiver.

Even though the solar simulator source is not considered a stable source, the data provided by Solarus and the results obtained by simulation are in a good agreement to each other.

The uncertainties obtained for the tabulated data are within the expected range levels, according the equations presented in Appendix-II.

5.3 Prototype circuit: results and comparative analysis

A circuit setup was tested as a prototype in Instituto Superior Técnico (IST) at Lisbon University (UL) to model the effects of shading and temperature. The circuit setup is represented in Fig.5.7. The diodes D_1 to D_{18} are plastic silicon rectifiers IN4003. With this experiment we intended to create an analogy with the effect of radiation on solar cell behavior. The current source associated to the illumination I_{PV} is replaced by a voltage source (V_1 to V_4) in series with a resistor of 1MΩ. This means that each voltage source V, expressed in volt, corresponds indeed to a current source expressed in microampere. V_5 is an adjustable DC voltage source connected in series with an ammeter. The setup consists of four groups of diodes, in a sequential arrangement of 2+5+5+2, each group having its own bypass diode across it. In order to change the current value, the voltage sources V_1, V_2, V_3, and V_4 are modified to meet the required current through each group of solar cells to demonstrate the shading effect.

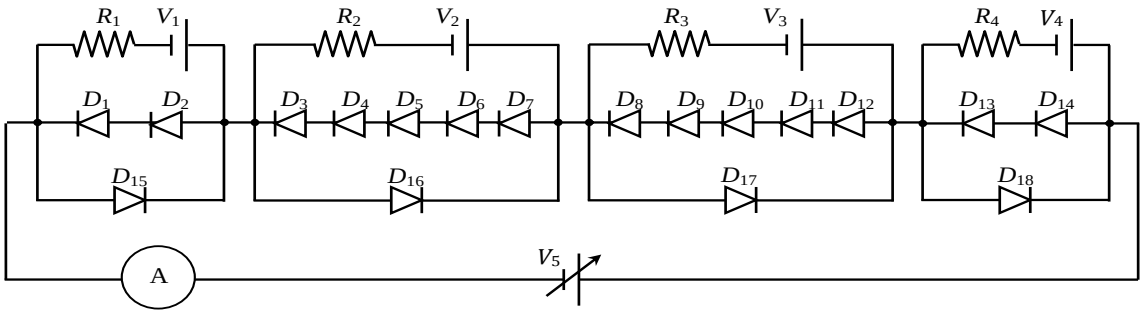

Figure 5.7: Prototype circuit.

From now on, each example under analysis will be identified by the set of numbers I1-I2-I3-I4. For instance, the sequence 15-20-20-20 will represent the PV module with the first set of solar cells under a radiation associated to a current of 15μA and the remaining three have an illumination current of 20μA. The effect of temperature on the PV characteristics is also studied by placing the circuit assembly inside an oven for temperatures of 25°C and 40°C (figure 5.8).

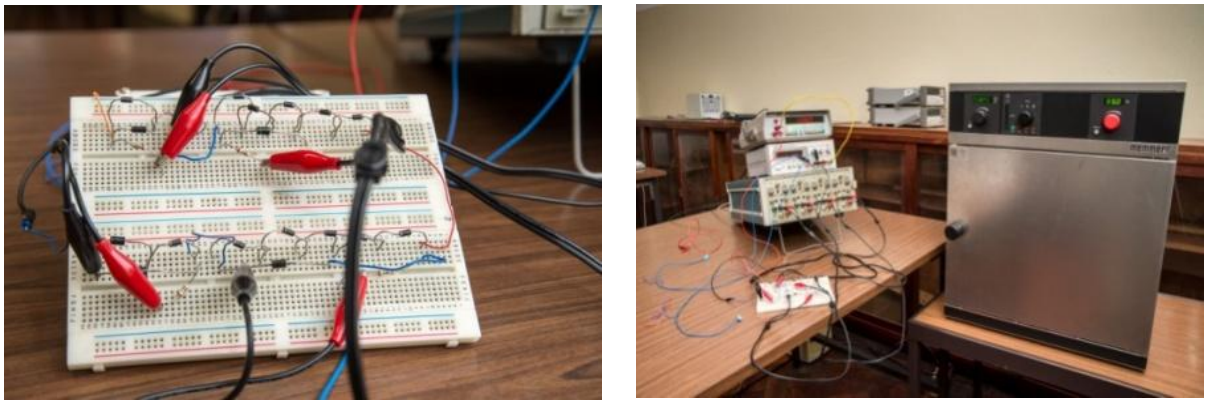

Figure 5.8: Circuit assembly in lab at IST.

The lab circuit assembly of the module with 14 diodes is shown in figure 5.8, at left. At right of the same figure it can be seen the oven, where the circuit has been inserted in order to be subjected to various temperature conditions.

By convention, solar cell efficiencies are always measured under STC (T = 25ºC and G = 1000 W/m^2), unless otherwise stated.

The presented results correspond to a module of 14 solar cells under different voltage (illumination) and temperature (25ºC and 40ºC) conditions.

As far as the equivalent irradiance is concerned, three situations are presented:

i. full uniform illumination (20-20-20-20);
ii. 50% illumination of the 1st group: (10-20-20-20)
iii. 50% illumination of the 2nd group: (20-10-20-20).

All the simulation results presented in this section were obtained in a LTSPICE environment, recurring to the single diode model with 5 parameters for the solar cell description represented in figure 5.1.

Figures 5.9 to 5.11 represent the *I-V* and *P-V* stationary characteristics concerning experimental and simulation results for the three solar cell string configurations referred above.

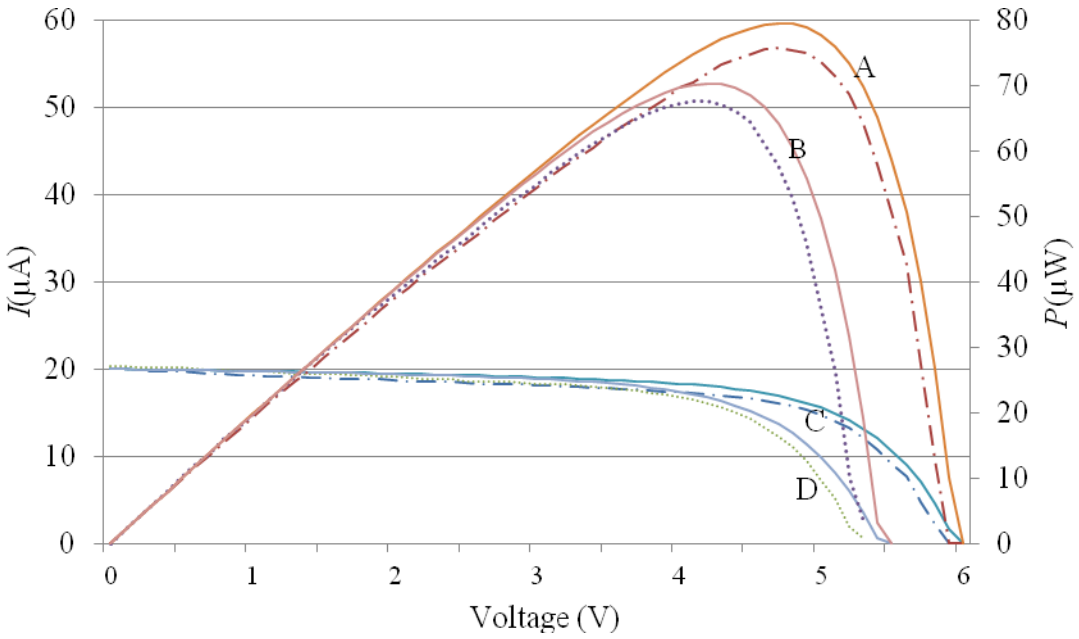

Figure 5.9: Experimental (broken line) and simulation (solid) results..

T=25ºC (case A, *P-V* curve and case C, *I-V* curve);
T=40ºC (case B, *P-V* curve and case D, *I-V* curve), when the conditions are 20-20-20-20.

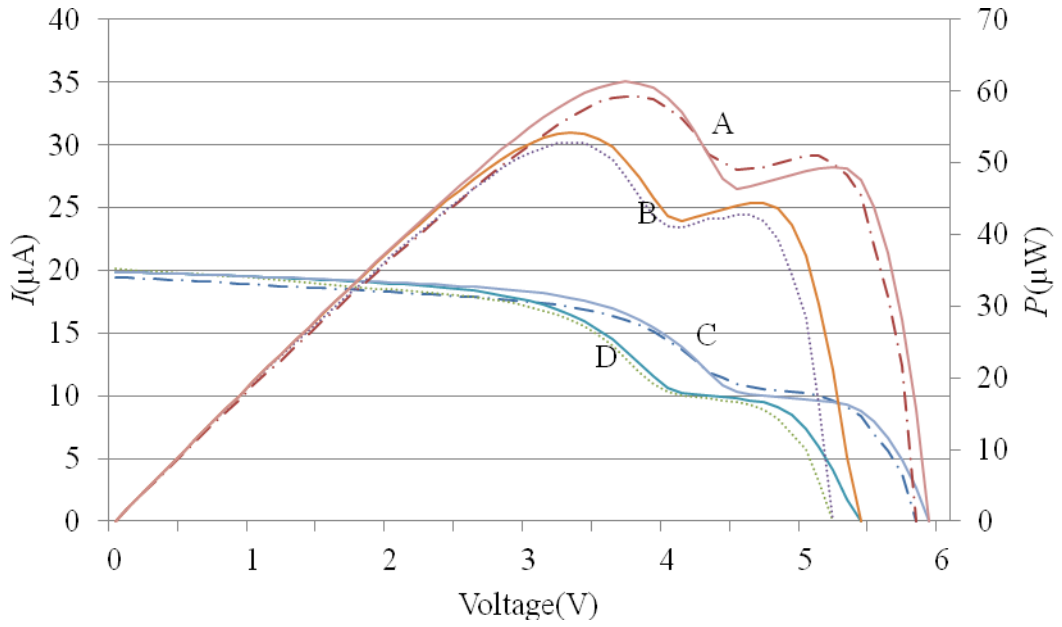

Figure 5.10: Experimental (broken line) and simulation (solid) results.
T = 25ºC (case A, *P-V* curve and case C, *I-V* curve);
T = 40ºC (case B, *P-V* curve and case D, *I-V* curve), when the conditions are 10-20-20-20.

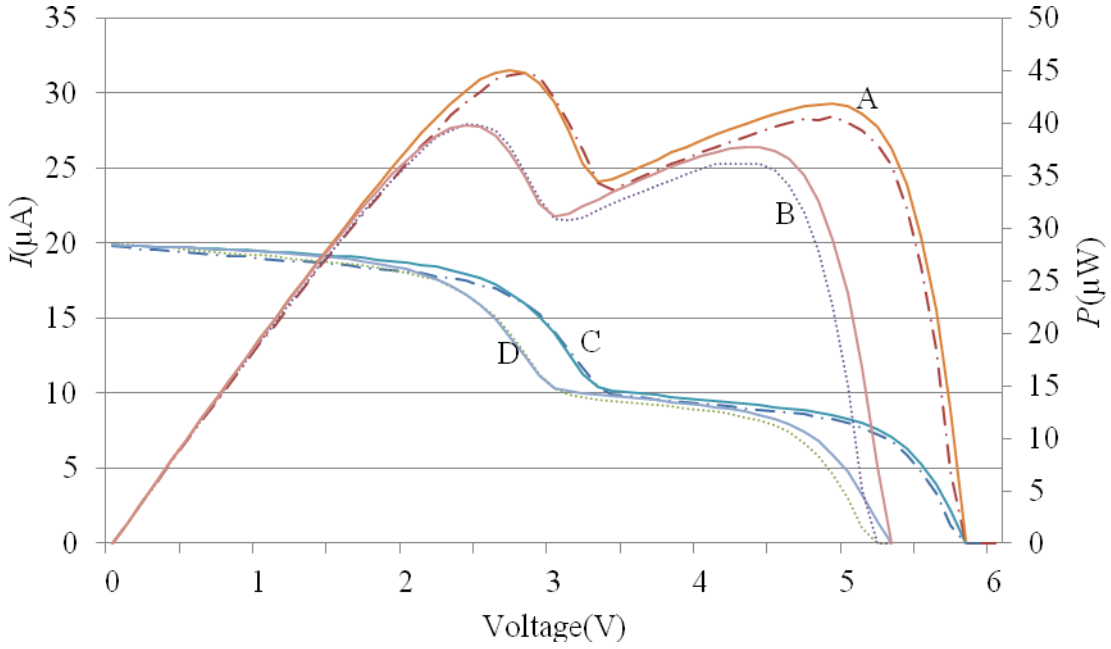

Figure 5.11: Experimental (broken line) and simulation (solid) results.

T = 25ºC (case A, *P-V* curve and case C, *I-V* curve);
T = 40ºC (case B, *P-V* curve and case D, *I-V* curve), when the conditions are 20-10-20-20.

Results at room temperature are summarized in table 5.7. The energy efficiencies are normalized to the value obtained for full uniform illumination conditions of the PV module.

20-20-20-20				
	Simulation	Experimental	$\lvert\Delta_{abs}\rvert$	$\lvert\Delta_{rel}\rvert$%
V_{oc}	5.96 V	5.90V	0.06 V	1.00
I_{sc}	20.00 μA	20.00 μA	0 μA	0
V_{max}	4.70V	4.70V	0V	0
I_{max}	16.92 μA	16.10μA	0.82 μA	5.00
P_{mp}	79.50μW	75.67 μW	3.83 μW	5.00
FF	0.67	0.64	0.03	5.00
η_e	1	0.95	0.05	5.00
10-20-20-20				
V_{oc}	5.85V	5.80V	0.05V	1.0
I_{sc}	19.87 μA	19.40 μA	0.47 μA	2.00
V_{max}	3.70V	3.80V	0.10V	3.00
I_{max}	16.57 μA	15.60μA	0.97 μA	6.00
P_{mp}	61.30 μW	59.28 μW	2.02 μW	3.00
FF	0.53	0.53	0	0
η_e	0.78	0.77	0.01	1.00
20-10-20-20				
V_{oc}	5.80V	5.75V	0.05V	1.00
I_{SC}	19.87 μA	19.80 μA	0.07 μA	0.40
V_{max}	2.70V	2.80V	0.10V	4.00
I_{max}	16.69 μA	16.00 μA	0.69 μA	4.00
P_{mp}	45.10 μW	44.80 μW	0.30 μW	1.00
FF	0.39	0.39	0	0
η_e	0.57	0.57	0	0

Table 5.7: Comparative analysis at room temperature.

Solar cell modelling and simulation in LTPSPICE environment has been presented and validated by a comparative analysis of the associated results with those obtained in laboratory. The effects of the temperature and the shading on the PV module have been analyzed. The obtained results show a remarkable agreement between experimental and simulation results, which ensures that the model can indeed be used as an important tool to the analysis of the main figures of merit related to the PV system. Moreover, the modelling can be used to define the solar cell string layout associated to different PV cell configurations in order to improve their performance.

The analysis presented in sections 5.2 and 5.3 showed undoubtedly a remarkable agreement between the simulation results obtained with the proposed model and the

experimental results obtained either from data provided by Solarus (outdoor test an solar simulator) or from a prototype in IST. We are in the right position to assume that the model can be used as an important tool for comparative analysis of different combinations of PV solar cell strings. The study of several cell string layout and bypass diode arrangements will be presented in the next section.

5.4 Simulation analysis concerning different cell string layout and bypass diode configurations

The following simulations were carried to determine the effect of shading on the characteristics concerning different types of strings of 38 solar cells (1/3 cell type) produced by Solarus. The shading movement from one cell to the next following the sunrise (shown in figure 2.8) may lead to a drastic change in the characteristics of the solar panel.

In the configuration reference the * sign indicates the group in which the solar cell affected by partial shading, and bridged by a bypass diode, is placed. For instance, the denomination 3*-16-16-3 stands for a string of 38 solar cells with 4 bypass diodes in which at least one of the 3 solar cells bridged by the first bypass diode is affected by the frame's shade.

Case A: **38 solar cells without bypass diodes**

F	1	0.9	0.8	0.7	0.6	0.5	0.4	0.3	0.2	0.1	0
P_{mp}	57.23	51.23	45.28	39.22	33.30	27.43	21.66	15.94	10.35	4.92	0
V_{mp}	20.48	20.36	20.21	20.03	19.87	19.67	19.41	19.07	18.58	17.75	0
I_{mp}	2.79	2.51	2.23	1.96	1.68	1.39	1.12	0.83	0.56	0.28	0
V_{oc}	24.20	24.02	23.88	23.75	23.55	23.32	23.00	22.67	22.14	21.27	0
I_{sc}	2.97	2.67	2.38	2.08	1.78	1.49	1.19	0.89	0.59	0.30	0

Table 5.8: Simulation results for different shading levels in a string of 38 series connected solar cells (no bypass diode).

Case B: 3*-16-16-3

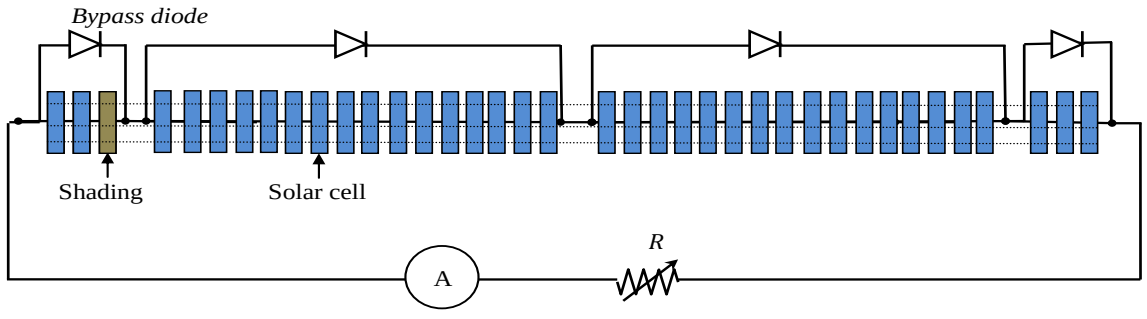

Figure 5.12: 3*-16-16-3 string layout.

F	1	0.9	0.8	0.7	0.6	0.5	0.4	0.3	0.2	0.1	0
P_{mp}	57.23	55.62	51.27	51.05	51.02	50.99	50.97	50.96	50.94	50.93	50.92
V_{mp}	20.5	20.98	21.68	18.28	18.28	18.28	18.28	18.25	18.25	18.25	18.25
I_{mp}	2.8	2.652	2.365	2.793	2.792	2.79	2.789	2.792	2.791	2.791	2.79
V_{oc}	24.18	24.15	24.15	24.13	24.13	24.10	24.08	24.05	24	23.95	22.28
I_{sc}	2.973	2.973	2.973	2.973	2.973	2.973	2.973	2.973	2.973	2.973	2.973

Table 5.9: Simulation results for different shading levels in a string 3*-16-16-3.

Case C: 4*-15-15-4

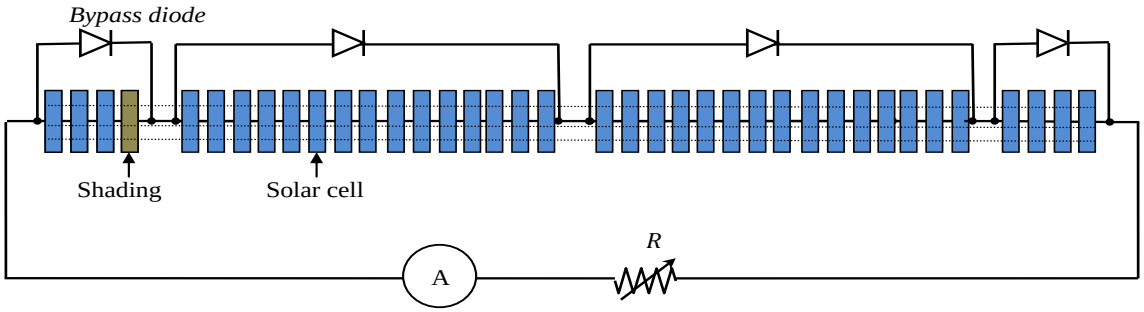

Figure 5.13: 4*-15-15-4 string layout.

F	1	0.9	0.8	0.7	0.6	0.5	0.4	0.3	0.2	0.1	0
P_{mp}	57.23	55.4	50.98	49.54	49.50	49.48	49.46	49.44	49.43	49.42	49.41
V_{mp}	20.5	20.95	21.60	17.75	17.75	17.73	17.73	17.73	17.7	17.7	17.7
I_{mp}	2.79	2.645	2.36	2.79	2.79	2.79	2.79	2.79	2.793	2.792	2.791
V_{oc}	24.18	24.15	24.15	24.13	24.10	24.08	24.08	24.00	23.95	23.85	21.63
I_{sc}	2.973	2.973	2.973	2.973	2.973	2.973	2.973	2.973	2.973	2.973	2.973

Table 5.10: Simulation results for different shading levels in a string 4*-15-15-4.

Case D: 5*-14-14-5

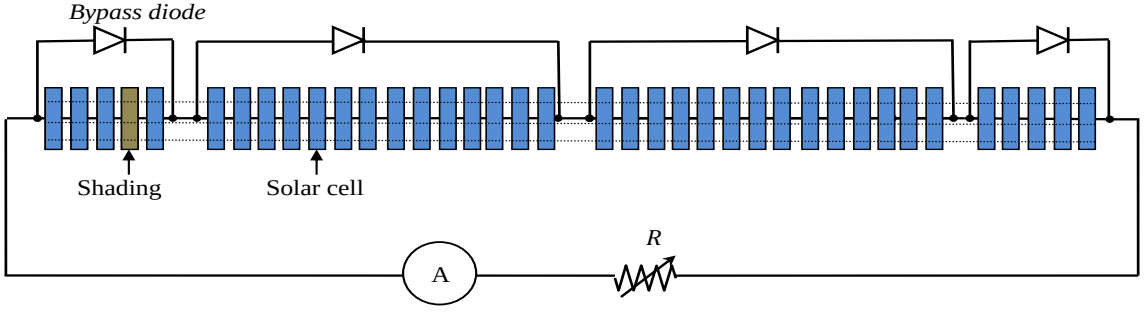

Figure 5.14: 5*-14-14-5 string layout.

F	1	0.9	0.8	0.7	0.6	0.5	0.4	0.3	0.2	0.1	0
P_{mp}	57.23	55.2	50.71	48.02	48.0	47.96	47.94	47.93	47.92	47.90	47.89
V_{mp}	20.5	20.93	21.53	17.2	17.2	17.2	17.18	17.18	17.18	17.18	17.15
I_{mp}	2.79	2.64	2.36	2.792	2.79	2.79	2.792	2.791	2.79	2.79	2.793
V_{oc}	24.18	24.15	24.13	24.1	24.08	24.03	24.03	23.98	23.90	23.78	21.0
I_{sc}	2.973	2.973	2.973	2.973	2.973	2.973	2.973	2.973	2.973	2.973	2.973

Table 5.11: Simulation results for different shading levels in a string 5*-14-14-5.

Figure 5.15 shows an histogram of the power generated by the PV module for the 4 strings of 38 cells previously referred as cases A, B, C and D for different levels of shading. It is apparent from the graphic that:

- The configurations with bypass diode present clear advantageous in the power conversion process;
- the power generation is a decreasing function of the shading level;
- the best solution is case B, since it is the combination that corresponds to the minimum number of shaded solar cells for a given shading level.

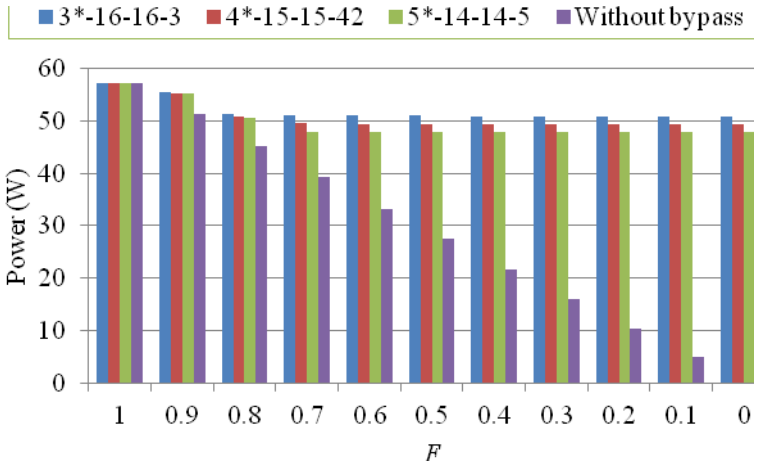

Figure 5.15: Power generated *vs* shading percentage.

Figures 5.16 to 5.21 show the evolution of

- the power losses;
- the open circuit voltage V_{oc};
- the short circuit current I_{sc};
- the voltage at MPP, V_{mp};
- the current at MPP, I_{mp};
- the fill factor, FF,

as functions of the shading levels in the 4 solar string configurations under analysis.

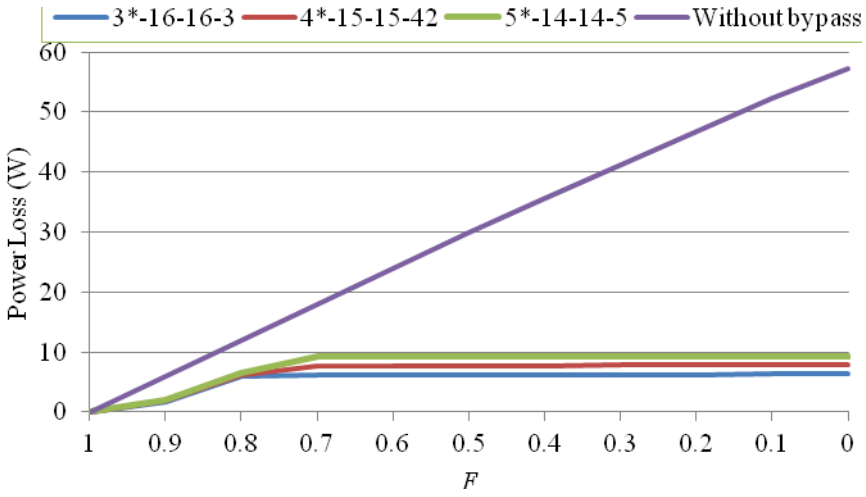

Figure 5.16: Power loss *vs* shading percentage.

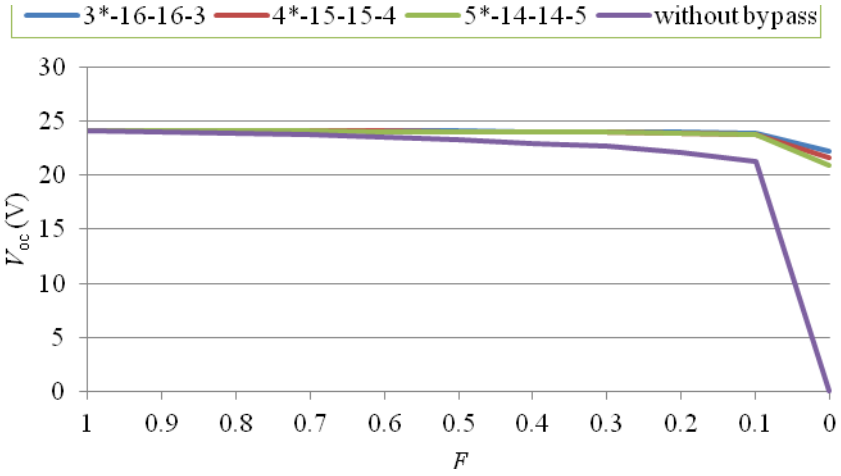

Figure 5.17: Open circuit voltage *vs* shading percentage.

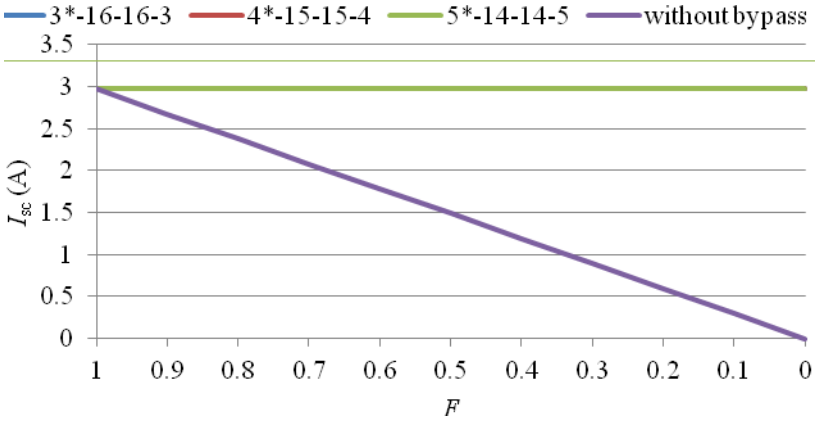

Figure 5.18: Short circuit current *vs* shading percentage.

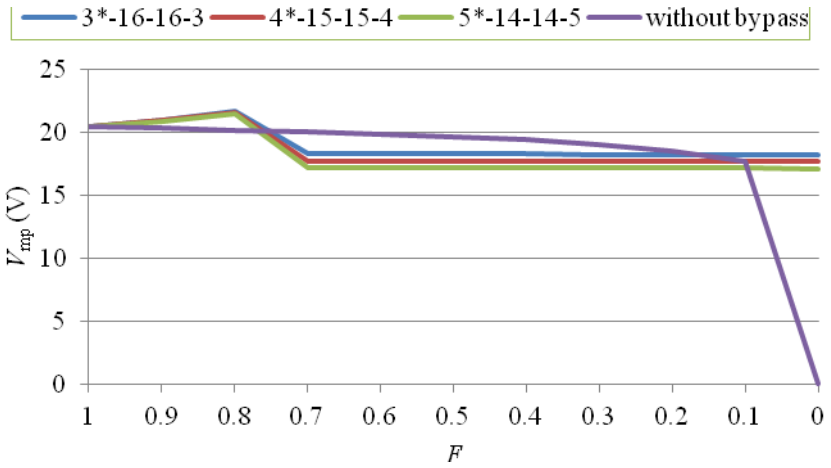

Figure 5.19: V_{mp} *vs* shading percentage.

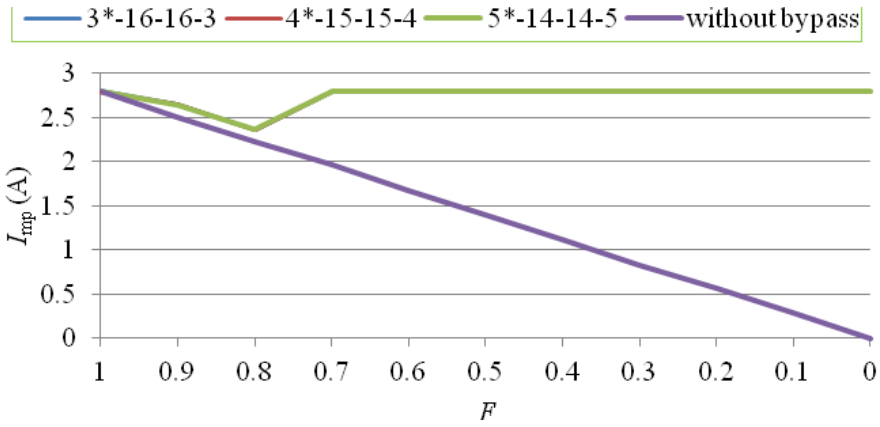

Figure 5.20: I_{mp} *vs* shading percentage.

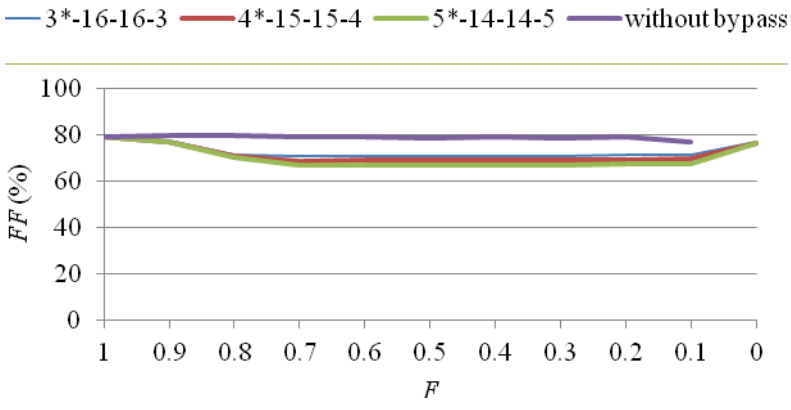

Figure 5.21: *FF vs* shading percentage.

Figure 5.22 shows the stationary *I-V* characteristic for the configuration related to case C for STC and for ten levels of shading percentage in steps $\Delta F = 0.1$. It is worth noticing the existence of two steps in the *I-V* characteristic whenever shading is present ($F < 1$).

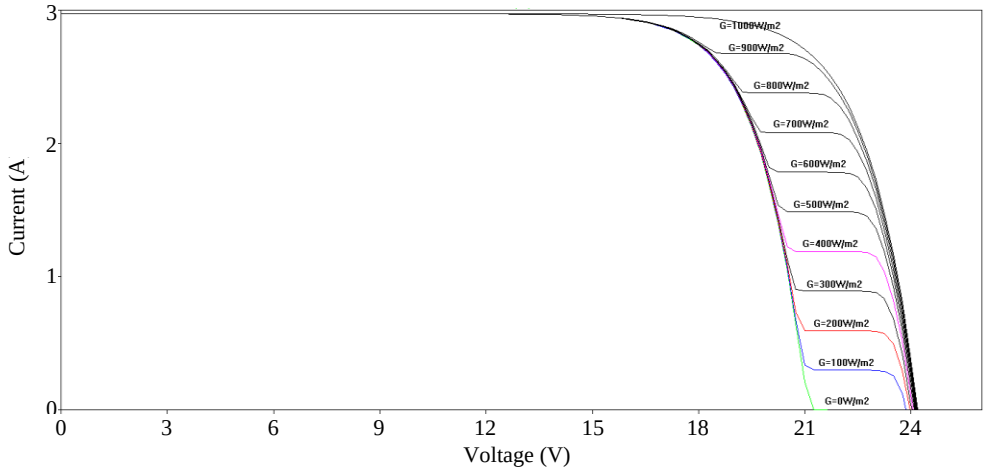

Figure 5.22: *I-V* curve (4*-15-15-4).

Figure 5.23 shows the stationary *P-V* characteristic for the same configuration (case C) considering STC and ten levels of shading percentage in steps $\Delta F = 0.1$.

One important detail is the presence of two power peaks (PP) whenever shading is present ($F < 1$). Let us refer them as PP_{low} and PP_{high}, for the peak power corresponding to the smaller voltage and to the higher voltage, respectively. For small shading percentages (F near 1) the MPP is PP_{high}. However, this one decreases quickly when F decreases, leading to a change of the MPP to the PP_{low}, which remains practically independent on F.

This fact explains the reason why the power loss *versus* shading percentage remains practically constant when F decreases, for all configurations using BP (see figure 5.16).

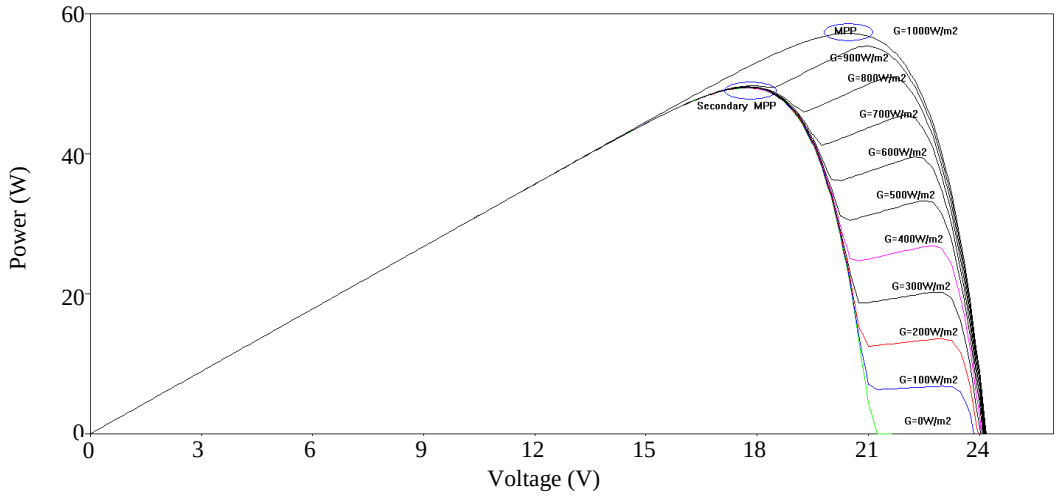

Figure 5.23: *P-V* curve (4*-15-15-4).

Similar simulation analysis where carried on when the shading affects the 2nd group of cells in the string. The string layouts are shown in figures 5.24 to 5.26 and the respective results summarized in tables 5.12 to 5.14.

Case A: 3-16*-16-3

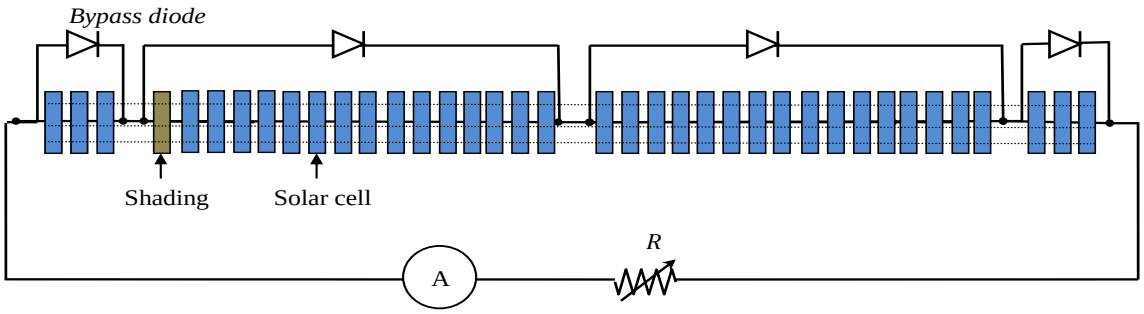

Figure 5.24: 3-16*-16-3 string layout.

F	1	0.9	0.8	0.7	0.6	0.5	0.4	0.3	0.2	0.1	0
P_{mp}	57.23	53.51	48.4	42.77	36.88	31.31	31.29	31.28	31.26	31.25	31.24
V_{mp}	20.5	20.7	20.95	21.13	21.23	11.2	11.23	11.23	11.23	11.23	11.2
I_{mp}	2.8	2.59	2.31	2.03	1.74	2.8	2.79	2.79	2.79	2.784	2.79
V_{oc}	24.18	24.13	24.05	23.98	23.90	23.8	23.68	23.53	23.30	22.93	14
I_{sc}	2.973	2.973	2.973	2.973	2.973	2.973	2.973	2.973	2.973	2.973	2.973

Table 5.12: Simulation results for different shading levels of the string 3-16*-16-3.

Case B: 4-15*-15-4

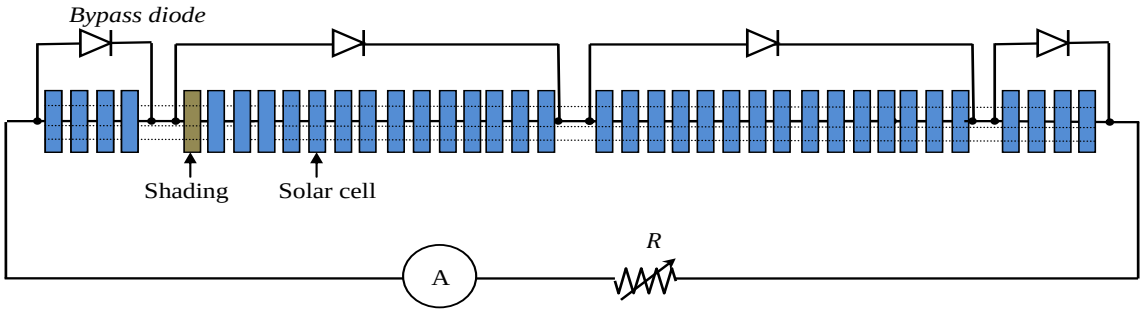

Figure 5.25: 4-15*-15-4 string layout.

F	1	0.9	0.8	0.7	0.6	0.5	0.4	0.3	0.2	0.1	0
P_{mp}	57.23	53.64	48.58	43.00	37.1	32.83	32.81	32.79	32.77	32.76	32.75
V_{mp}	20.50	20.70	21.00	21.18	21.3	11.78	11.78	11.78	11.70	11.75	11.78
I_{mp}	2.79	2.591	2.313	2.03	1.74	2.79	2.79	2.79	2.80	2.79	2.782
V_{oc}	24.18	24.13	24.05	24	23.93	23.83	23.7	23.58	23.35	23.0	14.62
I_{sc}	2.973	2.973	2.973	2.973	2.973	2.973	2.973	2.973	2.973	2.973	2.973

Table 5.13: Simulation results for different shading levels of the string 4-15*-15-4.

Case C: 5-14*-14-5

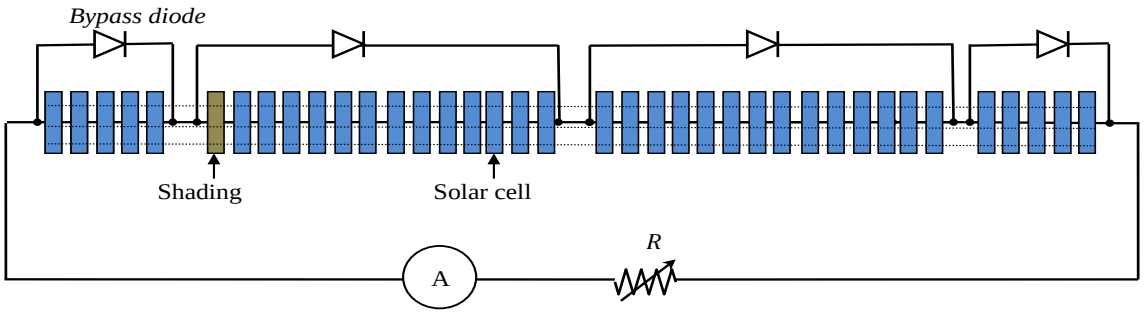

Figure 5.26: 5-14*-14-5 string layout.

F	1	0.9	0.8	0.7	0.6	0.5	0.4	0.3	0.2	0.1	0
P_{mp}	57.23	53.77	48.76	43.17	37.27	34.34	34.32	34.3	34.29	34.28	34.27
V_{mp}	20.5	20.73	21.05	21.25	21.38	12.33	12.33	12.3	12.3	12.3	12.3
I_{mp}	2.79	2.594	2.32	2.03	1.744	2.786	2.785	2.79	2.79	2.79	2.786
V_{oc}	24.18	24.13	24.08	24	23.93	23.85	23.73	23.60	23.43	23.1	15.25
I_{sc}	2.973	2.973	2.973	2.973	2.973	2.973	2.973	2.973	2.973	2.973	2.973

Table 5.14: Simulation results for different shading levels of the string 5-14*-14-5.

Figure 5.28 shows an histogram of the power generated by the PV module for the 4 strings of 38 cells previously referred as cases A, B and C for different levels of shading. The conclusions are qualitatively similar to those referred for figure 5.15, when the shading affected the 1st group of cells in the string. Quantitatively, there is a reinforcement of the negative effects associated to the shading, since the 2nd group bridged by the BP diodes has more cells than the 1st group.

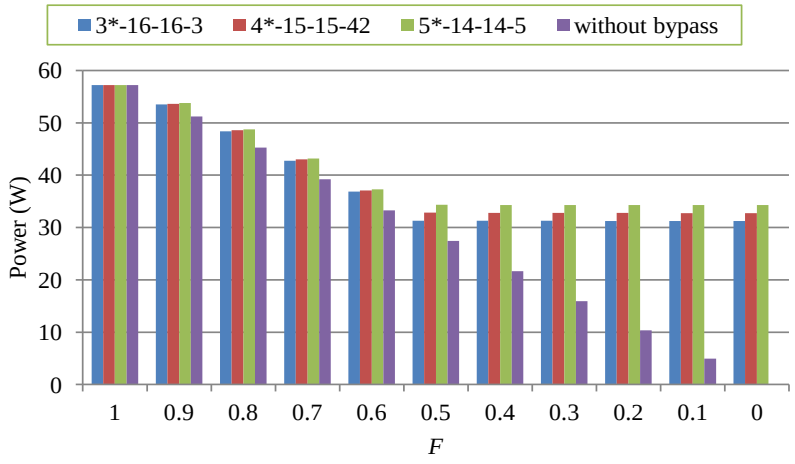

Figure 5.27: Peak power *vs* shading percentage.

Figures 5.29 and 5.30 show the stationary *I-V* and *P-V* characteristics for the string 4-15*-15-4. Comparing with figure 5.23, it is apparent that the modification of the MPP to PP_{low} is now reached for slower *F*: around 0.5 instead of approximately 0.75, obtained for the string 4*-15-15-4. This may be explained by the fact that in the present case (4-15*-15-4) the shading effect is stronger and PP_{low} is lower (around 30W) than for the string 4*-15-15-4 (around 50W).

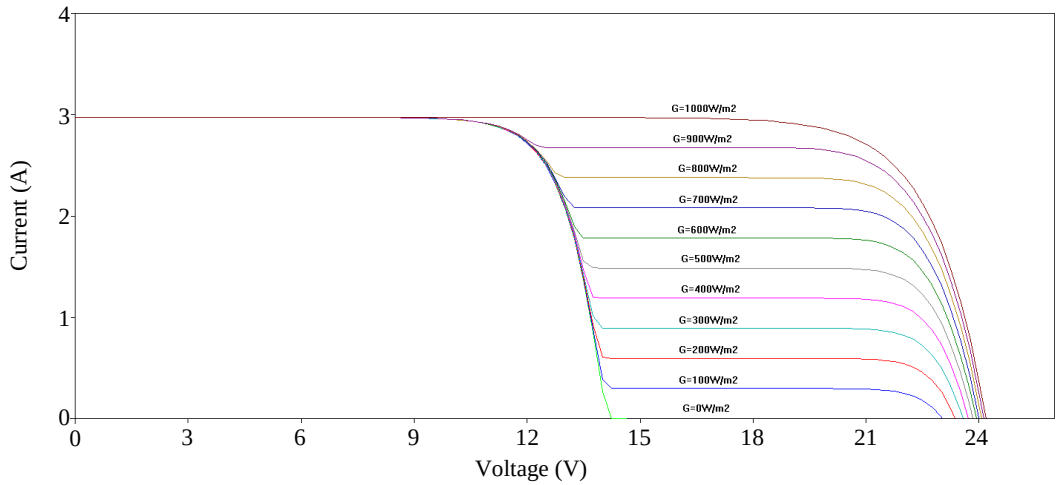

Figure 5.28: *I-V* curve for the string 4-15*-15-4.

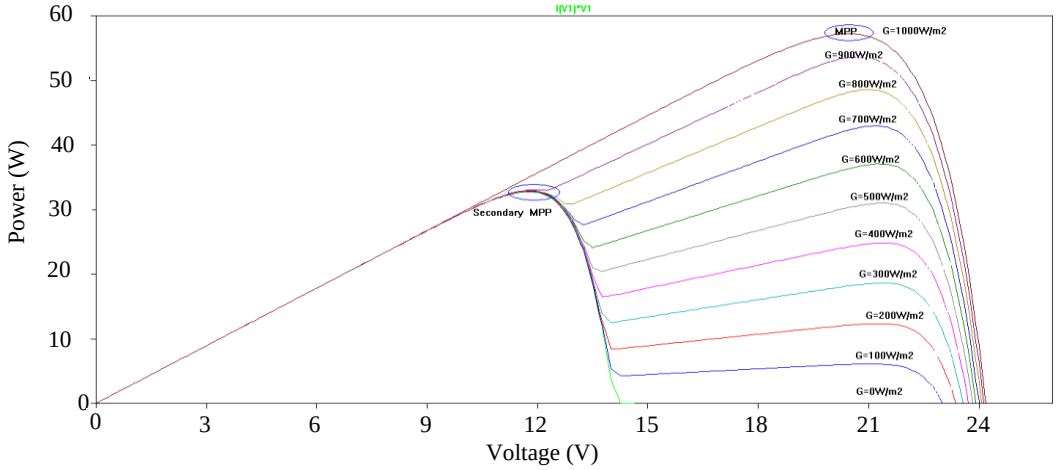

Figure 5.29: *P-V* curve for the string 4-15*-15-4.

From the simulation results presented previously, the following conclusions are apparent

- when BP diodes are not included in the circuit, shading has greater effect on short circuit current, power generated and little effect on open circuit voltage;
- the inclusion of bypass diode mitigates the adverse reduction in the power generated. This is due to the presence of multiple peak power points in the presence of shading or non-uniform illumination.

The initial thesis work was designed to minimize the effects of both longitudinal and transversal shading from the frame of the collector. The most predicted configurations and bypass diode arrangements were simulated accordingly, as 3-16-16-3, 4-15-15-4 and 5-14-14-5.

As the sun moves from sunrise to sunset, the movement of the shadow arising from the frame has different effect on the power generated from the cell string layouts. It has been concluded that the greater the number of solar cells bridged by the bypass diodes are affected by shading, the worst is the string´s performance: different configurations have different power generation capabilities. Therefore, comparing daily and annual energy production rates related to the string configurations is crutial, in order to optimize their performances by the reduction of shading/non-uniform illumination effects. However, other aspects should be taken into account when assessing the PV solar panel performance, which may compromise the choice. For instance, other constrains should be taken into account when considering the microinverter connected to the PV part of the PVT.

An inverter converts DC power coming from a solar panel or solar array into AC current, which can be used to power loads that run on alternating current electricity.

According to Solarus AB, some modifications were made in the PV modules, so that the concentrated side PV cell strings of both troughs are connected in parallel in the circuit that includes a micro-invertor. This one works for voltage levels that are between 50% of its maximum voltage to its maximum voltage rating (V_{max}). Below $0.5V_{max}$, the inverter output power is zero. This should be avoided at all costs. To avercome this, the number of cells closer to the frame must be increased, in order the voltage at peak power point would not fall below 50% of rated voltage when the shading affects the solar cells centrally located in the string.

The remainer work presented in the thesis dissertation has included the analysis of additional string configurations using 38 solar cells in parallell connection with 38 solar cells , that take into account the microinverter.

The simulation results are presented in the following paragraphs in figures 5.31 to 5.36 and summarized in tables 5.15 to 5.18.

Without bypass diode

F	1	0.9	0.8	0.7	0.6	0.5	0.4	0.3	0.2	0.1	0
P_{mp}	114.68	102.75	90.55	78.86	66.88	55.08	43.49	31.94	20.80	9.90	0
V_{mp}	20.38	20.30	20.20	20.06	19.88	19.71	19.46	19.09	18.62	17.72	0
I_{mp}	5.63	5.07	4.47	3.91	3.35	2.79	2.22	1.68	1.11	0.56	0
V_{oc}	24.20	24.06	23.91	23.74	23.55	23.29	23.02	22.66	22.13	21.24	0
I_{sc}	5.97	5.37	4.78	4.18	3.58	2.97	2.39	1.79	1.20	0.60	0

Table 5.15: Simulation results for different shading levels in a string 38//38.

6*-13-13-6 // 6*-13-13-6

F	1	0.9	0.8	0.7	0.6	0.5	0.4	0.3	0.2	0.1	0
P_{mp}	114.68	110.17	101.11	91.81	91.76	91.71	91.68	91.65	91.63	91.61	91.59
V_{mp}	20.38	20.75	21.50	16.50	16.50	16.50	16.50	16.50	16.50	16.50	16.50
I_{mp}	5.63	5.31	4.70	5.56	5.56	5.56	5.56	5.55	5.55	5.55	5.55
V_{oc}	24.20	24.18	24.14	24.10	24.08	24.04	24.00	23.95	23.87	23.73	19.75
I_{sc}	5.97	5.97	5.97	5.97	5.97	5.97	5.97	5.97	5.97	5.97	5.97

Table 5.16: Simulation results for different shading levels in a string 6*-13-13-6//6*-13-13-6.

7*-12-12-7 // 7*-12-12-7

F	1	0.9	0.8	0.7	0.6	0.5	0.4	0.3	0.2	0.1	0
P_{mp}	114.68	109.88	100.67	89.67	88.74	88.70	88.67	88.65	88.63	88.61	88.59
V_{mp}	20.38	20.88	21.38	21.75	15.88	15.88	15.88	15.88	15.88	15.88	15.88
I_{mp}	5.63	5.26	4.71	4.12	5.59	5.59	5.59	5.58	5.58	5.58	5.58
V_{oc}	24.20	24.18	24.14	24.10	24.06	24.02	23.97	23.93	23.83	23.67	19.11
I_{sc}	5.97	5.97	5.97	5.97	5.97	5.97	5.97	5.97	5.97	5.97	5.97

Table 5.17: Simulation results for different shading levels in a string 7*-12-12-7//7*-12-12-7.

8*-11-11-8 // 8*-11-11-8

F	1	0.9	0.8	0.7	0.6	0.5	0.4	0.3	0.2	0.1	0
P_{mp}	114.68	109.53	100.18	89.16	85.70	85.70	85.70	85.70	85.58	85.56	85.55
V_{mp}	20.38	20.88	21.38	21.63	15.38	15.38	15.38	15.38	15.25	15.38	15.25
I_{mp}	5.63	5.25	4.69	4.12	5.57	5.57	5.57	5.57	5.61	5.57	5.61
V_{oc}	24.20	24.16	24.14	24.10	24.04	24.00	23.95	23.89	23.77	23.58	19.00
I_{sc}	5.97	5.97	5.97	5.97	5.97	5.97	5.97	5.97	5.97	5.97	5.97

Table 5.18: Simulation results for different shading levels in a string 8*-11-11-8//8*-11-11-8.

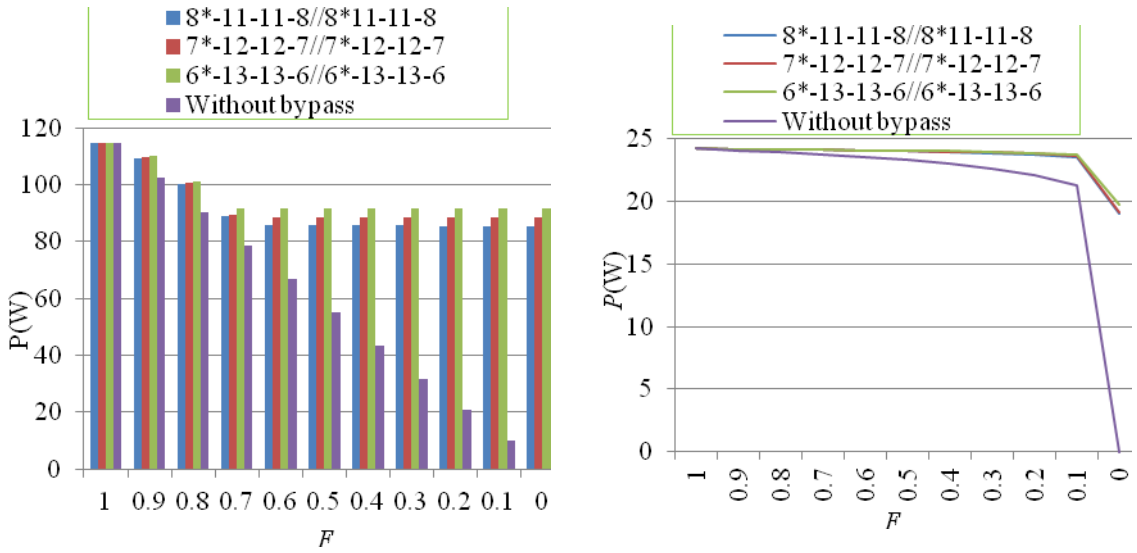

Figure 5.30: Shading *vs* peak power (left) and shading *vs* V_{oc} (right).

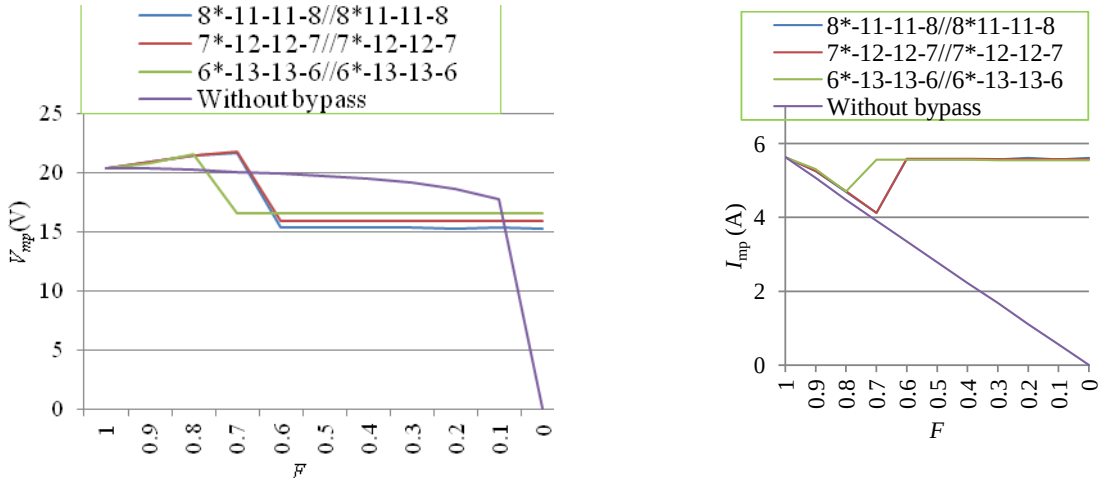

Figure 5.31: Shading *vs* V_{mp} (left) and shading *vs* I_{mp} (right).

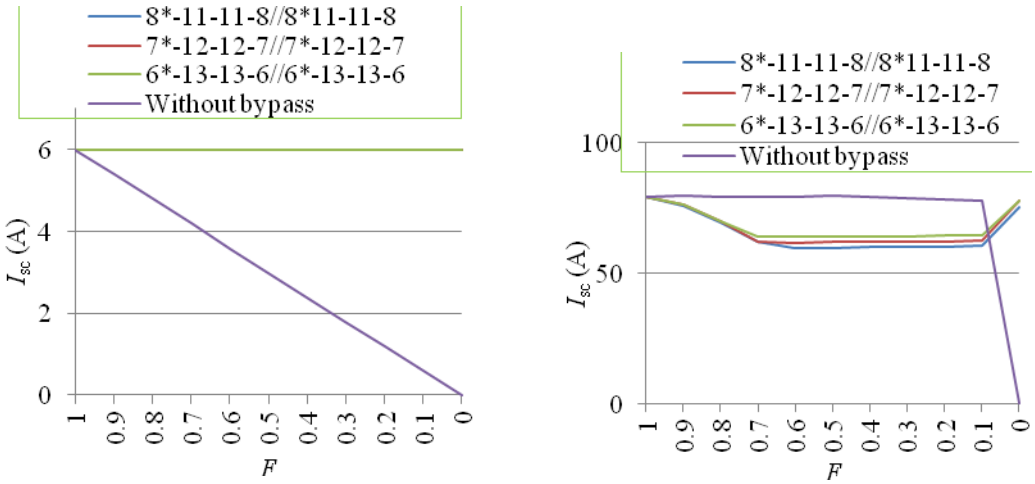

Figure 5.32: Shading *vs* I_{sc} (left) and shading *vs* *FF* (right)

6-13*-13-6 // 6-13*-13-6

F	1	0.9	0.8	0.7	0.6	0.5	0.4	0.3	0.2	0.1	0
P_{mp}	114.68	108.02	98.10	86.94	75.12	70.45	70.43	70.42	70.40	70.38	70.36
V_{mp}	20.38	20.75	21.00	21.25	21.50	12.50	12.63	12.63	12.63	12.63	12.63
I_{mp}	5.63	5.21	4.67	4.09	3.49	5.63	5.58	5.58	5.58	5.58	5.57
V_{oc}	24.20	24.14	24.08	24.02	23.97	23.88	23.80	23.66	23.51	23.20	15.25
I_{sc}	5.97	5.97	5.97	5.97	5.97	5.97	5.97	5.97	5.97	5.97	5.97

Table 5.19: Simulation results for different shading levels in a string 6-13*-13-6//6-13*-13-6.

7-12*-12-7 // 7-12*-12-7

F	1	0.9	0.8	0.7	0.6	0.5	0.4	0.3	0.2	0.1	0
P_{mp}	114.68	108.31	98.51	87.37	75.54	73.51	73.48	73.46	73.44	73.42	73.41
V_{mp}	20.38	20.75	21.13	21.38	21.50	13.13	13.13	13.13	13.13	13.13	13.13
I_{mp}	5.63	5.22	4.66	4.09	3.51	5.60	5.60	5.60	5.60	5.59	5.59
V_{oc}	24.20	24.14	24.12	24.04	23.99	23.91	23.82	23.70	23.55	23.26	15.89
I_{sc}	5.97	5.97	5.97	5.97	5.97	5.97	5.97	5.97	5.97	5.97	5.97

Table 5.20: Simulation results for different shading levels in a string 7-12*-12-7//7-12*-12-7.

8-11*-11-8 // 8-11*-11-8

F	1	0.9	0.8	0.7	0.6	0.5	0.4	0.3	0.2	0.1	0
P_{mp}	114.68	108.60	98.91	87.78	76.58	76.54	76.51	76.49	76.47	76.45	76.43
V_{mp}	20.38	20.75	21.13	21.38	13.75	13.75	13.75	13.63	13.63	13.63	13.63
I_{mp}	5.63	5.23	4.68	4.11	5.57	5.57	5.56	5.61	5.61	5.61	5.61
V_{oc}	24.20	24.16	24.10	24.06	24.00	23.95	23.86	23.76	23.59	23.33	16.51
I_{sc}	5.97	5.97	5.97	5.97	5.97	5.97	5.97	5.97	5.97	5.97	5.97

Table 5.21: Simulation results for different shading levels in a string 8-11*-11-8//8-11*-11-8.

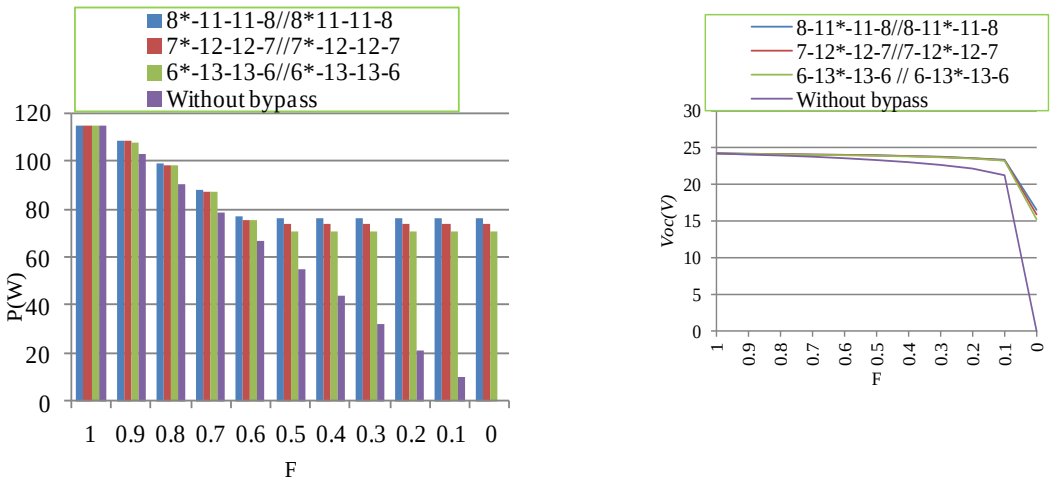

Figure 5.33: shading *vs* peak power (left) and shading *vs* V_{oc} (right)

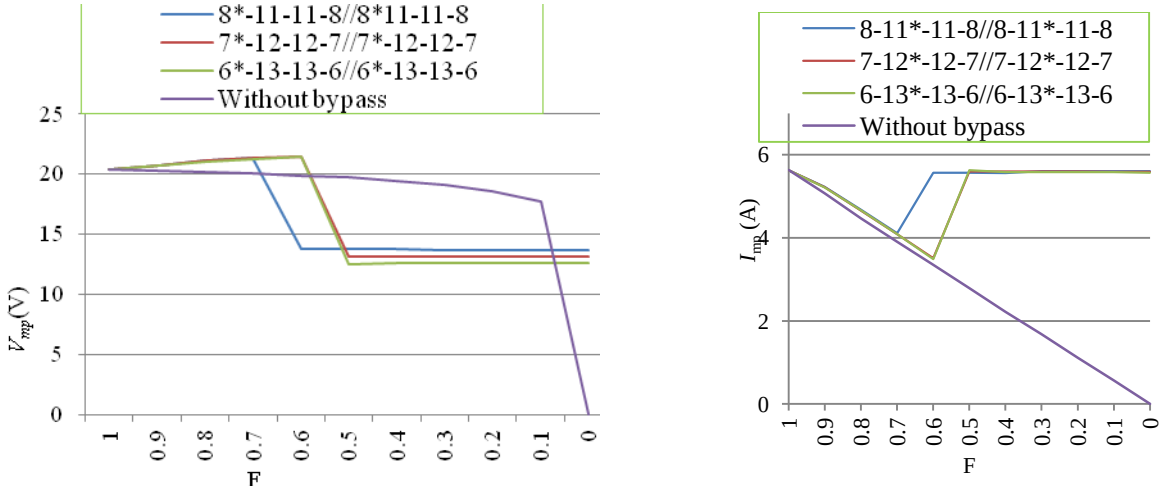

Figure 5.34: shading *vs* V_{mp} (left) and shading *vs* I_{mp} (right)

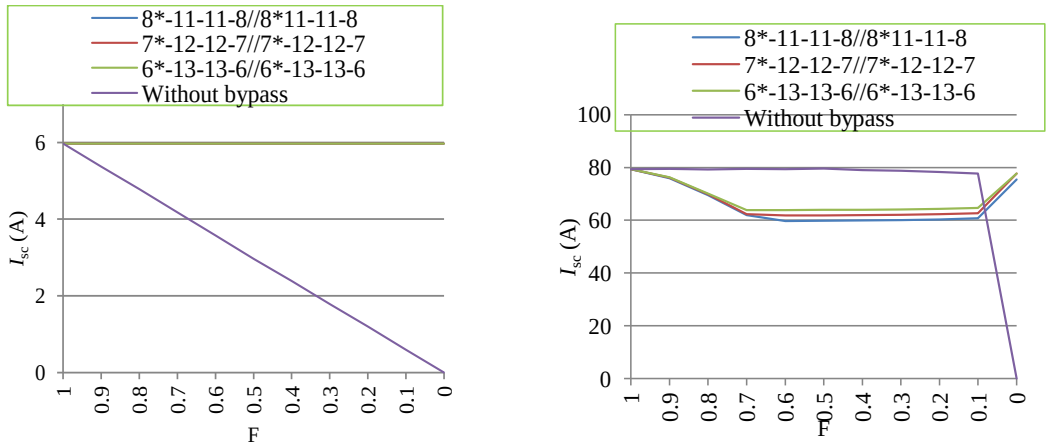

Figure 5.35: shading *vs* I_{sc} (left) and shading *vs* *FF* (right)

6. Conclusion

It has been considered all along this work PV modules that are combinations of strings of solar cells manufactured by Solarus AB (38 cells and 4 bypass diodes).

Solar cell modelling and simulation in a PSPICE environment has been presented and validated by a comparative analysis of the associated results with those obtained in laboratory in IST and from Solarus AB. The effect of shading on the PV module has been analyzed. The results show a remarkable agreement with experimental data, which ensures that the simulation model can indeed be used as an important tool for the analysis of the main figures of merit related to the PV solar module. Moreover, the modelling can be used to define the solar cell string layout associated to different PV collector configurations in order to improve their performance accordingly with he defined requeriments.

As it is known, sun continuously changes position throughout the day and with seasonal alterations. The non-uniform distribution of light in the concentrated side of the Solarus PVT collectors will have different effects on the electrical output of the PV cells in a string, depending on the configuration of the PV cells and the bypass diode arrangements. According to the obtained results, it may be concluded that there is a substantial power loss due to non-uniform illumination or shading of solar cell strings. It is thus advisable that all solar cells connected in series receive uniform illumination, all the time, with the smallest possible level of shading. This will allow a better protection of the array, minimizing the energy losses and, therefore, increasing the total energy generated by the PV module.

In shadow conditions, the decrease of the current in the branch where the PV cell is placed is proportional to the reduction in the irradiance. The bypass diode introduces a new peak in the *P-V* curve of the string characteristic, which may become the MPP of the string, depending on the shading levels. The number of peak power (PP) depends on the number of bypass diodes activated. This one depends on the extent of shading along the string, which is given by the distribution of illumination along the day. This distribution varies along the year and it depends on the place where the panel is located: the requirements for a solar panel adapted for high latitudes will be surely different from those for a solar panel near the equator. Therefore, it should be emphasized that this task is indeed a multi variable problem and that it should be kept in mind that the “best” solution does not exist and a search for adequate solutions will request compromises to be taken.

Even though, some simplifications have been introduced in the model and have clarified some aspects that should be relevant in the optimization of the performance of the PV solar panel. For instance, for all the available configurations of Solarus solar cell strings that have been simulated, when only one of the bypass diodes close to the frame is affected due to shading, the secondary PP will become the string MPP when the illumination falls below 75%. Moreover, the MPP reduction of the array will then remain constant, even if shadow levels increase.

On the other hand, if one of the central bypass diodes is affected by shading, the new PP point will become the MPP of the whole string if illumination falls below 50%. Another conclusion that should be referred is the following: no matter the configuration adopted for the Solarus strings, the bypass diodes maintain the MPP reduction due to shading arising from the frame below 43%.

It is hoped that this work will give some insight in the attempt to minimize the effects of shading or/and non-uniform illumination in different cell string layouts.

Finally, we shall refer some recommendations:

- the frame should be as thin as possible;
- the inclusion of blocking diodes in the electric circuit may help;
- reconfigurable bypass diode may be an option in order to increase the flexibility of possible options,

and also some future trends:

- simulation models to estimate the daily and annual production from a given string;
- the inclusion of thermal aspects to the analysis of PVT collectors and the necessary interfaces with the electric analysis.

Appendix I

The LTSPICE net list for the program is given below

```
* C:\Users\Samuel\Downloads\4-15-15-4.asc
D1 N020 0 DI_BAT54
B1 0 N020 I=(2.973+0.005*(temp-25))*((V(N001,0))/1000)
R1 N001 0 1000
R2 N020 0 1000
R3 N025 N020 0.001
V39 N112 0 0
V1 N001 0 1000
D2 N026 N025 DI_BAT54
R4 N027 N026 0.001
B2 N025 N026 I=(2.973+0.005*(temp-25))*((V(N002,0))/1000)
R5 N026 N025 1000
V2 N002 0 1000
R6 N002 0 1000
D3 N028 N027 DI_BAT54
B3 N027 N028 I=(2.973+0.005*(temp-25))*((V(N003,0))/1000)
R7 N028 N027 1000
V3 N003 0 1000
R8 N003 0 1000
D4 N021 N029 DI_BAT54
B4 N029 N021 I=(2.973+0.005*(temp-25))*((V(N004,0))/1000)
R9 N004 0 1000
R10 N021 N029 1000
R11 N030 N021 0.001
V4 N004 0 1000
D5 N031 N030 DI_BAT54
R12 N032 N031 0.001
B5 N030 N031 I=(2.973+0.005*(temp-25))*((V(N005,0))/1000)
R13 N031 N030 1000
V5 N005 0 1000
R14 N005 0 1000
D6 N033 N032 DI_BAT54
B6 N032 N033 I=(2.973+0.005*(temp-25))*((V(N006,0))/1000)
R15 N033 N032 1000
V6 N006 0 1000
R16 N006 0 1000
D7 N022 N034 DI_BAT54
B7 N034 N022 I=(2.973+0.005*(temp-25))*((V(N007,0))/1000)
R17 N007 0 1000
R18 N022 N034 1000
R19 N035 N022 0.001
```

```
V7      N007   0      1000
D8      N036   N035   DI_BAT54
R20     N037   N036   0.001
B8      N035   N036   I=(2.973+0.005*(temp-25))*((V(N008,0))/1000)
R21     N036   N035   1000
V8      N008   0      1000
R22     N008   0      1000
D9      N038   N037   DI_BAT54
B9      N037   N038   I=(2.973+0.005*(temp-25))*((V(N009,0))/1000)
R23     N038   N037   1000
V9      N009   0      1000
R24     N009   0      1000
D10     N023   N038   DI_BAT54
B10     N038   N023   I=(2.973+0.005*(temp-25))*((V(N010,0))/1000)
R25     N010   0      1000
R26     N023   N038   1000
R27     N039   N023   0.001
V10     N010   0      1000
D11     N040   N039   DI_BAT54
R28     N041   N040   0.001
B11     N039   N040   I=(2.973+0.005*(temp-25))*((V(N011,0))/1000)
R29     N040   N039   1000
V11     N011   0      1000
R30     N011   0      1000
D12     N042   N041   DI_BAT54
B12     N041   N042   I=(2.973+0.005*(temp-25))*((V(N012,0))/1000)
R31     N042   N041   1000
V12     N012   0      1000
R32     N012   0      1000
D13     N024   N043   DI_BAT54
B13     N043   N024   I=(2.973+0.005*(temp-25))*((V(N013,0))/1000)
R33     N013   0      1000
R34     N024   N043   1000
V13     N013   0      1000
R35     N029   N028   0.001
R36     N034   N033   0.001
R37     N043   N042   0.001
R38     N044   N024   0.001
D14     N045   N044   DI_BAT54
B14     N044   N045   I=(2.973+0.005*(temp-25))*((V(N014,0))/1000)
R39     N045   N044   1000
V14     N014   0      1000
R40     N014   0      1000
R41     N046   N045   0.001
```

```
D15     N047    N046    DI_BAT54
B15     N046    N047    I=(2.973+0.005*(temp-25))*((V(N015,0))/1000)
R42     N047    N046    1000
V15     N015    0       1000
R43     N015    0       1000
R44     N048    N047    0.001
D16     N049    N048    DI_BAT54
B16     N048    N049    I=(2.973+0.005*(temp-25))*((V(N016,0))/1000)
R45     N049    N048    1000
V16     N016    0       1000
R46     N016    0       1000
R47     N050    N049    0.001
D17     N051    N050    DI_BAT54
B17     N050    N051    I=(2.973+0.005*(temp-25))*((V(N017,0))/1000)
R48     N051    N050    1000
V17     N017    0       1000
R49     N017    0       1000
R50     N052    N051    0.001
D18     N053    N052    DI_BAT54
B18     N052    N053    I=(2.973+0.005*(temp-25))*((V(N018,0))/1000)
R51     N053    N052    1000
V18     N018    0       1000
R52     N018    0       1000
R53     N054    N053    0.001
D19     N055    N054    DI_BAT54
B19     N054    N055    I=(2.973+0.005*(temp-25))*((V(N019,0))/1000)
R54     N055    N054    1000
V19     N019    0       1000
R55     N019    0       1000
R56     N056    N055    0.001
D20     0       N030    DI_BAT53
D21     N030    N056    DI_BAT53
D22     N076    N056    DI_BAT54
B20     N056    N076    I=(2.973+0.005*(temp-25))*((V(N057,0))/1000)
R57     N057    0       1000
R58     N076    N056    1000
R59     N081    N076    0.001
V20     N057    0       1000
D23     N082    N081    DI_BAT54
R60     N083    N082    0.001
B21     N081    N082    I=(2.973+0.005*(temp-25))*((V(N058,0))/1000)
R61     N082    N081    1000
V21     N058    0       1000
R62     N058    0       1000
```

```
D24     N084    N083    DI_BAT54
B22     N083    N084    I=(2.973+0.005*(temp-25))*((V(N059,0))/1000)
R63     N084    N083    1000
V22     N059    0       1000
R64     N059    0       1000
D25     N077    N085    DI_BAT54
B23     N085    N077    I=(2.973+0.005*(temp-25))*((V(N060,0))/1000)
R65     N060    0       1000
R66     N077    N085    1000
R67     N086    N077    0.001
V23     N060    0       1000
D26     N087    N086    DI_BAT54
R68     N088    N087    0.001
B24     N086    N087    I=(2.973+0.005*(temp-25))*((V(N061,0))/1000)
R69     N087    N086    1000
V24     N061    0       1000
R70     N061    0       1000
D27     N089    N088    DI_BAT54
B25     N088    N089    I=(2.973+0.005*(temp-25))*((V(N062,0))/1000)
R71     N089    N088    1000
V25     N062    0       1000
R72     N062    0       1000
D28     N078    N090    DI_BAT54
B26     N090    N078    I=(2.973+0.005*(temp-25))*((V(N063,0))/1000)
R73     N063    0       1000
R74     N078    N090    1000
R75     N091    N078    0.001
V26     N063    0       1000
D29     N092    N091    DI_BAT54
R76     N093    N092    0.001
B27     N091    N092    I=(2.973+0.005*(temp-25))*((V(N064,0))/1000)
R77     N092    N091    1000
V27     N064    0       1000
R78     N064    0       1000
D30     N094    N093    DI_BAT54
B28     N093    N094    I=(2.973+0.005*(temp-25))*((V(N065,0))/1000)
R79     N094    N093    1000
V28     N065    0       1000
R80     N065    0       1000
D31     N079    N094    DI_BAT54
B29     N094    N079    I=(2.973+0.005*(temp-25))*((V(N066,0))/1000)
R81     N066    0       1000
R82     N079    N094    1000
R83     N095    N079    0.001
```

```
V29     N066    0       1000
D32     N096    N095    DI_BAT54
R84     N097    N096    0.001
B30     N095    N096    I=(2.973+0.005*(temp-25))*((V(N067,0))/1000)
R85     N096    N095    1000
V30     N067    0       1000
R86     N067    0       1000
D33     N098    N097    DI_BAT54
B31     N097    N098    I=(2.973+0.005*(temp-25))*((V(N068,0))/1000)
R87     N098    N097    1000
V31     N068    0       1000
R88     N068    0       1000
D34     N080    N099    DI_BAT54
B32     N099    N080    I=(2.973+0.005*(temp-25))*((V(N069,0))/1000)
R89     N069    0       1000
R90     N080    N099    1000
V32     N069    0       1000
R91     N085    N084    0.001
R92     N090    N089    0.001
R93     N099    N098    0.001
R94     N100    N080    0.001
D35     N101    N100    DI_BAT54
B33     N100    N101    I=(2.973+0.005*(temp-25))*((V(N070,0))/1000)
R95     N101    N100    1000
V33     N070    0       1000
R96     N070    0       1000
R97     N102    N101    0.001
D36     N103    N102    DI_BAT54
B34     N102    N103    I=(2.973+0.005*(temp-25))*((V(N071,0))/1000)
R98     N103    N102    1000
V34     N071    0       1000
R99     N071    0       1000
R100    N104    N103    0.001
D37     N105    N104    DI_BAT54
B35     N104    N105    I=(2.973+0.005*(temp-25))*((V(N072,0))/1000)
R101    N105    N104    1000
V35     N072    0       1000
R102    N072    0       1000
R103    N106    N105    0.001
D38     N107    N106    DI_BAT54
B36     N106    N107    I=(2.973+0.005*(temp-25))*((V(N073,0))/1000)
R104    N107    N106    1000
V36     N073    0       1000
R105    N073    0       1000
```

```
R106    N108    N107    0.001
D39     N109    N108    DI_BAT54
B37     N108    N109    I=(2.973+0.005*(temp-25))*((V(N074,0))/1000)
R107    N109    N108    1000
V37     N074    0       1000
R108    N074    0       1000
R109    N110    N109    0.001
D40     N111    N110    DI_BAT54
B38     N110    N111    I=(2.973+0.005*(temp-25))*((V(N075,0))/1000)
R110    N111    N110    1000
V38     N075    0       1000
R111    N075    0       1000
R112    N112    N111    0.001
D41     N056    N113    DI_BAT53
D42     N113    N112    DI_BAT53
.model D D
.lib C:\Program Files (x86)\LTC\LTspiceIV\lib\cmp\standard.dio
.dc V39 0 25 0.25
.include DI_BAT54.txt
.backanno
.end
```

The Diode models for DI_BAT53 and DI_BAT54 are presented below

```
*SRC=BAT54;DI_BAT54;Diodes;Si;  30.0V  0.200A  5.00ns   Diodes Inc. Schottky
.MODEL DI_BAT54 D  ( IS=17.9n RS=2.0u BV=30.0 IBV=2.00u
+ CJO=13.3p  M=0.333 N=1.3 TT=7.20n )

*SRC=BAT53;DI_BAT53;Diodes;Si;  30.0V  0.200A  5.00ns   Diodes Inc. Schottky
.MODEL DI_BAT53 D  ( IS=1.26n RS=1.0u BV=15.0 IBV=2.00u
+ CJO=13.3p  M=0.333 N=1 TT=7.20n )
```

Appendix- II

Electrical Power

$$P_{mp} = V_{mp} \cdot I_{mp}$$

The uncertainty in power is given by

$$\delta P_{mp} = \pm P_{mp} \cdot \sqrt{\left(\frac{\delta V_{mp}}{V_{mp}}\right)^2 + \left(\frac{\delta I_{mp}}{I_{mp}}\right)^2}$$

Fill Factor (*FF*)

FF describes how close the *I-V* characteristics of solar cell are close to the ideal characteristics; it is normally expressed as percentage.

$$FF = \frac{V_{mp} \cdot I_{mp}}{V_{oc} \cdot I_{sc}}$$

The uncertainty in FF is given by

$$\delta FF = \pm FF \cdot \sqrt{\left(\frac{\delta V_{mp}}{V_{mp}}\right)^2 + \left(\frac{\delta I_{mp}}{I_{mp}}\right) + \left(\frac{\delta I_{sc}}{I_{sc}}\right) + \left(\frac{\delta V_{oc}}{V_{oc}}\right)^2}$$

Efficiency (η)

Solar cell electrical efficiency is given by

$$\eta_{el} = \frac{P_{mp}}{A_{cell} \cdot G}$$

The uncertainty in efficiency is given by

$$\delta \eta_{el} = \pm \eta_{el} \cdot \sqrt{\left(\frac{\delta P_{mp}}{P_{mp}}\right)^2 + \left(\frac{\delta A_{cell}}{A_{cell}}\right)^2 + \left(\frac{\delta G}{G}\right)^2}$$

References

[1] J. Cubas, S. Pindado, C. de Manuel , "Explicit Expressions for Solar Panel Equivalent Circuit Parameters Based on Analytical Formulation and the Lambert W-Function", http://www.mdpi.com/1996-1073/7/7/4098, 1st Int. E-Conference on Energies *Whither Energy Conversion? Present trends, Current Problems and Realistic Future Solutions*, June 2014.

[2] A. Acakpovi, E. Hagan, "Novel Photovoltaic Module Modelling Using Matlab /Simulink", http://www.ijcaonline.org/archives/volume83/number16/14535-2978, *International Journal of Computer Applications*, (0975-8887), vol 83, No.16, December 2013.

[3] V. Perraki, G. Tsolkas, "Temperature Dependence on the Photovoltaic Properties of Selected Thin-Film Modules", doi: 10.11648/j.ijrse.20130204.12 *International Journal of Renewable and Sustainable and Green Energy*, vol. 2, No. 4, pp. 140-146, 2013.

[4] Swedish enterprise: http://www.solarus.se/the-hybrid-system/

[5] http://environ.andrew.cmu.edu/m3/s2/02sun.shtml

[6] *An Assessment of Solar Energy Conversion Technologies and Research Opportunities*, Summer 2006 http://gcep.stanford.edu/pdfs/assessments/solar_assessment.pdf, Stanford University , Global Climate and Energy project.

[7] *Solar cells*, chapter 2 : Solar radiation, http://ocw.tudelft.nl/fileadmin/ocw/courses/SolarCells/res00026/CH2_Solar_radiation.pdf

[8] *Solar Energy*, http://www.inforse.org/europe/dieret/Solar/solar.html

[9] *Oriel Product training, solar simulation*, http://assets.newport.com/webDocuments-EN/images/12298.pdf

[10] *Solar cells*, chapter 4: Operational Principle, http://www.aerostudents.com/files/solarCells/CH4SolarCellOperationalPrinciples.pdf

[11] http://www.alternative-energy-tutorials.com/energy-articles/solar-cell-i-v-characteristic.html

[12] Md. Nayeem-Ur-Rahman Chowdhury, "Technical and economic analysis of a novel asymmetric PVT hybrid solar collector", Ph.D. Thesis, September 2013 http://upcommons.upc.edu/pfc/bitstream/2099.1/19692/1/Master%20Thesis_Nayeem-Ur-Rahman%20Chowdhury.pdfhttp://upcommons.upc.edu/pfc/bitstream/2099.1/19692/1/Master%20Thesis_Nayeem-Ur-Rahman%20Chowdhury.pdf

[13] http://www.nordicgreen.net/startups/solar/solarus-ab

[14] http://www.solarus.se/solutions/

[15] Solar thermal power, 2020 Exploiting the heat from the sun to combat climate change http://www.greenpeace.org/international/PageFiles/24870/SolarThermalPower.pdf

[16] *Concentrating Solar Power* http://mcensustainableenergy.pbworks.com/w/page/20638019/Concentrating%20Solar%20Power

[17] J. M. Puerto, "Performance Evaluation of the Solarus AB Asymmetric Concentrating Hybrid PV/T Collector", Ph.D. Thesis, 2013-2014. http://www.diva-portal.org/smash/get/diva2:727716/FULLTEXT01.pdf

[18] C. Giovinazo, L. Bonfiglio, J. Gomes, B. Karlsson, "Ray Tracing model of an Asymmetric Concentrating PVT", *International Solar Energy*, September 2014,,
[19] A. Helgesson, "Optical Characterization of Solar Collectors from Outdoor Measurements, Incidence Angle Dependence of Asymmetric Collectors", Ph. D. Thesis http://www.ebd.lth.se/fileadmin/energi_byggnadsdesign/images/Publikationer/Bok_EBD-T-04_1_web_Anna_H.pdf
[20] M. Adsten, B. Hellström and B. Karlsson, "Measurement of Radiation Distribution on the Absorber in an Asymmetric CPC Collector" http://solar.org.au/papers/01papers/P821.pdf
and Bjørnar Sandnes, Exergy Efficient Production, Storage and Distribution of Solar Energy, November 2003. https://www.ecn.nl/fileadmin/ecn/units/egon/pvt/pdf/exergy.pdf
[21] http://www.ebd.lth.se/fileadmin/energi_byggnadsdesign/images/Publikationer/Bok_EBD-T-04_1_web_Anna_H.pdf
[22] Monika Adsten, Solar Thermal Collectors at High Latitudes, Design and performance of non tracking Concentrators, http://pointfocus.com/images/pdfs/csphighlatitude.pdf
[23] http://bigladdersoftware.com/epx/docs/8-0/engineering-reference/page-101.html
[24] *http://www.estif.org/solarkeymarknew/images/downloads/QAiST/qaist%20d2.1%20r2.2%20experience%20from%20tests%20on%20concentrating%20and%20tracking%20collectors.pdf*
[25] R. Bernardo, H. Davidsson, N. Gentile, J. Gomes, C. Gruffman, L. Chea, C. Mumba, B. Karlsson, "Measurements of Electrical Incidence Angle Modifiers of an Asymmetric PVT CPC collector", Scientific Research 2012
[26] J. Gomes, L. Diwan, R. Bernardo, B. Karlson, "Minimizing the impact of shading at oblique solar angles in a fully enclosed Asymmetric concentrating PV/T collectors", http://scholar.google.pt/scholar?q=Minimizing+the+Impact+of+Shading+at+Oblique+Solar+Angles+in+a+Fully+Enclosed+Asymmetric+Concentrating+PVT+CollectorSystem&btnG=&hl=en&as_sdt=0%2C5&as_vis=1
ISES Solar World Congress, *Energia Procedia*, 2013.
[27] https://www.jstage.jst.go.jp/article/jee/6/3/6_3_680/_pdf
[28] M. Kaya, "Thermal and Electrical Performance Evaluation of PV/T Collectors in UAE", http://scholar.google.pt/scholar?q=Thermal+and+Electrical+Performance+Evaluation+of+PV%2FT+Collectors+in+UAE&btnG=&hl=en&as_sdt=0%2C5&as_vis=1
KTH School of Industrial Engineering and Management Energy Technology EGI-2013-037MSC Division of Applied Thermodynamics and Refrigeration SE-100 44 Stockholm.
[29] R. Bernardo, H. Davidsson, B. Karlsson, ''Performance Evaluation of High Solar Fraction CPC collector System'', *Japanese Society of Mechanical Engineers –Journal of Environment and Engineering*, vol. 6, pp. 680-692, 2011. http://dx.doi.org/10.1299/jee.6.680
[30] S. Silvestre and A. Chouder, "Effects of Shadowing on Photovoltaic Module Performance", *Progress in Photovoltaics: Research and Applications*, May 2007, http://www.researchgate.net/profile/Chouder_Aissa/publication/227869114_Effects_of_shadowing_on_photovoltaic_module_performance/links/02bfe51249275cf149000000.pdf?disableCoverPage=true
[31] S. Silvestre, A. Boronat, A. Chouder, "Study of bypass diodes configuration on PV modules", *Applied Energy* , ELSEVIER, January 2009

[32] http://www.avdweb.nl/dummy/6-fietsroute-maastricht-vise/detail/73-maastricht-vise-005.html?tmpl=component
[33] R. Aloulou, P. de Peslouan, J. Armand , H. Minf, F. Alicalapa, M. Loulou, L. Luk, "Improved Circuit Model of Photovoltaic Cell for Energy Harvesting Application", 17th *IEEE Mediterranean Electro technical Conference*, Beirut, Lebanon, 13-16 April 2014.
[34] M. Edouard, D. Njomo, "Mathematical Modeling and Digital Simulation of PV Solar Panel using MATLAB Software", *International Journal of Emerging Technology and Advanced Engineering* Website: www.ijetae.com (ISSN 2250-2459, ISO 9001:2008 Certified Journal, vol 3, Issue 9, September 2013 http://www.ijetae.com/files/Volume3Issue9/IJETAE_0913_05.pdf
[35] S. Kumar, "Shading Impact on Solar PV Module", *American International Journal of Research in Science, Technology, Engineering & Mathematics*, ISSN (Print): 2328-3491, ISSN (Online): 2328-3580, ISSN (CD-ROM): 2328-3629 http://iasir.net/AIJRSTEMpapers/AIJRSTEM14-374.pdf